On the equilibrium of self-balanced shells under construction

Cross-herringbone technology

by

Vittorio Paris

Doctor of Philosophy in Engineering and Applied Sciences
XXXII cycle

At the

University of Bergamo
Department of Engineering and Applied Sciences

Thesis Supervisors:
Attilio Pizzigoni

Thesis Supervisors:

Attilio Pizzigoni
Professor of Architectural Design
University of Bergamo

On the equilibrium of self-balanced shells under construction

Cross-herringbone technology

by

Vittorio Paris

Abstract

The equilibrium of self-balanced masonry shells, during their construction, is the focus of this research. Through an evaluation of various historical self-supporting technologies, isolation of the primary factors that contribute to their self-balanced state under construction, a general approach to assess the equilibrium of masonry structures during their construction is proposed. This approach, based on two steps, can consider J. Heyman's hypotheses and can be adapted to consider the characteristics concerning different self-supporting technologies used. Among the historical technologies observed, the cross-herringbone technique (developed starting from the famous Brunelleschi's one) has been mainly observed. Its characteristics are derived from two types of sources: historical documents and surveys of real structures. A two-stepped approach is implemented to assess the self-balanced state of two case studies built adopting cross-herringbone technology. The research places the basis for future research on the evaluation of the stability of masonry under construction, and development of the cross-herringbone technology.

Keywords: Self-balancing, self-supporting, masonry, historic structures, cross-herringbone, herringbone, limit analysis, equilibrium analysis, discrete element method, Sangallo, Brunelleschi.

Acknowledgements

This document bears witness to the progress made in these years of study, very intense, exciting years, full of unexpected events and challenges that honestly more than once seemed like enormous obstacles. However, despite the difficulties, Attilio Pizzigoni has always wisely guided me by demonstrating his attention to me more than once, committing himself much more to what his professorship obligations were. Thank you very much for this. I would also like to thank Professor Sigrid Adriaenssens, for supporting me and helping me during my time in Princeton and for the following one, advising me wisely and showing great patience in waiting for the first results of the research.

I would like to say a few words of thanks for all those people who have chosen to work with passion, and in particular, I would like to thank Professor Santiago Fernandez Huerta, Professor Maurizio Angelillo, Professor Roberta Fonti.

I further extend my thanks to Professor Gian Marco de Felice, Professor Rosa Ana Guerra, Giuseppe Ruscica, Professor Giulio Mirabella Roberti, Ignacio Javier Gil- Crespo, Paula Fuentes, Alba de Luis, Carlo Olivieri, Isabella Elia and Diego Pezzoli. The surveys for the development of the research were carried out in collaboration with SABE directed by Prof. Alessio Cardaci and materially carried out by Pietro Azzola, an unrelenting worker, whom I want to thank, just as I want to thank Itasca C.G. who granted free use of the 3DEC software under the Education Partnership Program, fundamental for the analyses performed, and thanks also to Rhima Gazal for its availability in tutoring me.

I do not want to forget either Antonino Iannuzzo and Nicola Lepore, and Nandini Priya Thatikonda for the endless discussions (at all hours of the day and night) which have certainly provided a fundamental contribution to writing the document presented here, and for helping in editing.

Thanks also to those who in recent years, despite not understanding anything about my research, listened to me. Among them particular attention to Mattia Agazzi and all the guys at FabLab Bergamo. Finally, I want to thank my family that allowed me to arrive at this moment with serenity, helping me in the challenges that have arisen in these years.

Table of contents

List of figures

List of tables

Part I

1. Introduction

In this dissertation, an approach to evaluate the self-balanced state of masonry shells during the construction phase is proposed. The approach illustrated has been implemented to assess the equilibrium of domes built with the cross-herringbone spiralling technique.

1.1 Design and technology

In recent decades, masonry shells have been the subject of considerable study, in particular, with the development of computers and digital fabrication tools that influence the direction of research in this area. A witness of this development is the Armadillo Vault pavilion [1] where the extreme shape has been designed and fabricated, only through the aid of computer numerical control tools. Also, from the structural behaviour point of view, considerable progress has been made. The formulation of plastic theory for masonry structures [2] has been placed the basis for thriving research [3] [4] [5]. According to this theory, the geometry is the crucial factor for guarantee the equilibrium of masonry structures, from the simple study of geometry, it is possible to determine the state of the structure. Concerning the construction of masonry buildings, Byzantine builders believed that the stability, geometry and construction were fundamental elements for understanding these structures [6] [7]. They also believed that these three elements were deeply related to each other, and as mentioned above, nowadays, we know that there is a close relationship between the first two aspects: the stability and the geometry. However, much of the research developed in the last decades points to the development of advanced construction systems [8] [9] that do not always consider geometry and stability. Undoubtedly, the new digital fabrication technologies and the use of robotic instruments can reduce the costs of masonry structures

[10], in particular, referring to the relative costs of fabrication and formwork. The issues encountered in the context of productivity and economic efficiency of curved spatial structures are certainly not new, not in the current day nor throughout history when various self-supporting and/or self-centering technologies have been developed. Around the world, several studies, installations and architectural works give evidence of work being conducted in the area of self-supporting technologies, in particular, related to the tiling vaulting technique. Nevertheless, very few scientific researches are dedicated to defining an approach for evaluating the equilibrium of these structures under construction.

1.2 Statement of the problem

The economic factor in terms of productivity is the main issue faced in the building field [11]. Starting from the existing and historical techniques, the development of efficient and sustainable construction technologies should be the scope of the current day research. From the previous discussion, and to achieve this purpose, it is needed to develop a theory to evaluate the state of equilibrium of structures during their construction and concerning masonry buildings, this approach should consider the peculiar masonry behaviour.

1.3 Outline of chapters

The remainder of this document is organized as follows: in **Part I**., after introduction chapter 2. and chapter 3. give an overview of the principal historical self-balanced technologies and an introduction on the theory and method adopted for assessing the equilibrium of masonry structures. **Part II** is constituted by chapters 4, 5. and 6.. Chapter 4. describes the characteristics of the cross-herringbone spiralling pattern a self-supporting technology developed by Sangallo architects, while the approach to evaluate masonry structures during their construction is also illustrated in chapter 5. and applied to assess the equilibrium addressed in chapter 6.. The conclusions are illustrated in **Part III**, constituted by chapter 7.. Three appendixes follow the conclusions: Appendix A reports the list of domes built using herringbone or cross-herringbone spiralling technology, Appendix B gives the results of limit state analysis, and Appendix C the results of discrete element method.

2. Self-Balanced vaulting technologies

Arches, vaults and domes are among of the most significant expressions of civilisation and cultural and technological progress. These structural systems have numerous applications, varying from providing shelter, defining a space, and in the creation of monuments. Among these, thin shell structures can define architectural forms and resist loads efficiently at the same time [12]. However, they require a significant investment in terms of resources, since centering or formwork is needed during the construction, which impacts at 20-30% of the entire project cost [13] [14].

Every culture has sought towards building methods and techniques based on the principles of efficiency. In this process, they have explored efficient technologies that permit to build vaults, arches and domes without the need for any formwork or shoring throughout various phases of its construction. As witnessed in scientific documents, several efficient technologies have been developed throughout history [15] [16]. Unfortunately, over the last few centuries, this knowledge is lost.

The literature refers to these efficient vaulting technologies, through the adoption of various terms: self-centering [17], self-supporting [18] or self-balancing [19]. Self-supporting and self-centering are terms related to the construction aspect with slightly different meanings: not all self-supporting technologies are self-centering; but, all self-centering technologies are self-supporting. The self-supporting techniques do not require the use of formwork, and in the self-centering ones, even the use of centering is not needed. The term self-balancing, on the contrary, is related to the static aspects. Self-balancing indicates the ability of a structure to find a balanced state without any support during all the construction phases. Therefore, in this document, the author refers to the following terms: self-supporting, self-centering or self-

balancing, depending on the aspect analysed: constructive or structural.

The focus of this chapter remains solely on the most relevant historical self-supporting technologies: vaulted masonry shells. The literature on various other self-supporting or self-centering technologies is available; nevertheless, this research does not include them, e. g. the armchair voussoirs technique [20] used in the Roman Empire to build self-supporting structures, displayed in figure 2.1, or the nuraghe vaulting technique [21].

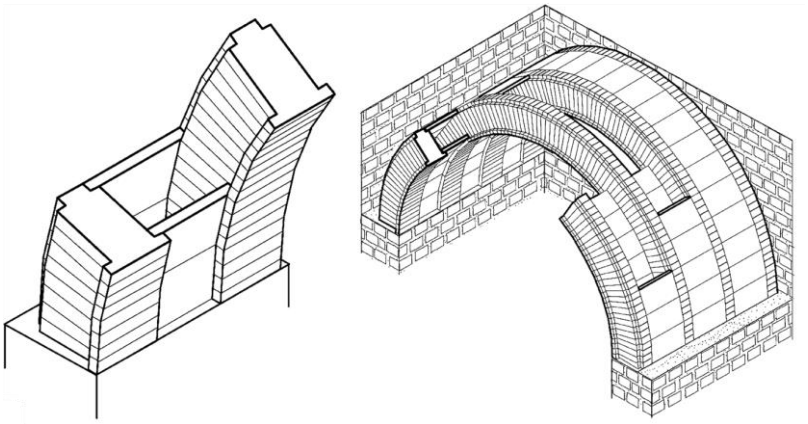

Figure 2.1 Armchair voussoirs vault. Left detail. Right, vault under construction. Drawing of L. C. Lancaster [20] [22].

The technologies chosen for the literature review are representative and among the most diffused. For each technique, a historical and critical overview is presented, showing their main peculiarities, and the construction principles. The following chapters give a brief introduction to these technologies

2.1 Pitched vault

2.1.1 Notes on the history of pitched vault

The pitched vaulting technique, also called the "Nubian" technique, is it the first or among the first self-centering method developed. The history of the pitched vaults is strictly related to the history of the arches: the origin of this technology dates back to the same period of the origin of the arch. Evidence of the existence of this constructive method dates back to as early as the 21st century B.C.E. [23] [24] [25], and it is in use in the current day in few parts of North Africa [26]. Traces of these kinds of structures can be found on three continents: Asia (Middle East), North Africa and Europe, which suggests that this construction technology had spread through the Mediterranean Sea and the cultures surrounding it [7] [16] [20] [27]. Several sources document the use of the pitched vaulting technique: on one hand through domes at Taq-I Kisra (Sassanid Empire, around the 6th century, ancient city of Ctesiphon in modern-day Iraq) [16] or the Byzantine domes [28] as the substructure of the apse hall of the Palace of Byzantine Emperors (Byzantine Empire, ancient Constantinople in modern Istanbul) [7], and on the other hand by historical documents such as the A. Choisy's treatise [6].

2.1.2 Principles of pitched vaulting technique

To understand how the pitched vaulting technique allows building a structure without centering, it is essential to first visualize a barrel vault under construction. Traditionally to build these vaults, the bricks are laid radially as shown in figure 2.1.1 a), thus, to prevent sliding, it is necessary to use auxiliary structures. A peculiar pattern characterizes the barrel vaults built with the pitched vaulting technique, figure 2.1.1 b): the bricks are laid radially to form arches placed in an inclined plane, and laid one next to another with the new arch resting over the previous one [29]. Referring to figure

2.1.2, it is possible to observe the construction method, where the first arch laid is placed against a boundary wall, and that has a crucial role in supporting the barrel vault during its construction. The first bricks are placed such a way to push against the wall and to form an arch. Once the first arch is completed, the next one can be laid. Following this construction sequence, the new brick course is placed over the previous one, allowing each brick to interact with the previous arch, these contacts prevent the slippage of bricks during the placing of the subsequent.

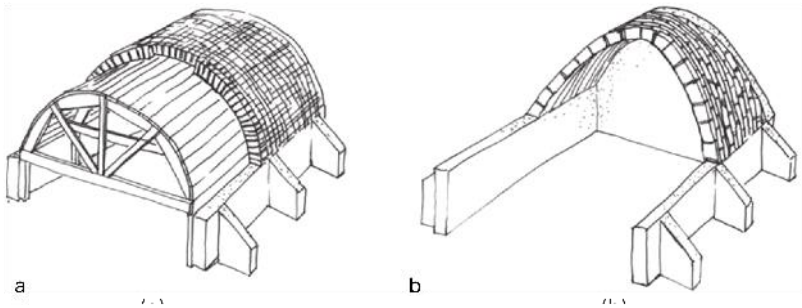

Figure 2.1.1 Barrel vault and pitched vault under construction. Drawing by J.F.D. Dahmen [16].

Figure 2.1.2 Pitched vault under construction. Photography by Adobe alliance [16].

As mentioned, the arches formed do not lay in vertical planes and display inclinations that are not evenly defined; some examples of this variation are shown in figure 2.1.3 [7] [27].

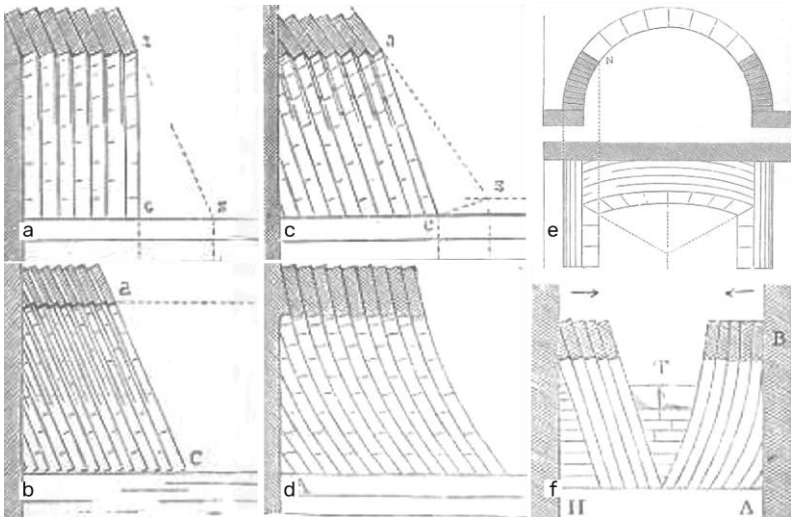

Figure 2.1.3 Pitched vaulting technique, different scheme to lay bricks. a), b), c) and d) are a lateral view of barrel vaults each one show different scheme and inclination of arches. e) and f) represent a combined method [6].
Drawing of A. Choisy.

The shape of arches is not clearly defined, but research studies and evidences from archaeological remains, testify that the geometry of the arch adopted is parabolic [20]. This shape gives both structural and constructive advantages: the parabola being the geometry most similar to catenary [30], the ideal geometry to support the uniform distributed load. Therefore, once the first arch is laid, the geometry of all the subsequent next arches is defined, thus eliminates the need for centering. During construction, the equilibrium state is facilitated by the portion of the vaults already built.

The equilibrium of the pitched vault is guided by the arch's stability and by the stability of the supporting wall, both of which depend essentially on their geometries [2].

2.1.3 Geometries of the pitched vault

As displayed in figure 2.1.3 e) and f) cases, the pitched technique could combine different laying methods within a structure. Certainly, the geometry most suitable for this self-centering technology is the barrel vault, owing to the analogy to an arch. However, it can be used to build domes with different geometries such as hemispherical domes, cross vaults, dominical vaults and more complex shells [27]. In order to build these complex structures using the pitched vaulting technique, it is necessary to design the orientation of mortar joints. The constructive process also assumes great importance here, and figure 2.1.4 illustrates a possible pattern for building a cross vault [27].

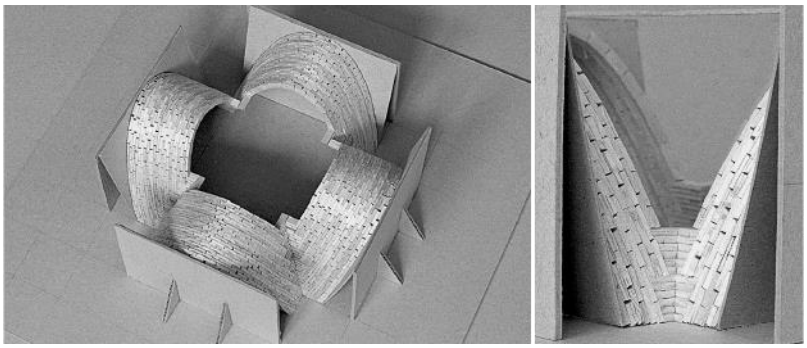

Figure 2.1.4 Pitched vaulting technique. Scaled model of cross vault under construction: different pattern orientation [27] [31]. Photography by D. Wendland.

2.2 Clay tubes vault

2.2.1 Notes on the history of Clay tube vault

Among the several technologies that flourished during the Roman Empire, the origins of the tube vaulting technique can be traced back to the 4th century B.C.E. [32] [33]. Over the following centuries the tube vaulting technique, developed mainly in Africa proconsularis (today Tunisia, Libya, Algeria and Morocco) and spread throughout Europe, especially in Italy, France, Spain and Britain [20] [24] [33]. Even after the fall of the Roman Empire, this technique was used until the 7th century C.E. by civilizations in North Afric, such as Vandals, Byzantines and the Arabs [34]. Nowadays, the tubes vaults and domes are used as low-cost alternatives in India [20].

The first use for this technology could be linked to a pre-existing building technique used for clay kilns [35], this also includes the tube vault covered food storages where the clay fireproofing properties protected the food from fire-related dangers [20].

2.2.2 Principles of Clay tube vaulting technique

As witnessed during the archaeological campaigns of Sicily and North Africa [33] [24], until the 2nd century C.E. the shape of the clay tubes changes constantly and the technique underwent refinements and variations. These tubes used in the clay vaulting technique are hollow clay cylinders with a small nozzle. Their sizes vary with the period and the context in which they were manufactured. Broadly viewing, they have the length of less than $20\ \mathrm{cm}$ and diameter around 6-10 cm [20].

The reduced dimensions of the clay tubes guaranteed lightness, allowing the mason to place them easily. Their peculiar shape, also allows the tubes to be stacked, in a way that the nozzle rests within the hollow end of the next clay tube. During construction, just

before the two tubes are piled one upon the other, gypsum mortar is laid between the two interacting surfaces: the nozzle and the cylindrical lateral surface of the tube [34]. Therefore during construction, the hollow end is partially filled, and immediately, the two tubes are joined together. However, in the pitched vaulting technique (chapter 2.1), the first arch placed requires to be supported under construction. In the case of barrel vaults construction wich the tube vaulting technique, as shown in figure 2.2.1, the tubes are oriented as parallel vertical arches and start from an end wall or by placing a light formwork [32].

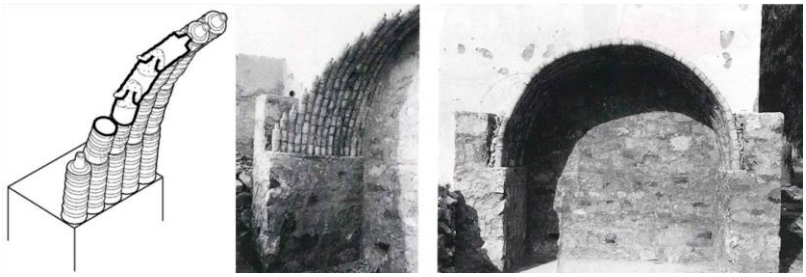

Figure 2.2.1 Tube vaulting technique. Left detail under construction, the clay tubes and gypsum mortar Drawing of L. C. Lancaster [20]. Center and right, reconstruction of a barrel vault, Chemtou (Tunisia) [34].

The use of gypsum-based mortar and the pipes stereotomy does not make the construction sequence fundamental: it is not necessary to complete the previous arch before being able to proceed with the subsequent arches. Therefore the tubes vaulting technique allows creating self-supporting structures and construction of simple structures without centering.

2.2.3 Geometries of clay tube vault

The tube vaulting technique allows building complex geometries, such as hemispherical domes, cross vaults, pavilion domes, squinch domes, and even more complex geometries. For building these complex structures, the study of the orientation pattern of

tubes is needed, figure 2.2.2 clarifies some orientation patterns: interesting are the cases related to revolution geometries where the orientation patterns are possible by arches or rings [34].

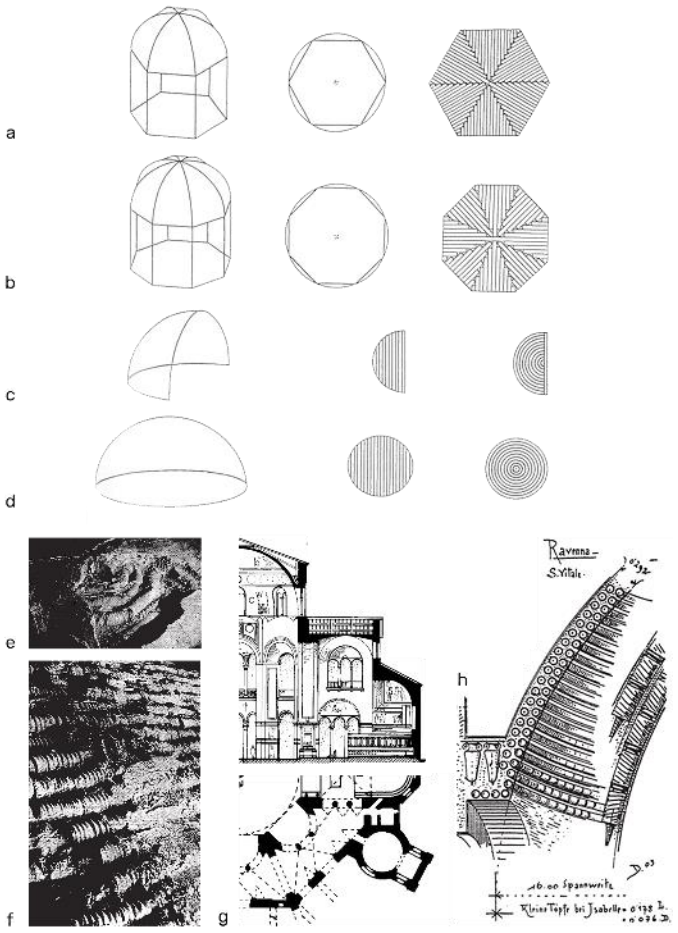

Figure 2.2.2 a), b), c), d) orientation pattern of clay tubes. For cases c) and d) two different patterns can be adopted [34]. e), f), g), h) San Vitale basilica (Ravenna, Italy). e) and f) are details of the dome, which was built with the tube vaulting technique. e) Detail near the crown, the tubes are laid to form rings. f) Detail near the base of the dome, as well as e) the tubes form rings [36] [37]. g) Section and plan view of San Vitale in Ravenna. h) Detail of a section of San Vitale dome, the horizontal orientation of the tubes [38].

2.3 Tiling vault

2.3.1 Notes on the history of tile vault

The tile vault is the most famous self-supporting technology that developed in Spain around the 13-14th C.E. [39]. This technology is an efficient method to build curved structures using only mortar and tiles.

Although extensive literature reports the history of the tile vaulting technique [40] [41], the origin of this technology is not clear. However, it is reasonable to think that the encounter between Islamic and Romanesque culture has favoured the birth of this constructive system. This interaction could have taken place in the Spanish peninsula, due to, the scarce availability of the wood for auxiliary structures. The use of tiles and the presence of gypsum [41] combined with constructive knowledge of Byzantine and Islamic builders [15], forms the perfect environment to develop the tiling vaulting technique.

It is not the purpose of this document to report the complete historiography on the evolution of this technique [41], but it is fundamental to list the milestones in the evolution that have characterized the tile vaulting method. These milestones are broadly related to the aspects of efficiency and strength of the tile vaults The early known use, between the 12th-13th century, was for secondary structures such as stairs [39]or for filling space between ribs vaults [42] (span: 1.3 -1.5 m). Over the next centuries, the technique was used to build domes and vault without ribs. This is when, the knowledge of the tile structure behaviour increased, adding to its importance and applications (span: few meters). Along the 16th century, the method was systematically applied along the Spanish east coast [15], especially in the area of Catalonia, Valencia and Extremadura. Architects like Guastavino, had a significant role during the 19th and 20th century [43], when the tiling technology was transferred to North America and became one of the most

popularly used self-supporting technique [44] (span: > 15 m). Later since the 18th century, this constructive method was learnt and applied in other countries like Italy [15] and France [45]. Nowadays, tile vaults are used primarily in developing countries [26] [46].

2.3.2 Principles of tile vaulting technique

To raise a tile vault it is required following a construction sequence [47]: first, the centering is placed, as shown in figure 2.3.1 a) [48], and then tiles are laid according to the construction sequence, e.g. figure 2.3.1 b). Generally, the tile vaults are composed of 2-3 tile layers, which are laid using two different types of binders. The inner shell is placed by using gypsum mortar (plaster of Paris) or fast-setting cement; this layer supports the following layers and acts as formwork during the construction process. The remaining layers can be laid with non-hydraulic or hydraulic binder [49]. To avoid overlap of joint the orientation of the tile pattern must be changed between different layers, typically by rotating the first layer with respect to the second one by 45° [50] figure 2.3.1 c). The tile used to build the vaults are thin, once laid the overall thickness remains less than 12 cm.

The use of a fast-setting mortar does not provide by itself all the resources to prevent sliding and overturning of the structure during the construction phases. Only if all factors have been respected: the construction sequence, the feature of stiffness derived from the curved geometry [27], lightness and strength of the tiles and the fast-setting property of the binder [44] the tile vaulting is a self-supporting method.

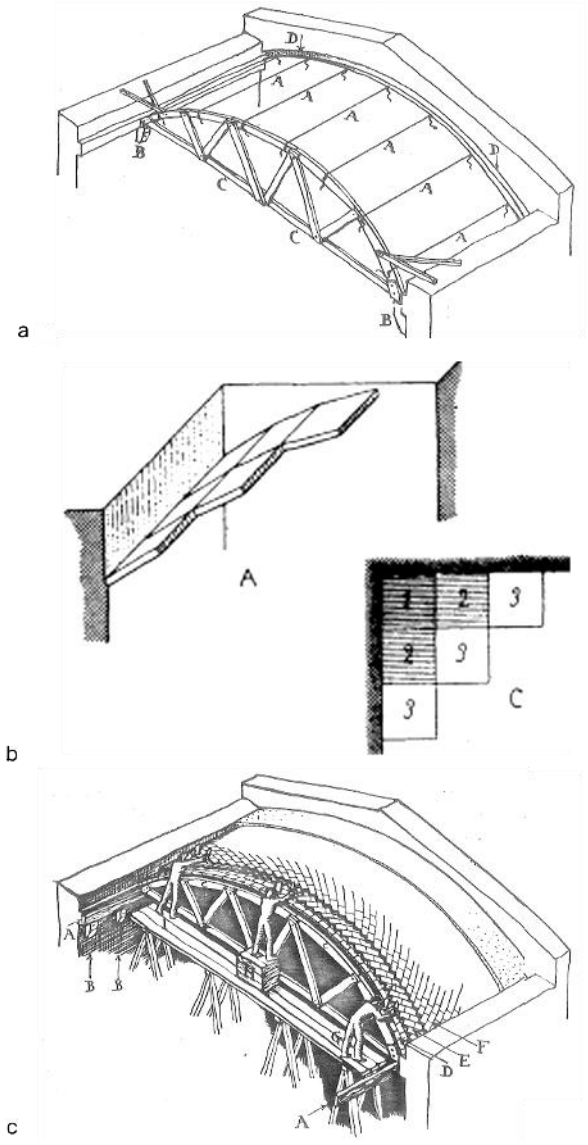

Figure 2.3.1 Tile vault under construction. a) Centering [48]. b) The construction sequence [51]. c) A portion of tile vault under construction [48]. Drawing of (from top to bottom) L. B. Moya, A.Choisy, L B. Moya.

2.3.3 Geometries of tile vault

Thanks to the peculiar constructive technique, the tiling vaulting technique permit to build practically any kind of compressed shells: from staircases [44] to barrel vaults. As displayed in figure 2.3.2, contemporary projects [46] [52] show the full potential of the tile vaulting technique [50].

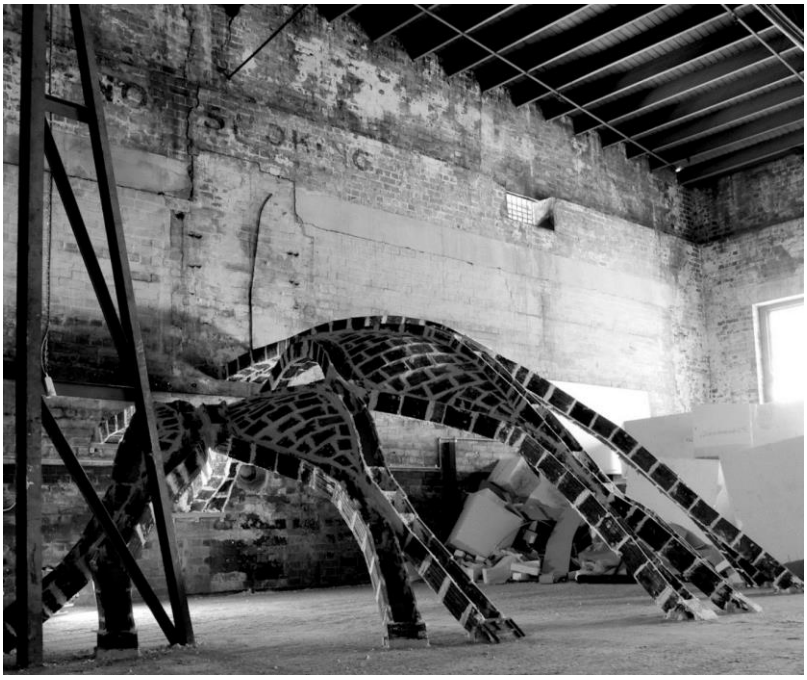

Figure 2.3.2 Complex ribbed vaults. Masterclass - Ribbed Catalan, Photography by M. Ford [52].

2.4 Herringbone vaulting technique

2.4.1 Notes on the history of Herringbone vaulting

The secret building process of the dome of the Santa Maria del Fiore (1418-1471) cathedral in Florence has fascinated researchers for around six hundred years [53] [54] [55] [56] [57]. Despite the resolution of numerous questions, the construction of these impressive structure remains a mystery.

The origins of the herringbone construction technology have been obscured by the fame of the dome of Santa Maria del Fiore. It is unreasonable to think that Filippo di Ser Brunellesco Lapi (1377-1446 [58]), commonly known by the name Brunelleschi, built his masterpiece without having a full grasp of the herringbone spiralling technology.

Some researchers believe that the herringbone spiralling technique can be derived from the Opus spicatum [59], a Roman technique, shown in figure 2.4.1 a), used to build wall whose pattern appears very similar to that of the Brunelleschi's herringbone.

Other researchers trace its origins to the east [60] [61] [62], based in the cultural contact that was evident between the Florentine, Byzantine and Arab cultures. As evidence of this, there are numerous testimonies: the council of Florence (1055) chaired by Victor II [63] or the commercial agreements between Tuscans and Arab kingdoms [64]. The influence of Arab and Byzantine in Florentine architecture begins at least one century before the construction of Santa Maria del Fiore's dome [64]. Therefore, for all of these reasons, it is not possible to pinpoint the origins of the herringbone spiralling technology, and even how Brunelleschi gathered his knowledge on this constructive system.

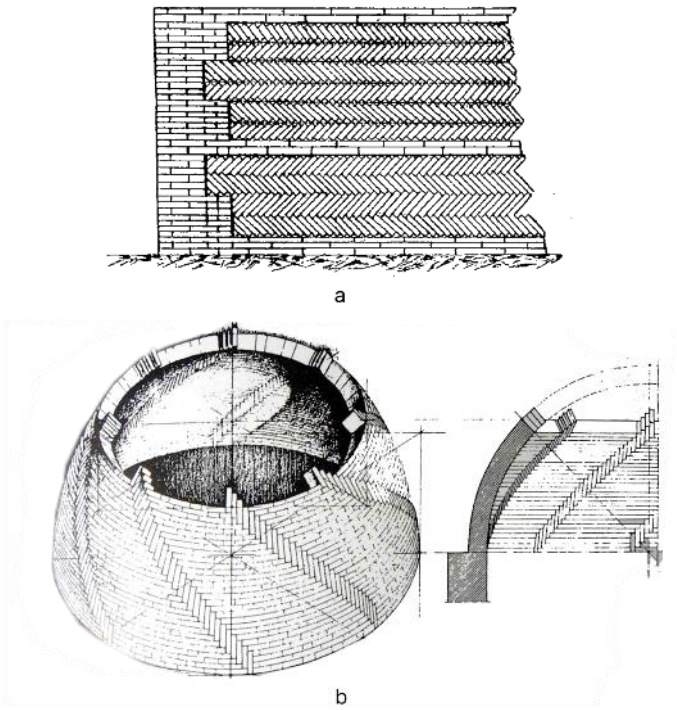

Figure 2.4.1 Herringbone spiralling pattern. a) Opus spicatum. Drawing of C. G. de Montauzan [65]. b) Revolution dome and herringbone spiralling pattern, the vertical bricks are highlighted. Drawing of F. Gurrieri [66].

The Venetian master masons, during the 11th century, used the herringbone spiralling technique in the area close to Venice [60], as the same period, the Seljuks applied it to build mosques [61]. Figure 2.4.2 shows the dome of Northern Prayer Hall (completed in 1088) of the Isfahan Friday Mosque (Isfahan, Iran), the herringbone spiralling pattern is visible in the lateral half-domes. Nowadays, the Ardestan Friday Mosque (completed in 1158, Ardesan, Iran), displayed in figure 2.4.3, is proof of the great skill of Arab masons in the use of the herringbone spiralling technique. The invention of this technology could be even more ancient since it is interwoven with the history of traditional Iranian wind towers (the Bādgir) and

the traditional Iranian water cisterns (the Ab Anbar) whose origins are very ancient even millennia B.C.E., figure 2.4.4 [67].

Figure 2.4.2 Northern Prayer Hall (completed in 1088 C.E.) of the Isfahan Friday Mosque (Isfahan, Iran). Photography by R. Piperno [68].

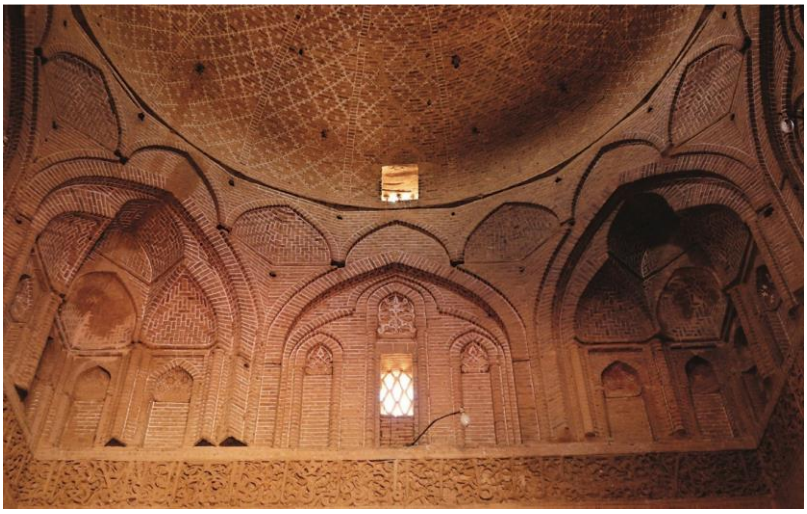

Figure 2.4.3 Ardestan Friday Mosque (completed in 1158 C.E., Ardesan, Iran). Photography by Selcuklu Belediyesi [69].

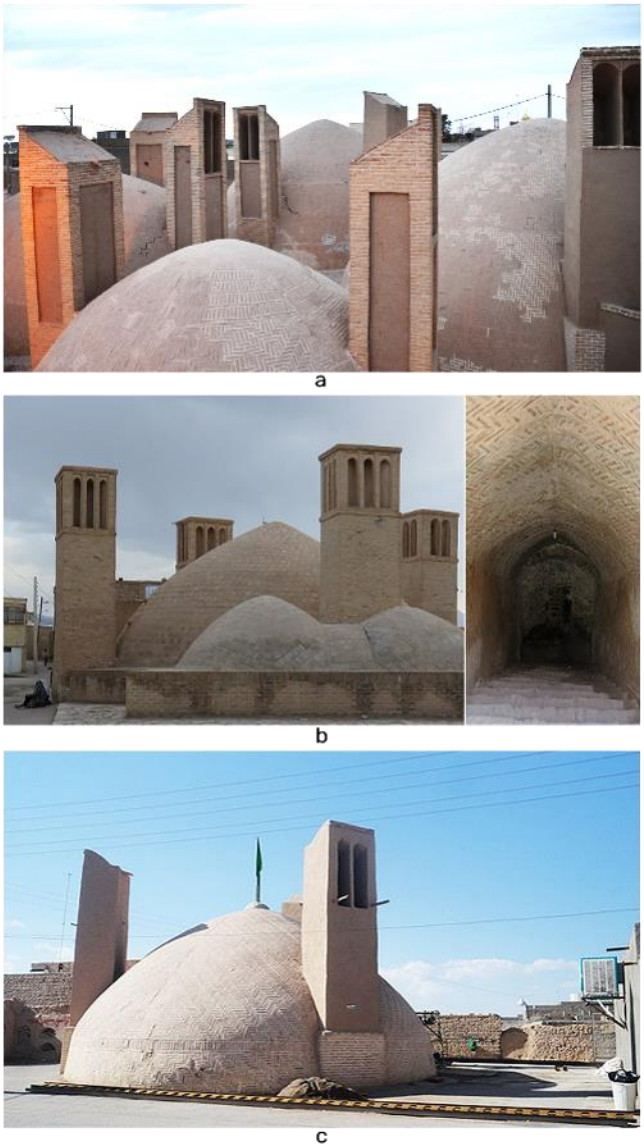

Figure 2.4.4 a) Traditional Iranian water cisterns (date unknown, Ardakan, Iran) Photography by unknown [70]. b) water cisterns facility of Ardestan Friday Mosque (completed in 1158 C.E., Ardesan, Iran). Photography by R. Piperno [68]. c) Traditional water cisterns (date unknown, Ardakan, Iran) Photography by unknown.

In Italy, until the second half of the 16th century. The herringbone spiralling technique was used systematically by florentine Sangallo architects [62] (Appendix A). Sangallo perfected this building technology, and from it, developed the cross-herringbone spiralling technique [71]. It also seems that the application of the technique ended with the Sangallo architects. However, the specific reasons why the use of this herringbone spiralling technique disappeared in Italy post 16th century are not known.

2.4.2 Principles of herringbone vaulting technique

To understand how the herringbone spiralling technique allows building structures without support it is necessary to examine its typical masonry pattern: as shown in figure 2.4.1 b), the herringbone spiralling pattern consists of an arrangement of horizontal brick courses interrupted by vertical bricks, in this document, they are called herringbone bricks. The herringbone bricks are laid at regular intervals and placed in the same plane of the horizontal bricks.

Through the different courses, the herringbone bricks describe a peculiar trajectory curve: the loxodrome also called rhumb line [72] [73][74]. The loxodromic curves are a class of mathematical curves: they are continuous, and they run on the entire surface of the structures. This geometrical continuity highlights the role of the herringbone spiralling pattern and in particular that of the arrangement of herringbone bricks: linking the courses together.

Figure 2.4.1 b) shows an incomplete dome with a herringbone spiralling pattern, and assuming to build through the complete course, i.e. placing bricks of a new course only when the previous one is completed, it is possible to understand how the vertical bricks tie two courses together. They belong to a closed course which is a balanced structure and stable; therefore the vertical bricks are fixed and capable of acting as constraints for the construction of the next course. Under construction, the

herringbone spiralling technique allows the formation of resistant substructures (see chapters 4.3 and 6.3.2) whose role is to prevent slippage and overturning.

2.4.3 Geometries of herringbone vault

The herringbone spiralling technique has been applied mainly to hemispherical or pavilion domes; however, as shown in figure 2.4.3 and 2.4.4 b) with appropriate precautions, it can also cater to other geometries.

3. Notes on masonry mechanics

The following chapters 3.1, 3.2 and 3.3 illustrate the mechanical assumptions and the essential characteristics of the theory and tools adopted to pursue the research presented in this thesis.

3.1 Notes of the history on the theory of arch and vaults

This chapter contains a brief history of the fundamental theories formulated over the last four centuries. The aim here is not to present the history of the structural arch theory, which is well known and documented, as evidenced by the vast literature [75] [76] [77]. The aim is to understand what the origins of the structural theories of the arch and vault are. Also, what today is commonly accepted. Only through this study of history and theories formulated in the past, it is possible to develop a critical capacity that avoids repetitions of mistakes.

The earliest scientific research published on an arch is written by R. Hooke (1670). He understood the link between the geometry of the catenary and the resistance capacity of the arch, figure 3.1.1 [78]. Twenty-seven years later, D. Gregory (1697) reached the same conclusion, adding for the first time what is now within Heyman's theory as the sufficient condition to guarantee equilibrium [75].

Simultaneously in France, by pursuing the medieval tradition, P. de La Hire (1695) initially [79] [80] and then B. F. de Belidor (1739) [81] [x] analysed the kinematics of the arch as a system of macroblocks. Today, a similar approach is adopted through D.E.M. [82].

Around the same time in France itself, although with some inaccuracies and without much mathematical rigour, A. Couplet (1730) in his second memoir [83] anticipated by almost two

centuries the hypotheses fundamental for the validity of the limit analysis [2]. From the observation of the real structures, Couplet understood that commonly the collapse of arches occurs due to the formation of kinematic mechanisms.

He illustrated the dual nature of structural analysis: the static approach aimed at determining equilibrium and the kinematic approach whose purpose is to analyse the possible mechanisms. Although indirectly, the Couplet's work, as well as that of de La Hire and Belidor, was enclosed and reformulated by C. A. de Coulomb (1773) [75], he was the first to introduce the concept of the upper and the lower limit of thrust and described the nature of crushing phenomena [78].

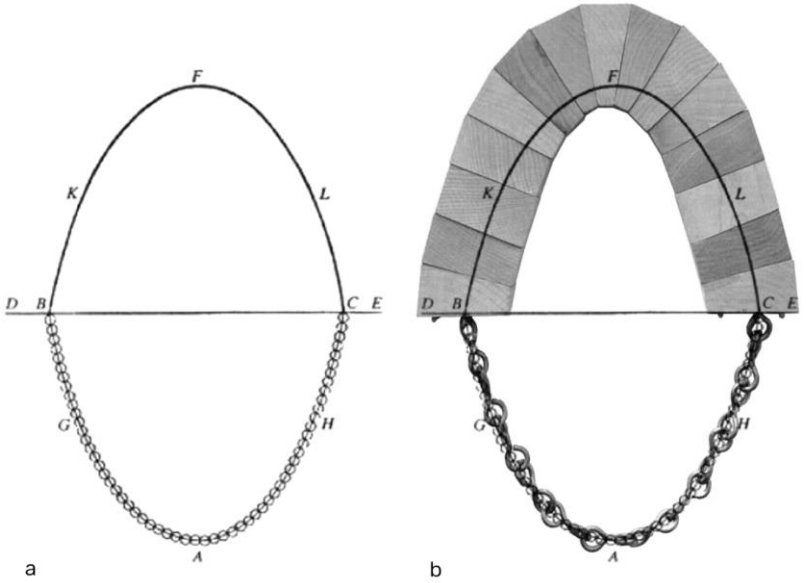

Figure 3.1.1 a) Poleni's drawing of Hooke's analogy. b) Overpostistion of: *The Catenary and The Arch* by R. Pedreschi and Poleni's drawing of Hooke's analogy.

The studies are based on the two approaches: static and kinematic pursued in search of a connection. This element was recognised in

the curve of pressure, whose first exhaustive formulation was by T. Young (1817) [76] [84].

The curve of pressure is a specific funicular polygon related to an arch, through which the real state of the structure can be described. The curve of pressure is the locus of the application points of the resultant internal forces. These resultants do not necessarily act orthogonal by to the masonry joints in the arch, but at the limit, in the hypothesis of finite friction, they must be contained within the friction cone. Furthermore, to reflect the real mechanical behaviour of masonry, i.e. zero tensile strength, the curve of pressure must be entirely contained within the arch thickness [85].

The question of determining the curve of pressure was the primary subject for research in the first half of the 19th century [86] [87].

In the same century, C. Navier (1826), JV Poncelet (1852), H. Bresser (1852), W. J. M. Rankine (1860), E. Winkler (1879) and A. Castigliano (1879) [76] investigated on the possible applications of the theory of elasticity for the analysis of arches and vaults. Winkler wrote the first complete formulation. The elastic theory permits to describe the correct curve of pressures of the ideal arch, once the data are known exactly hence for analysing the real structure, several coefficients should be considered. These coefficients called perturbations, justify the differences between the determined elastic curve and the behaviour of the real arch [88].

Due to the considerable computational complexity and the development of static graphical tools, the application of the elastic arc theory was limited only to the analysis of exceptional structures [2].

In the second half of the 19th century, the static graphical tools allowed the analysis of arches and vaults. In particular, as shown in

figure 3.1.2, H. T. Eddy (1877) determined a method for the analysis of shells of revolution [89].

The first studies for evaluating masonry shells date back to the 18th century by P. Bouguer (1734) [90]. A. F. Frezier (1737) who introduced the Slicing technique [91] an essential element for the method developed by H. T. Eddy. Towards the end of the 19th century using static graphics tools, G. Ungewitter (1892) published a manual for the static study of vaults [92].

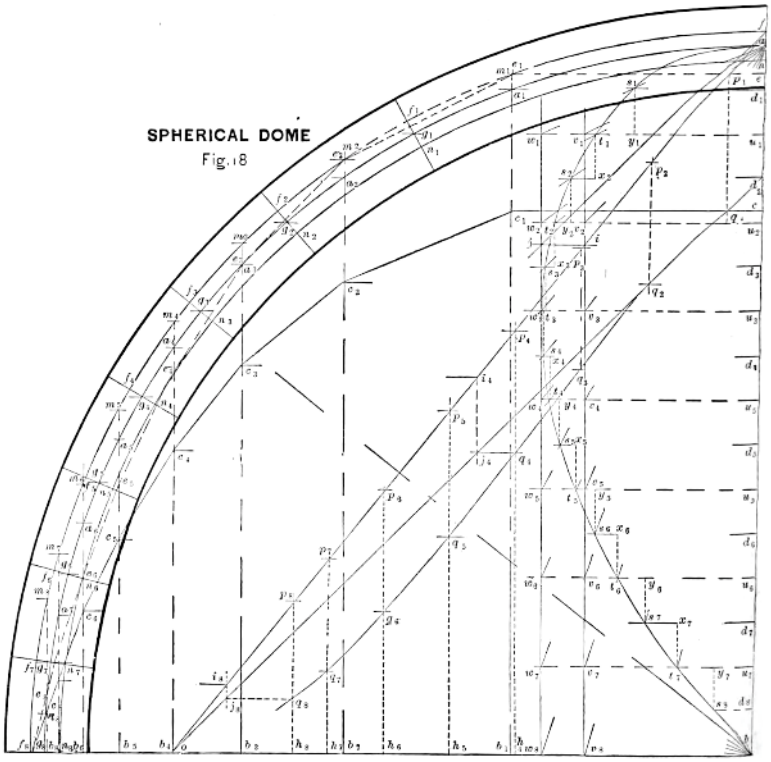

Figure 3.1.2 Eddy's method, analysis of hemispherical domes. Drawing of H.T. Eddy [89].

Despite the critical points highlighted, the theory of the elastic arch was considered the most correct until the second half of the 20th century when D.C. Drucker (1952) [93], A. Kooharian (1953) [94] and W. Prager (1959) [95], formulated the theory of plasticity and Limit Analysis for perfectly plastic solids. Following their studies, J. Heyman (1966) presented his Structural theory for masonry [2]. He revisited the traditional methods of analysis of masonry constructions (Hooke, Gregory, Couplet, Coulomb) in the framework of the plastic theory, and thus through the Heyman's formulation, it is possible to apply the principle of limit analysis to masonry structures [2].

Today, although with variations, the approach of the elastic theory is still predominant. This is mainly due to the development and the diffusion of F.E.M. commercial software based on the elastic approach. Commercials tools which permit to evaluate masonry structure within the framework of limit analysis approach are not yet been developed [30] [96] [97].

Finally, during the last decade of the 20th century, some researchers adopted distinct element methods to analyse masonry structures [98] [99] [100]. Distinct element method (D.E.M.), also called the discrete method, permits to evaluate masonry structures as a system of distinct blocks [101].

For this research, among all approaches developed in history, D.E.M. and Heyman's formulation have been adopted to evaluate the equilibrium during the construction. Chapter 6.4.2 presents the considerations and the assumptions needed to adapt them to evaluating the building phases.

3.2 Essential of the *Structural theory for masonry* [2]

The structural theory for masonry formulated by Heyman (1966) provides, under specific conditions [2], a method for evaluating masonry structures within the framework of the plastic theory and use limit analysis [102]. His formulation is based on three fundamental hypotheses:

I. Sliding failure cannot occur;
II. Masonry has no tensile strength;
III. Masonry has infinite compressive strength [2];

It is not a coincidence that the hypotheses mentioned were already derived by Couplet in the 18th century; they reflect the behaviour of the real masonry structures. Commonly, the collapse of the arch structure is strictly related to the formation of a sufficient number of hinges, for a kinematic mechanism to form. This is because of the absence of sliding failures and low compressive stresses that are present in ordinary masonry structures [103] [104] [100].

For ordinary conditions and common structures, the Heyman's hypotheses **I.**, **II.** and **III.** are usually respected, thus the lower bound theorem (or static theorem) provides the condition to guarantee the equilibrium of masonry structure. To evaluate the arch stability, the lower bound theorem can be expressed as follows:

> Under a given set of loads, if at least one line of thrust can be found entirely within the arch geometry. Then no kinematic mechanism can exist, and this is an absolute proof that under this set of loads, the structure is stable, and indeed that collapse can never occur.

This form of the lower bound theorem is called master 'safe' theorem. It provides sufficient condition to guarantee the equilibrium of an arch [2].

To trace the line of thrust, several methods can be adopted, most of them based only on the principle of equilibrium. Therefore, being the arch a hyperstatic structure, it is easy to understand that infinite lines of thrust can be traced [2]. Theoretically given a set of loads, a range of balanced solutions can be determined, figure 3.2.1 reports an example. The range is characterized by two factors: its bounds and the number of solutions contained. The bounds correspond to the minimal line of thrust and the maximal line of thrust.

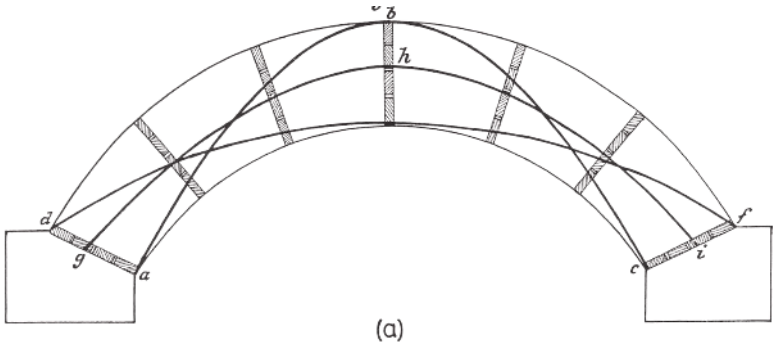

Figure 3.2.1 Different lines of thrust for an arch: curve d-f represents the maximum line of thrust, curve a-c the minimum line of thrust. Drawing of W. H. Barlow [105].

The number of solutions contained, instead, depends on several factors, as the arch geometry or the presence of cracks.

For particular cases, e. g. the existence of more than four hinges, the master 'safe' theorem is violated, the range is empty; hence the arch is not stable. To date, in the literature, several scientific documents can be found that introduce variations to conditions **I.**, **II.** or **III.**, these variations are due to justify local phenomena or particular circumstances [106] [107] [108].

As detailed in chapter 6.3, in the research here presented, limit analysis is used to evaluate the equilibrium under construction of domes. The master 'safe' theorem was used to provide the resources to assess the dome equilibrium under construction.

3.3 Discrete element method

The Distinct Element Method (D.E.M.) was conceived for geomechanical analysis, such as for caves or mines [98] [99]. However, some researchers have also demonstrated its validity for masonry structures [109] [110] [111].

D.E.M. is a computational method to study the time temporary evolution of structures. Through D.E.M., the masonry is assimilated to a system of discrete bodies consisting of two elements: blocks (the solid elements) and discontinuities (the interfaces) [98] [99]. The blocks can be rigid or deformable; in the second case, D.E.M. and F.E.M. methods are integrated, allowing to estimate stresses and deformations [112]. The discontinuities between the blocks could be described by elements or, in the simplified models by the interface between two blocks. The purpose of D.E.M. is to describe the time evolution of the system, to perform this the collisions between the bodies can be detected, and they influence the evolution of the system itself. D.E.M. uses an explicit time-marching scheme to solve the equations of motion directly [101], thus the determination of the different temporal states is calculated by the explicit numerical integration of the equations of the motion of rigid bodies in time [101].

The analyses are ruled by several parameters, some related to the blocks, such as the characteristics of the material, and other relevant to the discontinuities for simulating the joints [101]. However, the most decisive factors that influence the analysis are:

- The geometry of the blocks, whose choice must be weighted concerning different factors, including the type of analysis performed [113].
- The coefficients of the discontinuities, they depend on the scale of the model analysed, its geometry, and the failure criteria adopted to describe the joints [114].

Even if several documents propose several approaches on how the parameters should be chosen [115], their determination is subjective, at least partially. Thus, before defining any model, it is required to identify what the goal of the analysis is, only then the hypothesis can be formulated carefully. Wrong assumptions (e.g. the choice of discretisation) could lead to incorrect solutions, even though the equations are correctly solved.

The spreading of the technique in different fields has led to the development of different D.E.M. methods characterised by notable differences [116] [117].

Within the research conducted, here as described in chapter 6.4, the method D.E.M. was used to investigate the effect of cross-herringbone spiralling pattern on domes under construction.

Part II

4. Cross-herringbone vault

Essays, articles and other literature on the application of herringbone spiralling technology for Brunelleschi's dome: Santa Maria del Fiore in Florence are numerous, albeit how the Brunelleschi gained knowledge on this technology is still not well understood (see chapter 2.4.1). Undoubtedly, the use of this technology in the dome of Santa Maria del Fiore has influenced the diffusion and the affirmation of the herringbone spiralling technique in the buildings of the Florentine tradition. Even if Leon Battista Alberti explicitly writes about this technique in his treatise *De aedificatoria* [118], the most significant contribution to the knowledge and conservation of the herringbone spiralling technology is provided by the Florentine family of architects and master masons: the Sangallo.

Despite the diffusion of this technique, today, there are only two historical, scientific documents that describe the herringbone technique which are preserved in the Uffizi Museum. The first is the drawing 900A (n. 639051) GDSU (Gabinetto dei Disegni e Stampe Uffizi) and the second drawing 1330 (n. 594469) GDSU, illustrated in figure 4.1.1 and figure 4.2.10 respectively. Therefore, by reading these precious documents that describe the method of construction, and by studying the Sangallo's domes which are still standing, such as the dome of Santa Maria in Ciel d'Oro in Montefiascone (Viterbo) or the dome of Simon Mago of San Pietro cathedral in Rome, an attempt to interpret and to trace the various motivations behind this technology is made. The domes mentioned prove how the Sangallo, especially Antonio the Younger, has contributed to the growth of the herringbone spiralling technology. Hence they do not only systematically applied the herringbone spiralling technique, but they have also perfected.

The research of the Sangallo family led them to develop a building system the cross-herringbone spiralling technology. Even if such a technique is based on the same principles of Brunelleschi's one, the

differences are significant. Figure 4.1 b) illustrates the main variation is the presence of two orders of loxodromic curves, one right-handed oriented and another left-handed oriented.

a

b

Figure 4.1 a) Herringbone spiralling pattern, Santa Maria of Fiore dome in Florence. b) Cross-herringbone spiralling pattern, the dome of Simon Mago of San Pietro in Rome.

The cross-herringbone spiralling technique is the last self-balancing technique presented in this document and is perhaps the most modern one. The application of cross-herringbone spiralling technology requires a detailed preliminary study that influences the project from the first conceptual phases.

The following chapters illustrate the cross-herringbone spiralling technology through its history in chapter 4.1, its geometric characteristics illustrated in chapter 4.2, and the principles of technology and structural behaviour in chapter 4.3.

4.1 Traces of the cross-herringbone spiralling technology

The origins of the cross-herringbone spiralling technique are to be found in the works of architects and master masons of the 15th century. They had perhaps acquired the knowledge behind this technique at the building site of the Florentine Cathedral and were able to master as well as develop it until they had defined the cross-herringbone spiralling technique. Among the Florentine master masons, who jealously guarded the techniques behind this technology, were the Sangallo masters, descendants of Francesco Giamberti (1405-1480 [58]), who was the master mason contemporary of Brunelleschi. Surely Francesco and Brunelleschi must have known each other, and perhaps Francesco also might have worked under the leadership of Brunelleschi [119]. His sons: Antonio da Sangallo the Older (1455-1534 [58]) and Giuliano da Sangallo (1452-1512 [58]) were brilliant architects, worked alongside Pope Alessandro VI Borgia and Lorenzo il Magnifico respectively, but it was Antonio da Sangallo the Younger (1484-1546 [58]), who was also Francesco's nephew, who gave us the most significant amount of evidence and documents on the application of the cross-herringbone spiralling technique.

4.1.1 Development of herringbone and cross-herringbone spiralling technologies during the Renaissance

It is common knowledge that Brunelleschi's proposal for the dome of Santa Maria del Fiore (1418): to build the octagonal dome without formwork, were questioned by the jury of the Opera del Duomo. As evidence of their perplexity, in the early stages, Lorenzo Ghiberti was chosen as co-director and supervisor for Brunelleschi's work. Ghiberti, who was linked to the traditional approach, had never fully understood the Brunelleschi's approach or even the significance of the herringbone spiralling pattern. To testify this, several examples are recorded [120] [119], one for them is where Ghiberti accused Brunelleschi of not respecting the promise made a century before by the master masons to construct a gothic dome, but to build a dome of revolution [121]. The fact that this construction method was not a simple hypothesis is extensively documented in the Florentine Opera's records, through a certain record showing the purchase of a specific kind of bricks, called *Mezzane*. The *Mezzane* bricks were used to build a scale model of the dome, to prove the effectiveness of Brunelleschi's proposal. The records report that on the 26th of October 1418 had been paid 121 *lire*, 9 *soldi* and 4 *denari* to buy 13,725 bricks, the *Mezzane* from a furnace owner in Ghibellina street, in order to build a wall: *Pro modello Filippi ser Brunellesco* for the Brunelleschi's model [119]. Just from these two elements, the report of the bill of Mezzane bricks and the incapacity of the Ghiberti to understand the constructive method, prove how innovative the approach of Brunelleschi was, and that, at least, Brunelleschi already knew the herringbone spiralling technology .

Furthermore, this building method was usually practised for many years, even after Brunelleschi's death. It is known that many domes were built adopting to herringbone spiralling technology [62], Appendix A. Indeed, during the 16th century, the political and economic conditions and the spread of new weapons, such as the cannons [122], gave impetus to build several fortresses for defence.

Consequently, as testified by the domes still in existence and the historical reports, Sangallo architects used the herringbone to complete domes of these defensive structures [123].

Evidence and testimonies of use of herringbone and cross-herringbone is readable in many vaults built in the 15th and 16th centuries, such as in the vaults of the Vecchia Fortezza in Livorno (1519) [124], where Antonio da Sangallo the Younger built a hemispherical vault, as well as in the Sala d'Armi of the Fortezza da Basso in Florence (1534) [122]. Even in the dome of Santa Maria delle Carceri in Prato (1484) and in Basilica della Santa Casa in Loreto in Ancona (1468) Giuliano da Sangallo have applied the technology [125]. Figure 4.1.1 shows the location of the existing architectures, where probably the herringbone or cross-herringbone spiralling technologies could be applied by Sangallo. As shown in the figure, the buildings are mainly situated in the Tuscany region, exactly the same context where the Sangallo architects practiced. Inevitably the use of this technology led to perfecting it, and presumably, Sangallo introduced the use of the cross-herringbone spiralling technique in some of these fortresses, but this is however just a hypothesis. The presence of plastered surface in many of these domes does not allow observation of the masonry pattern [126].

As it is easy to understand by the restricted area of application of these building systems their use was kept confidential: a closely guarded secret, and, it is not by chance that after Sangallo, the herringbone and cross-herringbone spiralling techniques were lost. Today, the cross-herringbone spiralling pattern is visible in a few of the constructions all realised by Antonio the Younger, such the domes of octagonal rooms also called octagons, of San Pietro cathedral in Rome, or the dome of Santa Maria in Ciel d'Oro in Montefiascone which are the only octagonal domes known built with the cross-herringbone [127]. These non-plastered domes make the masonry model readable and allow to formulate hypotheses on how they were built.

These domes are certainly not comparable to the one in Santa Maria del Fiore in Florence, at least for size and for temporal context. Suffice to say that the building site of Santa Maria del Fiore ended about one hundred years before the one of Simon Mago of San Pietro in Rome.

Figure 4.1.1 Distribution of domes built probably using herringbone or cross-herringbone spiralling technologies, the complete list is reported in Appendix A.

4.1.2 Historical documents of herringbone and cross herringbone spiralling technologies.

Adding to the totality of the historical understanding of Herringbone spiralling technology, in addition to the previously mentioned testimonies, the two drawings: 900A (n. 639051) and 1330 (n. 594469) GDSU, drawings already introduced and shown in

figure 4.2.10 and figure 4.1.2 need to be given weightage. The former drawing is attributed to Antonio da Sangallo [128] the Younger and the latter to Guido Guidetti [59], who was a minor architect probably close to Antonio da Sangallo the Younger. The two drawings constitute further evidence of the existence of the Sangallesca school, where the herringbone spiralling technology was handed down and developed. However, beyond any possible verification, it is for sure that the first known record of the herringbone spiralling technology was in the building site of the Dome of Santa Maria del Fiore, as well as by the Sangallo family who knew the technique and used it until the first half of the 16th century. Besides, as witnessed at the dome of Santa Maria in Ciel d'Oro and at the domes of the octagons, it is indisputable that Antonio da Sangallo the Younger knew and used the cross-herringbone spiralling technique during his Roman permanence under Pope Paolo III.

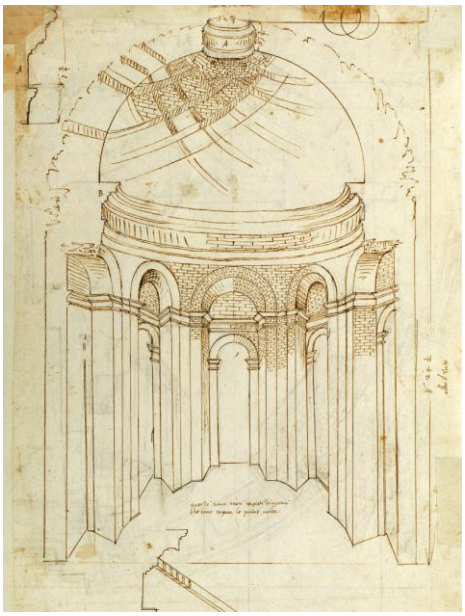

Figure 4.1.2 Drawing 1330 (n. 594469) GDSU. View of Simon Mago chapel, the cross-herringbone spiralling pattern is visible.

4.2 Cross-herringbone spiralling pattern

The study of existing structures is the primary source for understanding the behaviour of the structures themselves. In the following chapters 4.2.1, 4.2.2, 4.2.3 and 4.2.4, the geometric characteristics of the cross-herringbone spiralling technology, which are derived through the direct study and the survey of the domes of Santa Maria in Ciel d'Oro and Simon Mago of San Pietro are illustrated.

4.2.1 Overall information of cross-herringbone dome

As mentioned in chapter 4.1, Antonio da Sangallo the Younger designed the two domes: Santa Maria in Ciel d'Oro and Simon Mago of San Pietro. These two structures have histories that are quite similar. Santa Maria in Ciel d'Oro was designed around the year 1526 and was completed in 1548 [129]. The construction has been stopped several times for various reasons, such as the bubonic plague or the invasion of Lanzichenecchi. The initial idea was to build a monastery for pilgrims, but later only the church was realised. Figure 4.2.1 a) reports the plan view and a vertical section of the church. Antonio da Sangallo the Younger visited the building site only three times and the work was supervised by his brother Giovanni Battista Fiorentino. Simon Mago, as shown in figure 4.2.1 b) c) d) is a minor chapel at the first level in San Pietro cathedral. The historical documents do not say when its construction had precisely started, but there is evidence of Antonio da Sangallo the Younger working at the Fabbrica of San Pietro from 1520 until 1546 [123]. His presence in this building site is testified by numerous documents collected in the Archive of the Fabbrica of San Pietro. Thus, it is reasonable to think that Simon Mago was built with more accuracy and skill than Santa Maria in Ciel d'Oro. The two domes have similar dimensions, but one is an octagonal dome and the other a hemispherical one. As shown in detail in figure 4.2.2, Simon Mago is a perfect hemispherical dome whose inner radius is 4.83

meters, and the maximum deviation between the minimum and maximum radius is about 1.8 centimetres, it has an oculus of diameter 1.82 meters and no other openings.

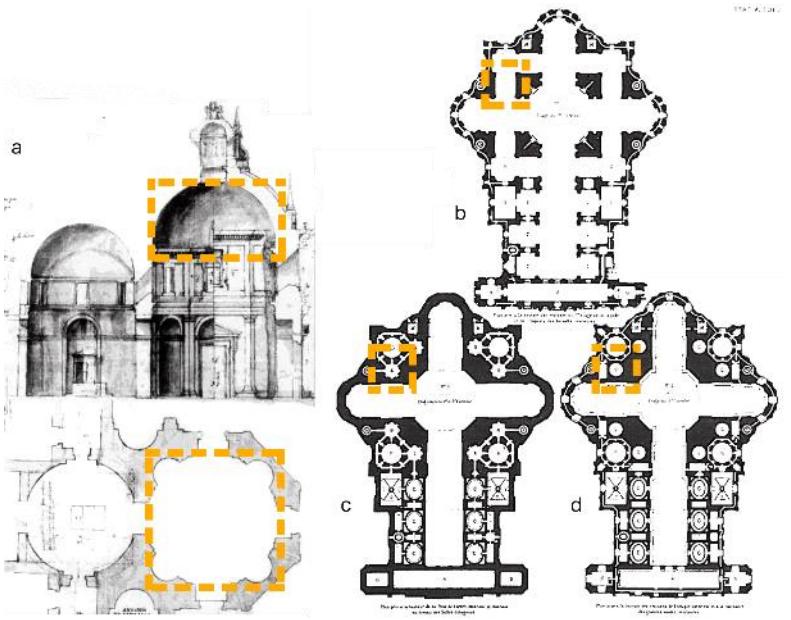

Figure 4.2.1 a) The drawing n. 173 Uffizi museum archive, plan view and vertical section of Santa Maria in Ciel d'Oro. Drawing of Antonio the Younger. b), c), d) Plans view of San Pietro Cathedral. b) Ground level. c) The first level above the secondary naves. d) View at the base of the dome of octagonal rooms. In all plans view, Simon Mago chapel is highlighted in yellow. Drawing of P.-M. Letarouilly [59].

Santa Maria in Ciel d'Oro, represented in figure 4.2.3, is an octagonal dome. The sails are described geometrically by portions of ellipsoidal cylinders. The ribs of the sails are circular arches whose radius is about 5.47 meters. The length of the four internal diagonals varies between 10.95 meters and 10.98 meters and the height is 5.31 meter.

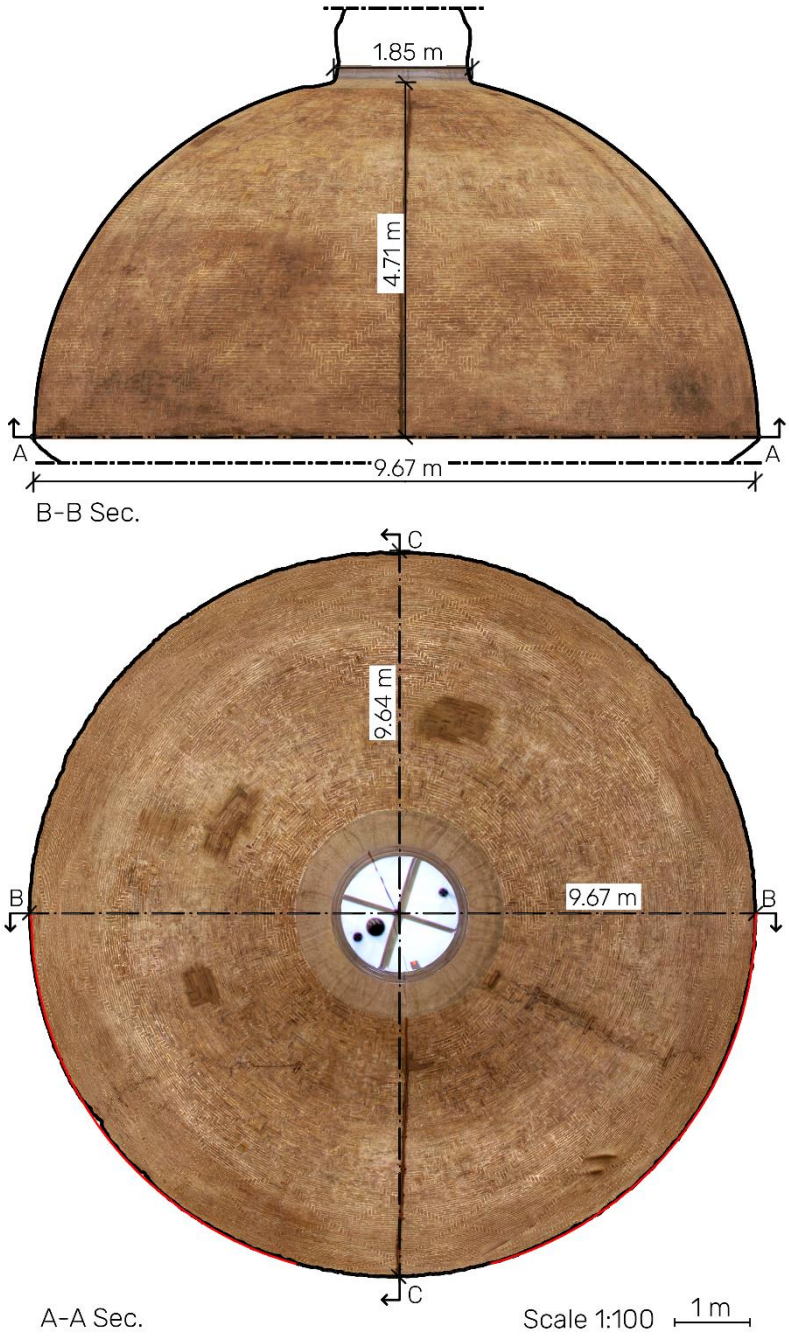

Figure 4.2.2 A-A Sec. Plans view, from bottom to top, of Simon Mago dome. B-B Sec. Vertical section.

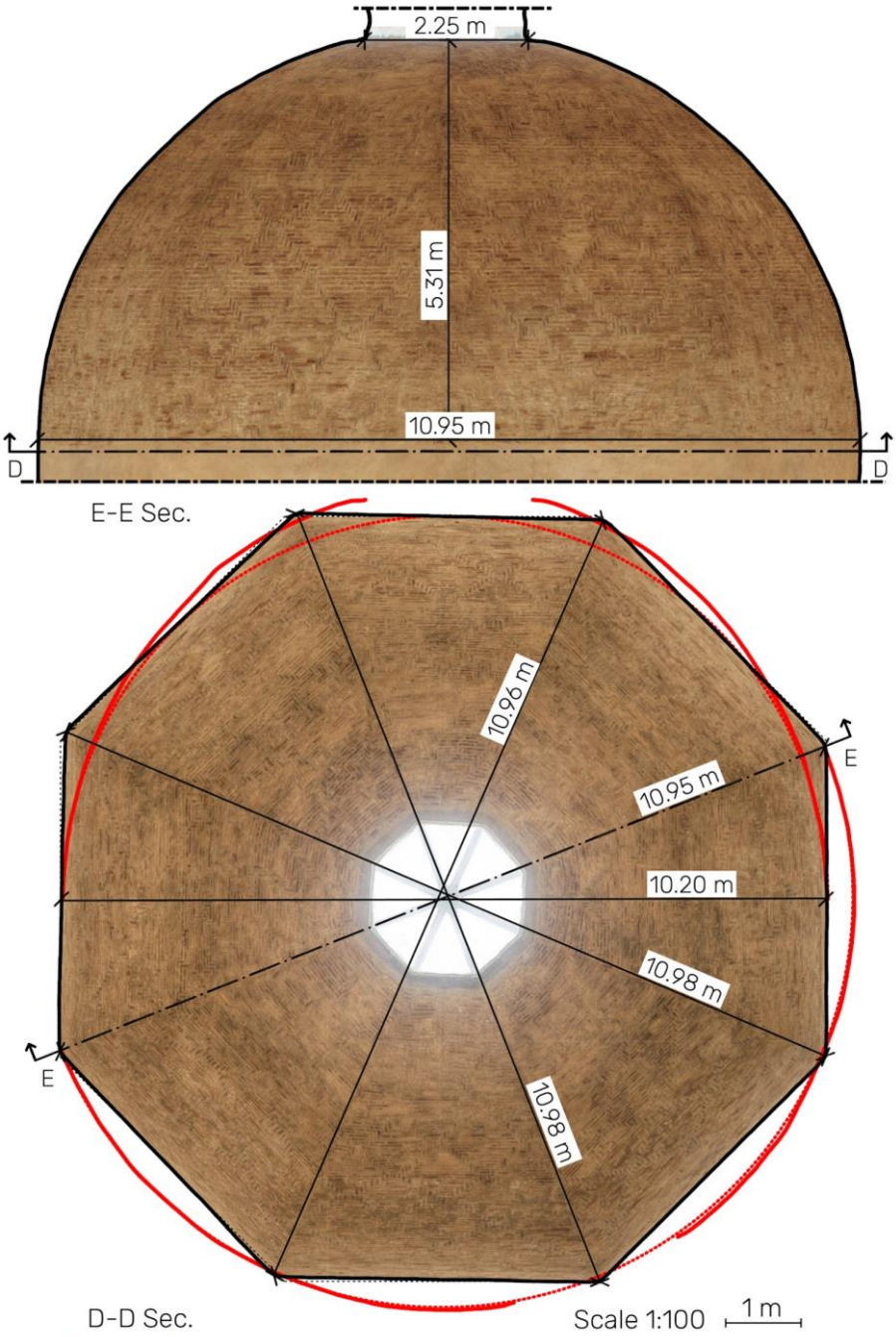

Figure 4.2.3 D-D Sec. Plans view, from bottom to top, of Santa Maria in Ciel d'Oro dome. E-E Sec. Vertical section.

4.2.2 Geometry of cross-herringbone spiralling pattern

The cross-herringbone spiralling pattern is a double herringbone path system, with one left-handed and one right-handed spiralling. Thus, referring to figure 4.2.4, at each of the intersection of two systems of the loxodromic curves, nodes are formed. The nodes are materialised by 1, 2 or 3 bricks placed one adjacent to another. The brickwork appears as a complex system of rhombi; each one is delimited by loxodromic trajectories. From the bottom to the crown of the dome, the size of the rhombi decreases. The geometry of loxodromic curves that trace rhombi is related to several factors: the thickness of mortar, the size of bricks and the dome geometry itself [130].

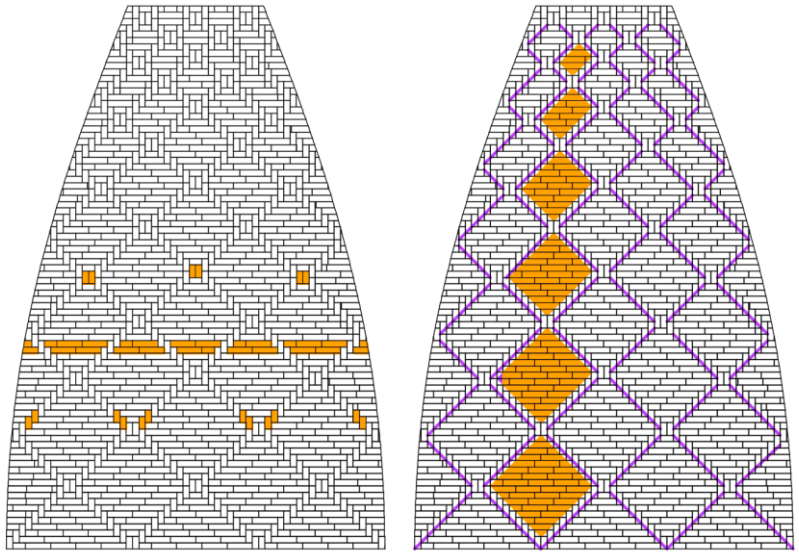

Figure 4.2.4 Cross-herringbone spiralling pattern: masonry pattern for a sail of an octagonal dome. a) Elements highlighted: nodes (top), horizontal courses (middle), herringbone bricks (bottom). b) Elements highlighted: left and right-handed loxodromic curves (thick lines) and rhombi (areas filled).

As shown in figure 4.2.5 and 4.26, the masonry pattern of Simon Mago domes exhibits that, the geometries of all loxodromic curves (one highlighted with continuous purple line) are the same. Thus, the rhumb lines have the same inclination with respect to the course of horizontal bricks, and all nodes are aligned radially (highlighted with dot orange lines). Santa Maria in Ciel d'Oro, on the other hand, presents several discontinuities. The reason for these discontinuities can be found in its history, as reported in chapter 4.2.1. The construction was interrupted and masons changed during the construction phase, with evidence to support the hypothesis that the builders did not know the cross-herringbone spiralling technique well. Also, Antonio da Sangallo the Younger did not follow the building site assiduously. Indeed, as shown in figures 4.2.7, the masonry pattern close to the dome's base is more regular than that at the crown, where the cross-herringbone spiralling pattern is not clearly visible. Furthermore, it is known that at least one intervention on the masonry dome was carried out during the last century. Despite the discontinuities in the masonry pattern of the Santa Maria in Ciel d'Oro dome, 6 loxodromic curves for each sail, 3 left-handed and 3 right-handed, can be visually identified. Figure 4.2.8 displayed the ideal sail of Santa Maria in Ciel d'Oro. Here within the sails, the position of the nodes describes a scheme 4 3 4 3 of rhombi, while near the ribs irregular nodes and spatial rhombi arise. The same pattern is visible in figure 4.2.7, (here, near the ribs of sails), the rhombi defined through paths lie in the two different sails. At the base of the dome, the distance between two loxodromic curves corresponds approximately to 1.15 m, which is around 2 Fiorentine arms (1 Florentine arm corresponds to 0.584 meters [127]). As far as with the Simon Mago dome reported in figures 4.2.5 and 4.2.6, is concerned 16 right-handed and 16 left-hand loxodromic paths are readable, hence 32 spirals in total. In this dome, all rhombi are regular, and the masonry pattern is visible throughout the structure. At the level of the spring of the dome, the spirals are spaced 3 Florentine arms, about 1.80 meters.

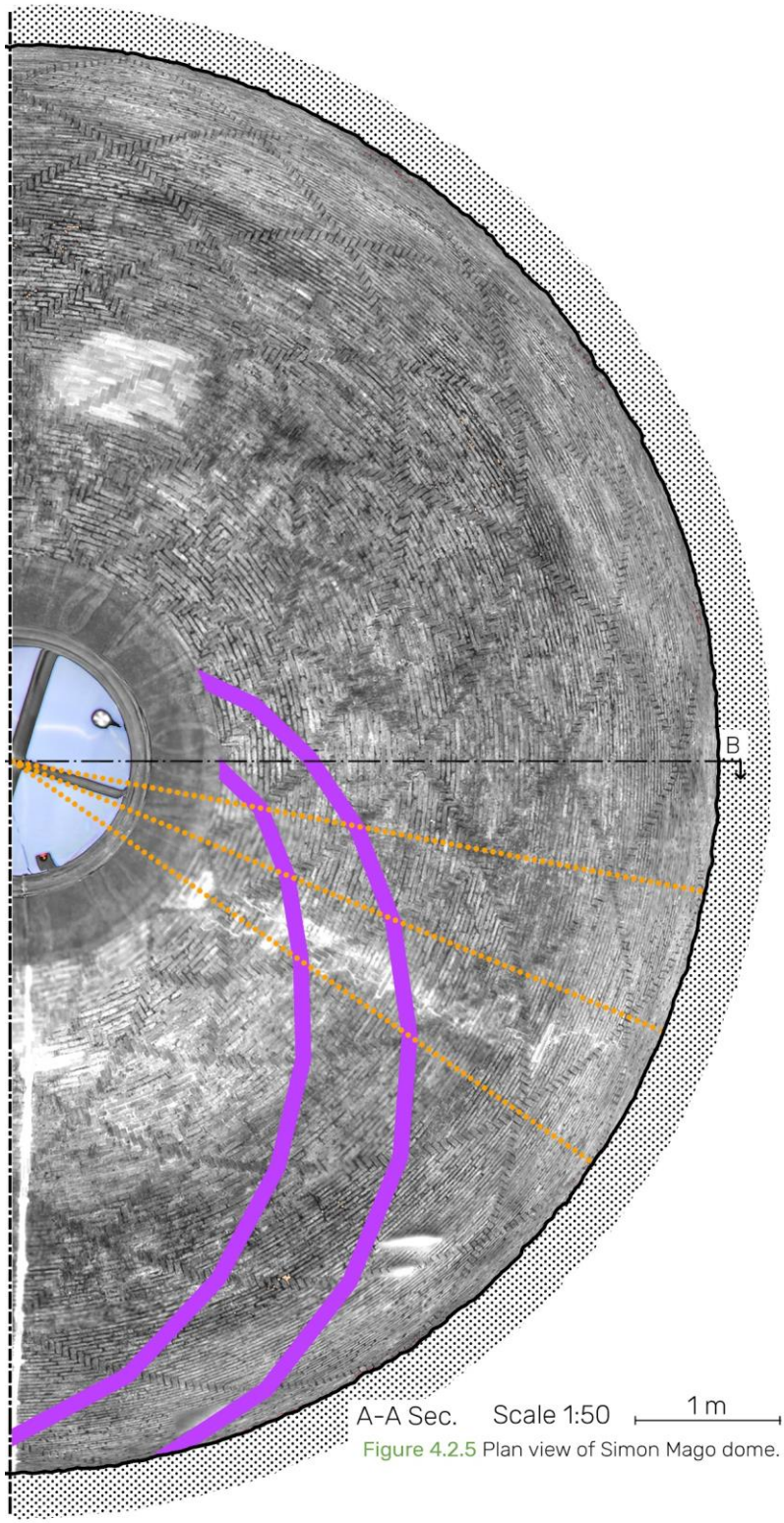

Figure 4.2.5 Plan view of Simon Mago dome.

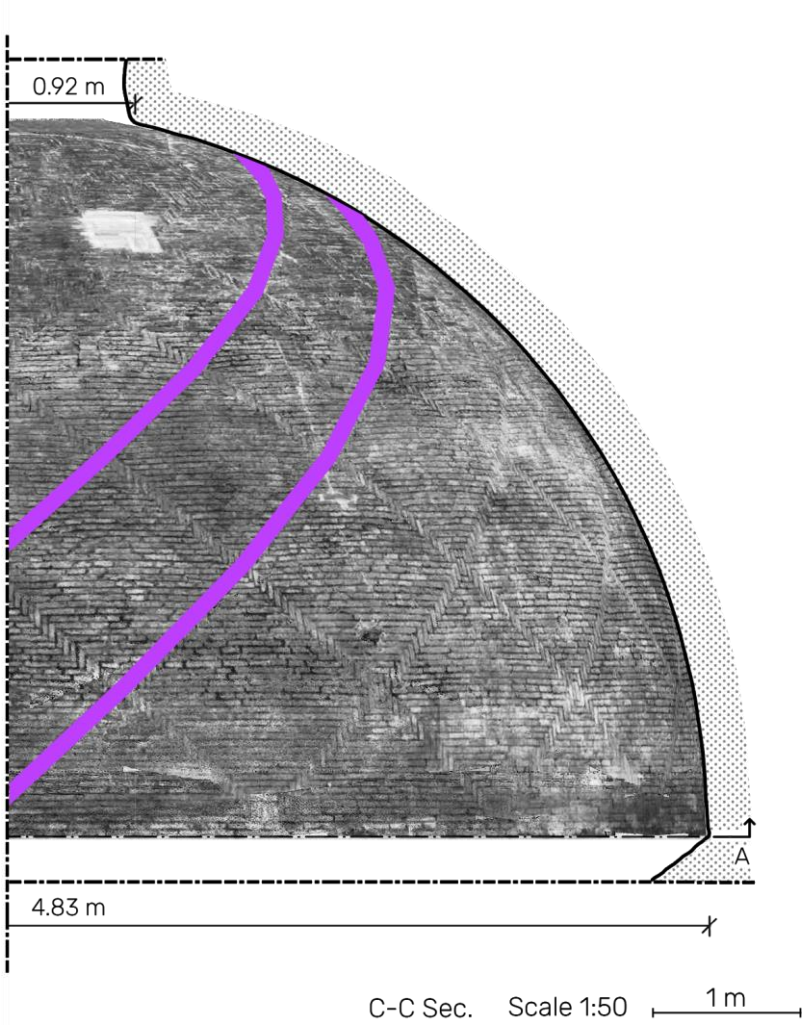

Figure 4.2.6 Vertical section of the dome of Simon Mago.

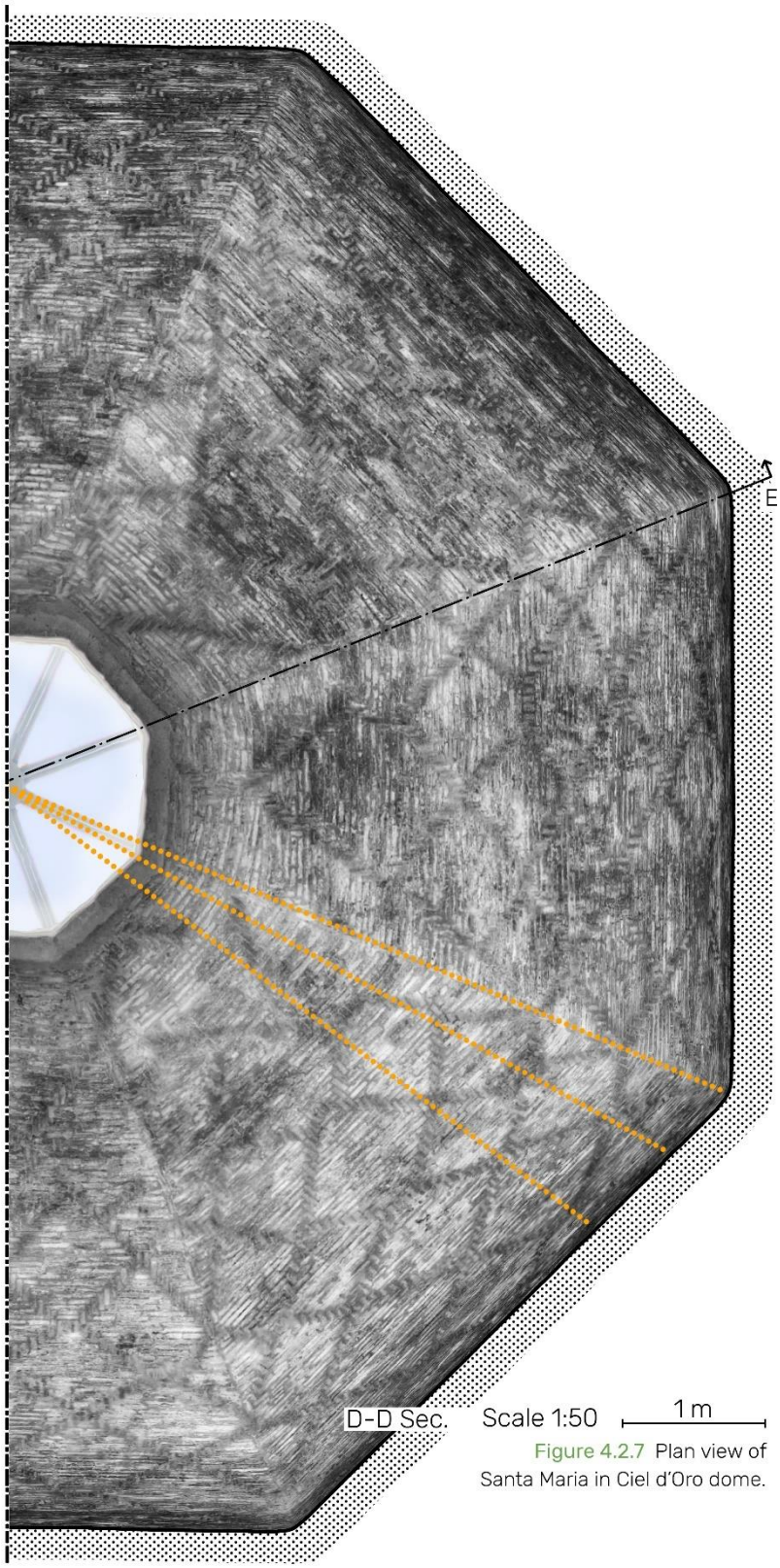

Figure 4.2.7 Plan view of Santa Maria in Ciel d'Oro dome.

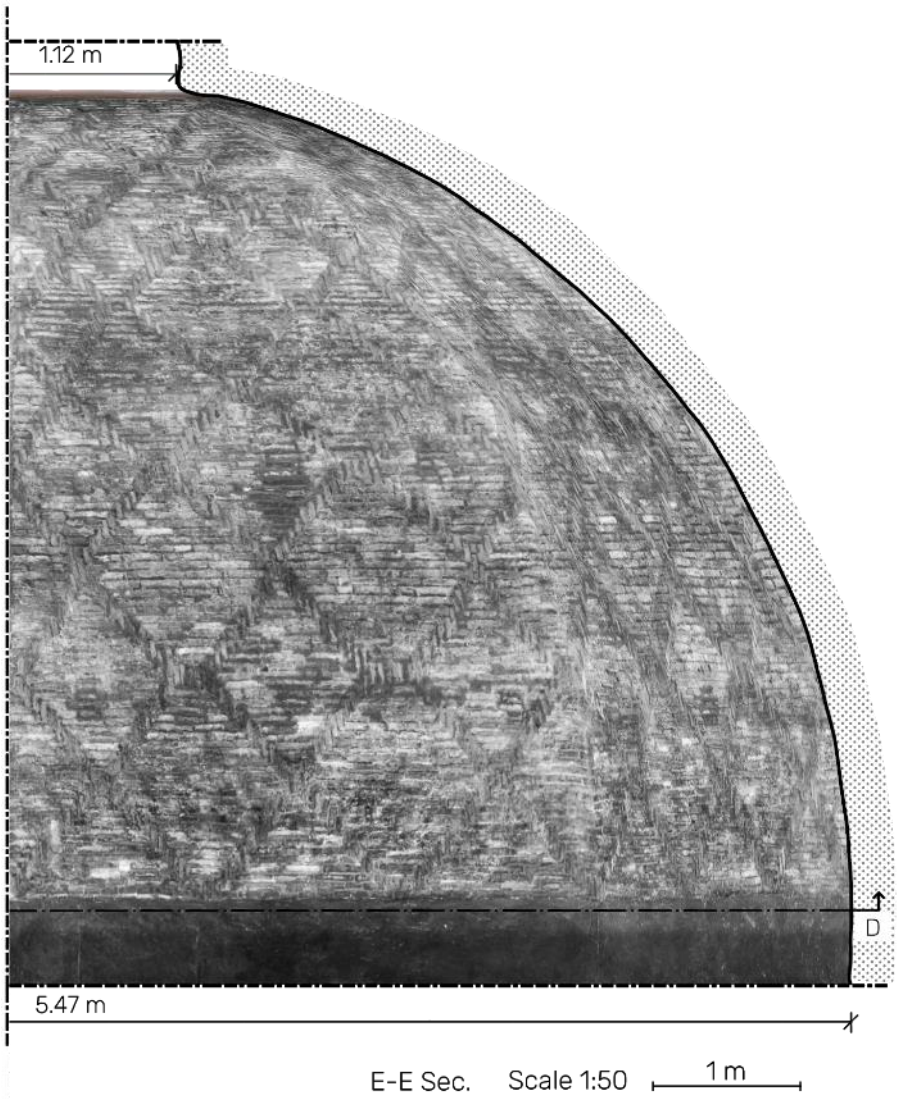

Figure 4.2.8 Vertical section of the dome of Santa Maria in Ciel d'Oro.

4.2.3 Brick dimensions

Two different types of bricks were adopted in the two domes discussed previously, as shown in figure 4.2.7 a), b) that exposes details of the masonry: the Simon Mago and Santa Maria in Ciel d'Oro. The sizes of Simon Mago's bricks are 4-13-27 centimetres (height-width-length), while the bricks used at Santa Maria in Ciel d'Oro have dimensions of 7-14-28 centimetres.

The bricks are quite similar, they have almost the same length, but it is more relevant to express the relationship between the three dimensions referring to height as a unitary quantity. Therefore, Simon Mago bricks can be described through the relation 1-3-6, Santa Maria in Ciel d'Oro as 1-2-4. Although the two types of bricks have different ratios, it is possible to identify a common root: 1-α·1-2·α.

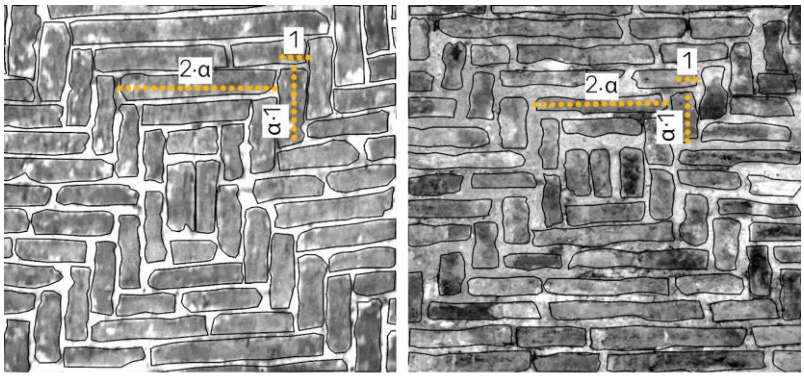

a b

Figure 4.2.9 Details of cross-herringbone spiralling pattern in correspondence of nodes. a) Detail of Simon Mago, ratio 1-3-6. b) Detail of Santa Maria in Ciel d'Oro, ratio 1-2-4.

4.2.4 The drawing 900A

The drawing 900A (n. 639051) GDSU, shown in figure 4.2.10 and previously mentioned in chapter 4.1, testifies the knowledge of Antonio the Younger of the herringbone spiralling technique. Despite its historical value, this document certainly has greater importance from a technological point of view.

The document displays one plan view, one vertical section and one caption that says: *'volte tonde di mezzane quali si voltano sanza armadura a Firenze'* that translates to hemispherical domes made of *mezzane* built without formwork in Florence. The drawing describes the herringbone spiralling technique, which displays several projections of loxodromic curves on the plan view of a hemispherical dome. Although the plan provides some information about the loxodrome trajectory, for the purpose of this research, the vertical section displayed on the right is of importance.

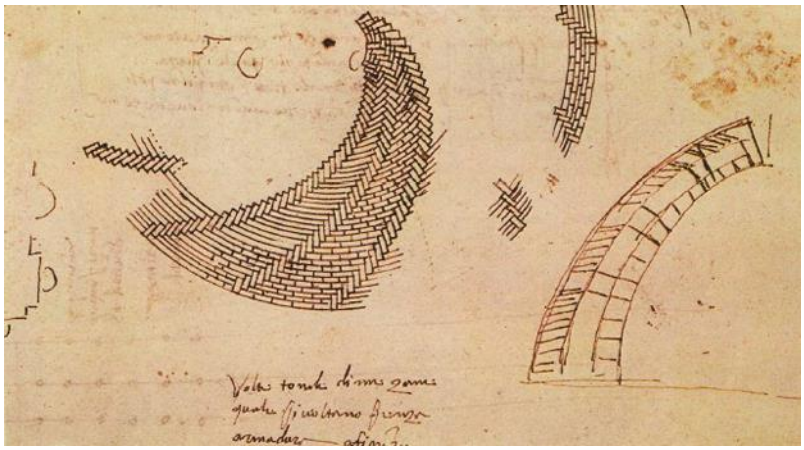

Figure 4.2.10 Drawing 900A (n. 639051) GDSU. Drawing by Antonio da Sangallo the Younger.

Few researchers suggest that this vertical section is associated to the Brunelleschi's dome [53] [128] [131], and according to them it

describes a double dome of the Santa Maria del Fiore. However, it is sufficient to observe the drawing further to realize that it cannot be a double-shells dome, the rectangular elements drawn can only be bricks.

Considering the accuracy of the drawing in the plan view, the vertical section appears to be just an explanatory scheme, the same hand that has designed such an accurate plan cannot have drawn so grossly vertical section if not just for explanatory purposes, the scale itself of the bricks is a clue. The vertical section reported in figure 4.2.11 a) is however associated with the same hemispherical dome seen in the plan view in figure 4.2.10. The figures drawn at the intrados can be assimilated to bricks laid according to a radial alignment. In the central portion of the vertical section others radial elements are illustrated, they seem to describe the same elements just mentioned, but with the double width (as highlighted in orange). Therefore revisiting the relationship $1\text{-}\alpha\cdot 1\text{-}2\cdot\alpha$, and the manner herringbone bricks are placed, in figure 4.2.11 b), it is possible to understand that these double-width elements are actually the herringbone bricks.

Therefore both the plan view and the vertical section describe the herringbone spiralling pattern for a hemispherical dome. The document explicitly provides some indications on the possible stratigraphy of the domes built with herringbone spiralling technique.

To date, this drawing is the only historical source which provides information on how the herringbone spiralling pattern links the layer in the direction of the thickness of the dome. Two other sources available give some information about the composition of the walls. The first is a historical dome near Brunelleschi's dome, which consists only of one brick layer, thus, from the point of view analysed, this structure is of no relevance [132]. The second source is a scale model of the Santa Maria del Fiore dome, called Antonella model, built at the end of the 20th century [133]. This model

presents similarities to the hypotheses made but fails to provide any historical information. It is reasonable to assume that the herringbone spiralling pattern can link the bricks layers through the thickness of the wall and this is also proved from the dimensions of bricks ($1\text{-}\alpha\cdot 1\text{-}2\cdot\alpha$) and their arrangement.

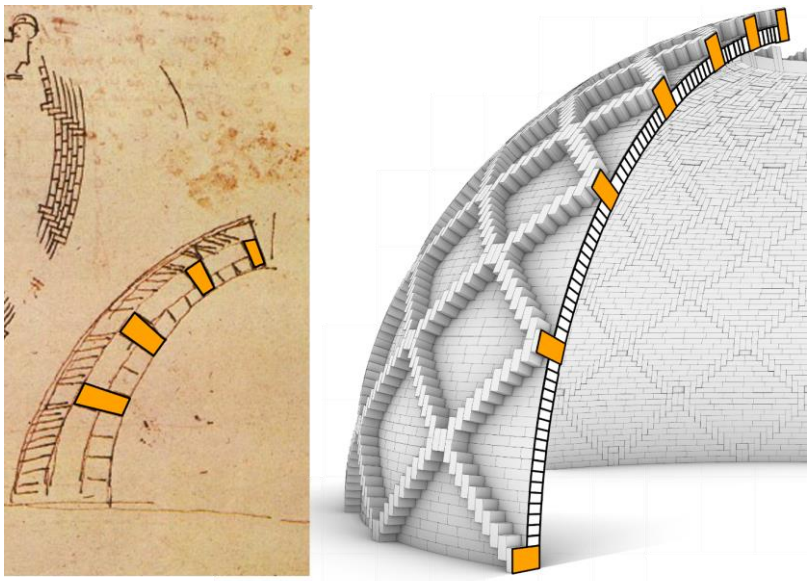

a b

Figure 4.2.11 Comparison of drawing 900A (n. 639051) GDSU. Drawing by Antonio da Sangallo the Younger.

Referring to figure 4.2.11 b), the model of the cross-herringbone spiralling pattern presents the same characteristics of the herringbone spiralling pattern, but the presence of the two systems of loxodromic curves increases the connection effect through the dome thickness. The cross-herringbone, differently from the herringbone pattern, permits to identify volumes completely delimited by herringbone bricks.

The analogy between these empty volumes and the empty spaces between the surfaces of the formwork is immediate. Perhaps the

stratigraphy of some domes built with cross-herringbone spiralling technique is similar to that of rubble masonry. Unfortunately, no one can affirm how to stratigraphy of the dome is, all the surveys carried out on such structures are not able to provide any information about this, but however the vertical section in figure 4.2.11 a) shows empty central areas which could be representative of empty volumes, as just described.

The last element displayed on the vertical section is an external layer of bricks, the extrados of the dome. The bricks are not arranged radially but lie within almost horizontal courses. The elements are only sketched, as to underline the scarce importance of the external layer with respect to the structure of the herringbone. Hence considering the purpose of the drawing 900A GDSU: explaining the herringbone spiralling technology, the bricks of the extrados play a marginal role, but do not constitute essential elements to reach the self-balance state during the phases of construction.

4.3 Principles of cross-herringbone vaulting technique

As already remarked above, the herringbone and the cross-herringbone spiralling techniques are based on the same principles. In this chapter, we refer to the cross-herringbone spiralling technology, but unless otherwise specified, the same concepts also apply for the herringbone one.

The ability to achieve the self-balance state of structures built using the cross-herringbone spiralling technique can be attributed to their construction process. Thus, even if it is not the specific scope of this chapter (in this respect see for example [71] [120] [127]), some elements of construction technique must be discussed.

To use the cross-herringbone spiralling technique an executive scheme is needed, whose goal is to identify the position and geometry of the nodes with respect to the whole structure, as well as to identify the number of herringbone bricks located between two nodes. Possible inaccuracies in the arrangement of these elements inevitably lead to mistakes that can compromise the self-balancing state of the structure itself. As shown in figure 4.3.1. a), Santa Maria in Ciel d'Oro dome exhibits several inaccuracies, probably due to the reasons mentioned in chapter 4.2.1. The realization of an accurate executive scheme is even more significant in double-curved structures such as the domes of revolution, indeed figure 4.3.1 b) shows the scheme for a hemispherical dome. Here, the non-alignments between herringbone bricks belonging to different rhumb lines (highlighted with an orange dotted line) are unquestionable.

Therefore the executive plan and the tracing operations are fundamental to guarantee the self-balancing state of these structures, while they have less importance when adopting the

herringbone spiralling technique. In this last case, the absence of nodes does not require such sophisticated executive drawing.

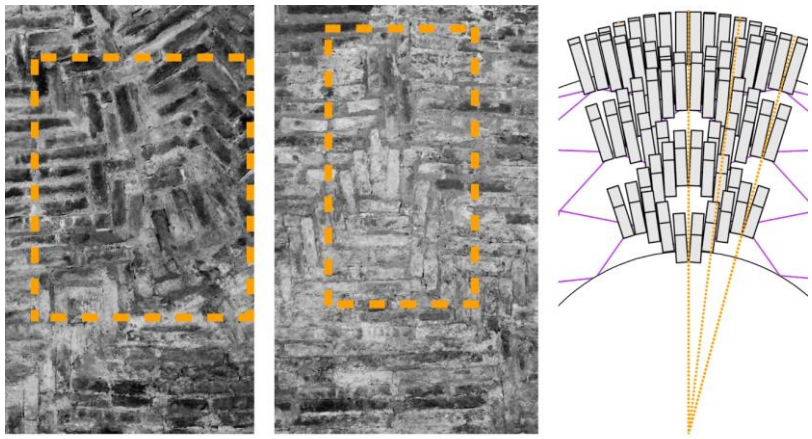

Figure 4.3.1 a) Details of nodes of Santa Maria in Ciel d'Oro. b) Scheme of herringbone bricks for a hemispherical dome. The herringbone bricks which belong to different loxodromic curves are not aligned.

The cross-herringbone spiralling technique permits to achieve the self-balanced state in the shells only by building through complete horizontal courses, i.e. during the construction before proceeding with the laying of a new course, all the courses at the lower courses must be complete (condition **A.**). Condition **A.** is the first of two requirements necessary to guarantee the effectiveness of the cross-herringbone spiralling technique. As evidence of this affirmation, it is noted that Brunelleschi claimed 8 teams of masons, one for sailing, to build the sails of Santa Maria del Fiore simultaneously [119]. Due to this and a few other reasons [119], Ghiberti accused him of building a dome of revolution within the walls of the dome of Santa Maria del Fiore [54]. Indeed, the condition **A.** combined with the radial symmetry of these structures constitutes a sufficient condition for achieving a self-balanced state. For the domes of revolution, during the laying of a brick course, the sliding of the elements can take place only before the

course itself is complete. Once closed, it can withstand compressive forces preventing sliding. Likewise, the cross-herringbone spiralling pattern allows the development of resistant sub-structures. To understand this, it is sufficient to think again about the domes of revolution. Referring to figure 4.3.2, when the course where two herringbone bricks (highlighted in orange) are laid is complete, the two mentioned bricks are fixed. Hence, they can support the upper course and once laid all bricks of the next course between the two herringbone elements a resistant arch exhibit. Therefore in domes built with cross-herringbone spiralling technique, whose pattern was discussed in chapter 4.2.2, the role of herringbone bricks is to link the courses together during the construction.

The goal of cross-herringbone is the development of sub-structures, like arches, that, under construction, provide the resources necessary to guarantee a self-balance state. Thus, the second condition necessary to guarantee the efficacy of the cross-herringbone spiralling technique is determined by the behaviour of the resistant sub-structures (condition **B.**), in the context of the analyses conducted it is generally correlated to the geometry of these sub-structures. If the conditions **A.** and **B.** are respected the cross-herringbone spiralling technology permit to build domes of revolution and polygonal domes without any formwork, furthermore within appropriates conditions, even other geometries of masonry shells could be built as self-supporting structures.

The following remark is in order, the presence of the double order of loxodromic curves differently from the herringbone technique permits to the materialisation of nodes reported in figure 4.2.9 and mentioned in chapter 4.2.2. During the construction phase, these elements play an essential role to achieve the self-balance state; they permit to adjust some errors by inserting wedges, bricks or elements to increase the compression forces within the horizontal brick courses. Indeed from the survey, especially in Santa Maria in Ciel d'Oro dome, several node adjustments are readable.

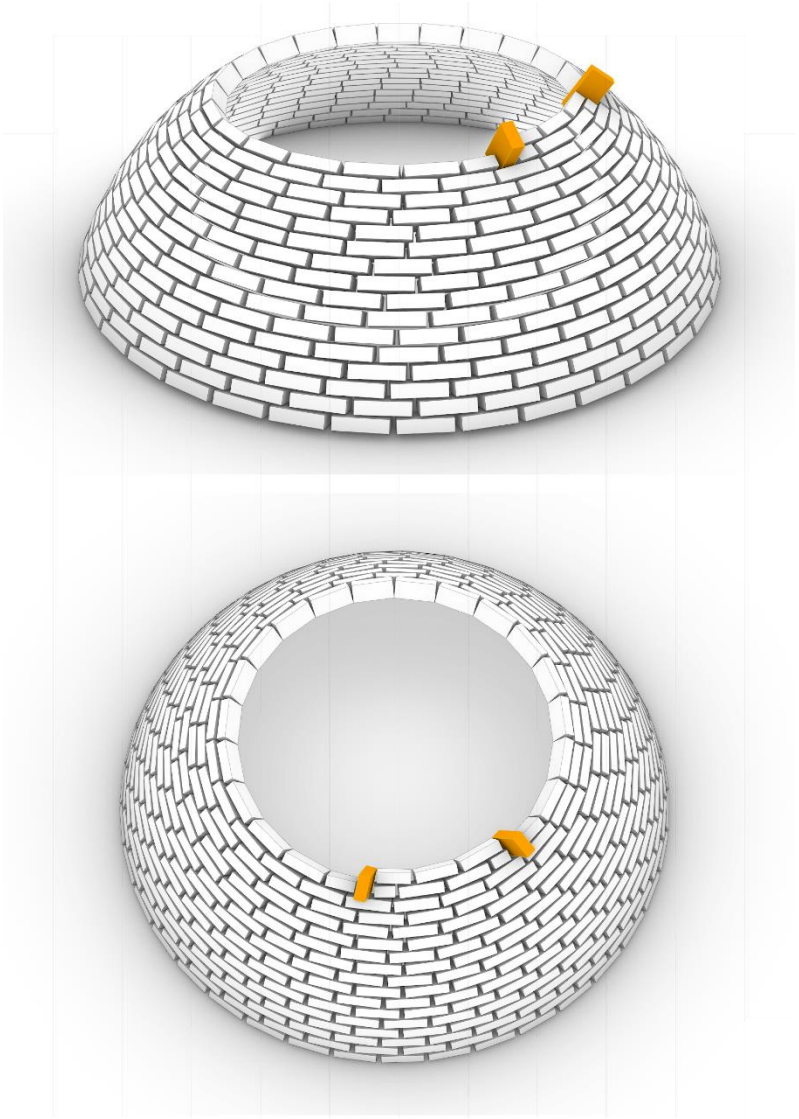

Figure 4.3.2 Hemispherical dome, the brick laid as herringbone bricks (highlighted in orange). Thank their orientation, the upper bricks course is constrained.

5. Learning from the history: equilibrium under construction

Chapters 2. and 4. present the significant technologies that allow building masonry vaults or domes without the aid of any temporary support. The study of these efficient techniques could contribute significantly to the formulation of a theory to evaluate the equilibrium under construction.

Chapter 5.1 summarises and organises the principles on which the self-balanced technologies are based, while in chapter 5.2, the guidelines to the evaluation of the stability of masonry structures during their construction are illustrated.

5.1 On the factors to reach the self-balanced state

The techniques illustrated in chapters 2. and 4. provide the resources to understand the self-balanced state of masonry structures under construction. All the technologies are ruled by factors whose principles can be geometric, constructive, mechanical, or a result of the properties of the material used. These factors are undoubtedly related to their effectiveness, e.g. it is not possible to build tile vaults without the use of fast-setting mortar or by the use of heavy blocks, because this would leads to their collapse.

The following factors have been derived from the study of the principles of the different self-supporting construction systems. These factors are:

- Bed joints orientation. For some technologies, such as pitched vaulting, this factor is the primary element that affects the self-balanced state. In others, like clay tubes vaulting technique, it is barely relevant. Examples are

given by figure 2.2.2 c) and d) where the tubes can be oriented in two different manners for the same structural geometry shown. If this factor is primary or relevant, a preliminary design is required, whose goal is to determine the correct orientation of the bed joints.

- Bricks stereotomy. During the construction phase, the geometry of the bricks significantly influences their stability, as witnessed by the clay tube vaulting technique or corbelled vaulting technique [37]. A wrong choice of the sizes or the geometry of the bricks lead to the sliding phenomena. The study of the stereotomy of bricks still represents an active research topic [134] [135].

- Resistant substructures. The existence of resistant sub-structures during the construction. This element is the primary factor for herringbone technology or even cross-herringbone, but it also influences the ability of self-balance in pitched vaults or clay tube vaults. Owing to the nature of this factor, the state of a structure based on it can be evaluated through mechanical analyses. The study of the equilibrium related to this factor is the primary subject discussed in chapter 6..

- Construction sequences. The construction sequence is a factor that influences all self-supporting technologies. This is essential for the correct construction of tile vaults and all those technologies whose balance is provided by resistant sub-structures.

- Material properties. A right choice of building material is always significant, but for technology such as tile vaulting technique the material properties are the primary factors to reach a self-balanced state.

Each of these factors can be decisive concerning the technology adopted. Table 01 summarises for all techniques discussed the incidence of factors mentioned above, three grades have been adopted: primary, relevant and not required:

- Primary is the factor that characterises the technology analysed. An incorrect application of the factor considered could lead to failures and collapse during construction.

- Relevant indicates a factor significant for a specific technology, but not primary.

- Not required is a factor that for the technology examined does not need a specific study, but as primary and relevant grades, if violated, could lead to failures.

E.g. for the right application of the herringbone vaulting technique it is assumed that the bed joints are arranged conventionally, and no particular study is required for the orientation of the joints. On the contrary, by adopting the pitched vaulting technique, the orientation of the bed joints is fundamental. However, even for the herringbone technique, errors of the orientation of beds joints could preclude the self-balancing ability of the structure built by herringbone vaulting technique.

The identification of the primary and relevant factors is fundamental to choose the method for assessing the equilibrium state during the building phase. For technologies based on different factors, a different method of evaluation should be adopted.

Technology	Bed joints orentation	Brick stereotomy	Resistant sub-structures	Construction sequence	Material properties
Pitched Vaulting	Primary	Not required	Relevant	Relevant	Not required
Clay tubes Vaulting	Relevant	Primary	Relevant	Not required	Relevant
Tiling vaulting	Not required	not required	Relevant	Relevant	Primary
Herringbone vaulting	Not required	Not required	Primary	Relevant	Not required
Cross - herringbone vaulting	Not required	Not required	Primary	Relevant	Not required

Table 01 Self-balanced technology and incidence factors.

5.2 Two-stepped approach

The evaluation of the state of a masonry building is the subject of studies by numerous researchers [136] [137] [138], however even today, the behaviour of these structures during the construction phase is scarcely analysed [17] [37]. One of the goals of the present study is to introduce the principles of a new theory which allow evaluating equilibrium during the construction phase. The development of this theory is significant for masonry arches, vaults or domes, but it can also be useful for other types of masonry structures. For this reason, the following rational refers to any type of masonry structure. Its validity is discussed in this chapter and also in the following ones, see chapter 5.2, 5.2.1 and 5.2.2.

Only from the observation of real structures and the study of historical technologies, the understanding of the reasons that guide the balanced state of domes and masonry vaults during the construction phase can be gained. Indeed, for the type of structures studied, the analyses conducted on self-balancing technologies have revealed that, although with considerable differences, they are influenced by common factors (see chapter 5.1 for the requirements to reach the self-balanced state under construction).

These factors affect only locally the behaviour of the structure. For example, referring to the tile vaulting technology, the fast setting properties of the mortar and lightness of the tiles allow the laying without manifesting any sliding phenomena, or the presence of sub-structures provides the support needed for the stability of bricks until the brick course is complete. Likewise, these factors do not alter the integrity of the whole structure, whose behaviour remains unchanged. To confirm this, it is enough to revisit hemispherical domes; by applying the building process discussed in chapter 4.3, it is possible to build them without any formwork. However, independently of the construction sequence adopted,

the stability of the hemispherical domes depends mainly on geometric factors [139], their overall behaviour does not change. Then, it is irrational to assume that the herringbone pattern governs the stability of a structure, like, for example, in the case of the dome of Santa Maria del Fiore. Although it may influence some aspects of its behaviour such as the position or shape of the cracks, it does not alter its collapse behaviour.

The same considerations discussed are also valid for different types of masonry structures, such as walls or structures which require support. Their overall behaviour is not modified by how they find the equilibrium during the construction phase because the overall equilibrium is determined by their geometries [2].

Therefore, to assess the balanced state of masonry structures during the construction phase, it is convenient to study their equilibrium through two analyses: one related to the local state and the other related to the global state. From here on, this approach is defined and referred to as the two-stepped approach. The first step consists of the evaluation of the local equilibrium and the second one of the assessments of the overall stability.

The two steps are called: **Local equilibrium step** and **Global equilibrium step**.

> The study of **Local equilibrium step (L.E.S.)** has the goal of detecting any possible local collapses. The evaluation criterion is relative to the construction techniques used, especially in the case of self-technology the criteria to assessing the stability of structures should be related to the factors that characterise the building technique itself (primary factors). It is not possible to adopt the same criterion to technologies based on factors whose principles are different. In this document, the calculation of local stability is carried out by referring only to the primary and relevant criteria of the cross-herringbone technology. The

determination of other criteria relating to other factors or technologies are not considered.

The study of **Global equilibrium step (G.E.S.)** aims to determine the stability of the entire structure built. It can be conducted with the traditional tools developed for determining the behaviour of complete structures.

Independently of the building technology adopted and of the type of structure considered, if no collapse phenomena (local or global) could occur for a given construction stage, all the conditions to guarantee a balanced state are provided. To guarantee the possibility to build a masonry structure, it is needed to evaluate all the construction stages and if for each one the balanced state is found (Local and Global), that structure could be built.

The flowchart shown in figure 5.2.1 describes the logic of the two-stepped process: before evaluating the global equilibrium (**G.E.S**.), it is required to determine the local balanced state (**L.E.S.**).This relation is justified by a simple assumption already mentioned: it is impossible to build any structure if, during the construction phase, local collapses occur. To explain the flowchart consider a wall under construction and defined by the i index the number of brick courses and by the n index the construction stages, it is possible to determine the equilibrium at the n^{th} stage evaluating the local stability, through **L.E.S.**, and then the global stability at that stage, through **G.E.S.** If no local or global failure phenomena are exhibited, the same logic process should be repeated for the next construction stage ($n+1$), and as mentioned before, the wall can be built if the equilibrium is found (local and global) for all stages.

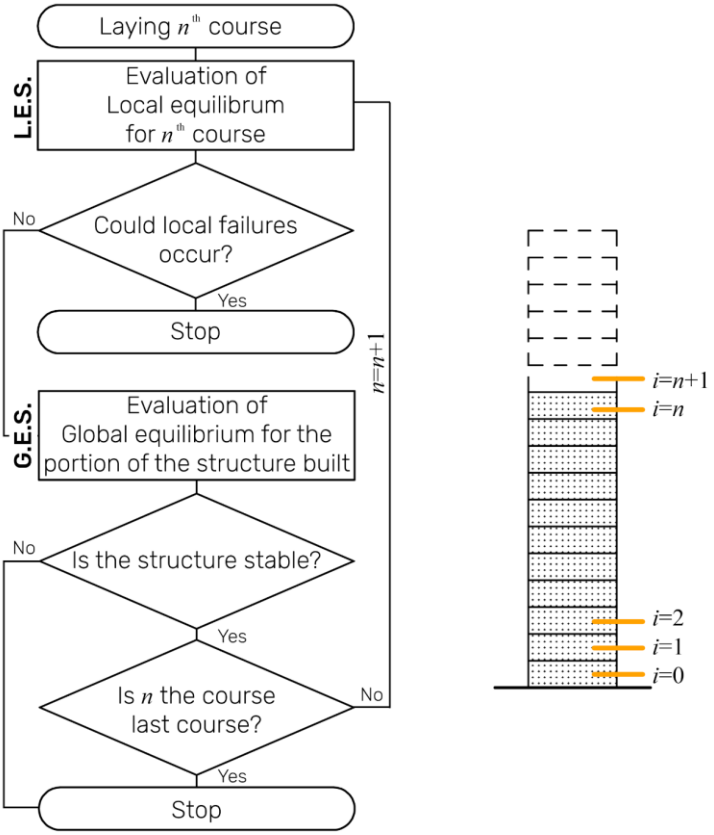

Figure 5.2.1 Right, flowchart to assess the equilibrium of a masonry structure during the construction. Left, a model of a wall during the construction, the i index indicates the course, while n index the last stage built.

5.2.1 Local equilibrium step

To build a structure it is necessary to prevent any failures, even the local ones. The **Local equilibrium step** has the purpose of identifying and verifying any possible collapses of masonry blocks or portions of brickwork at this local scale. Therefore, for each n^{th} construction stage, an analysis must be performed for determining the balanced state of the brick course just laid (n^{th} course), and the

balanced state of a portion of the structure. The choice of this portion concerns the type of structure considered and the building technology adopted, e.g. domes, arches and tower present different criticalities during the construction; thus, the different portion should be observed.

The following considerations concern the construction of a generic structure observed at the moment in which the bricks or blocks are being laid on a rough inclined plane, i.e. when the bricks are laid on the $i = n^{th}$ course. In this situation, the blocks are subject only to their weight, surely, they do not crack by themselves and the failures that could happen are through sliding or overturning. To understand this, we recall the **III.** Heyman's hypothesis (masonry has infinite compressive strength, chapter 3.2), if this statement is valid for complete structures, it is undoubtedly true also for the case investigated. Then the stability of the bricks or blocks are equivalent to the equilibrium of a rigid body and the causes of collapses are due to the low tensile strength of mortar joints, and the critical role assumed of the friction.

Referring to figure 5.2.2 and denoting by w the weight of a block, $w^{\parallel}$, $w^{\perp}$ its parallel and orthogonal components to the inclined plane and μ the Coulomb's friction, the equilibrium of the block at the n^{th} construction stage is described by (1) and (2) [140].

$$\mu \cdot w_n^{\perp} \geq w_n^{\parallel} \tag{1}$$

$$\frac{\mathrm{B}}{\mathrm{H}} \cdot w_n^{\perp} \geq w_n^{\parallel} \tag{2}$$

where H and B are the height and width of the considered block. The inequality (1) expresses the equilibrium condition at the translation of the block on an inclined plane, while (2) expresses the overturning equilibrium condition with respect to point A.

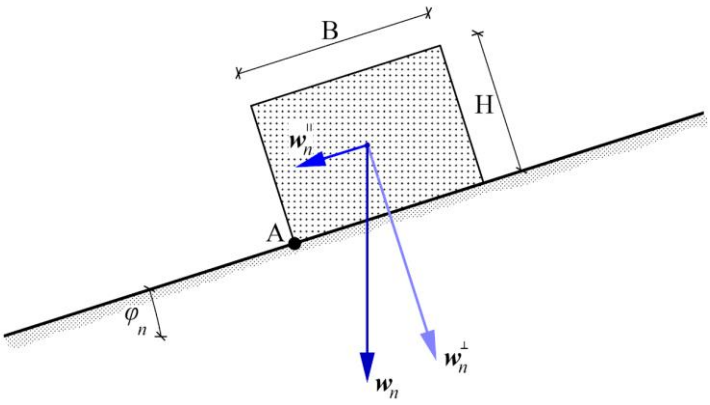

Figure 5.2.2 Block laid on the inclined plane at the n^{th} construction stage.

As long as both conditions (1) and (2) are verified, the system is balanced, while if one or both are violated, then motion occurs. Denoting φ the slope angle of the laying plane it is possible to express (1) and (2) in terms of φ:

$$\mu \cdot \cot\left(\varphi_n\right) \geq 1$$

$$\frac{\mathrm{B}}{\mathrm{H}} \cdot \cot\left(\varphi_n\right) \geq 1$$

Therefore the study of the block equilibrium is related to the geometric parameters B, H, φ, to the friction factor μ and the stage n, in particular, the limit condition for the equilibrium of the block is described by the equations (3) and (4).

$$\mu \cdot \cot\left(\varphi_n\right) = 1 \tag{3}$$

$$\frac{\mathrm{B}}{\mathrm{H}} \cdot \cot\left(\varphi_n\right) = 1 \tag{4}$$

For the purpose of this analysis, the φ angle could assume values within 0 and $\pi/2$. In such domain, the cotangent function is defined and is continuous, strictly monotone decreasing and superiorly not limited. Thus, independently of the values of B, H and μ, it exists a

limit value of the φ angle for which the block is not stable. This value is called the equilibrium limit angle and can be determined from (5).

$$\varphi_{n_L} = \left\{ \min(\varphi_n) \mid \frac{B}{H} \cdot \cot(\varphi_n) = 1 \ \vee \ \mu \cdot \cot(\varphi_n) = 1 \ ; \ 0 < \varphi_n \leq \frac{\pi}{2} \right\} \tag{5}$$

For angles greater than the equilibrium limit angle, (1) and (2) are violated, and failure occurs. The nature of the motion depends on B, H, μ and the relation to the angle of inclination φ. More precisely, in correspondence to the equilibrium limit angle, it is enough to study their relation as seen in (6) to understand the nature of the motion. If the (6) is verified, sliding occurs. Otherwise, the block overturns.

$$\frac{B}{H} > \mu \ ; \ \varphi_n = \varphi_{n_L} \tag{6}$$

Ultimately the block equilibrium condition is dictated by the condition described in (7), this condition is represented by the intersection of the areas illustrated in figure 5.2.3.

$$\frac{B}{H} \cdot \cot(\varphi_n) \geq 1 \ \wedge \ \mu \cdot \cot(\varphi_n) \geq 1 \ ; \quad 0 < \varphi_n \leq \frac{\pi}{2} \tag{7}$$

During the construction of arches, vaults or domes, the inclination of the plane increases through its construction stages, and the equilibrium limit angle can be exceeded; thus condition (7) is violated. In this case, the system represented in figure 5.2.2 is not able to supply all the resources needed to avoid slippage or overturn. Therefore, using traditional building techniques formwork and shoring is required. Self-supporting technologies aim to provide all resources to achieve the self-balanced state. Hence when φ is greater than the equilibrium limit angle, (7) cannot be valid and to express the block equilibrium, a new relation should be found. The nature of this new relations depends on factors that rule the self-supporting technology adopted to build the structure.

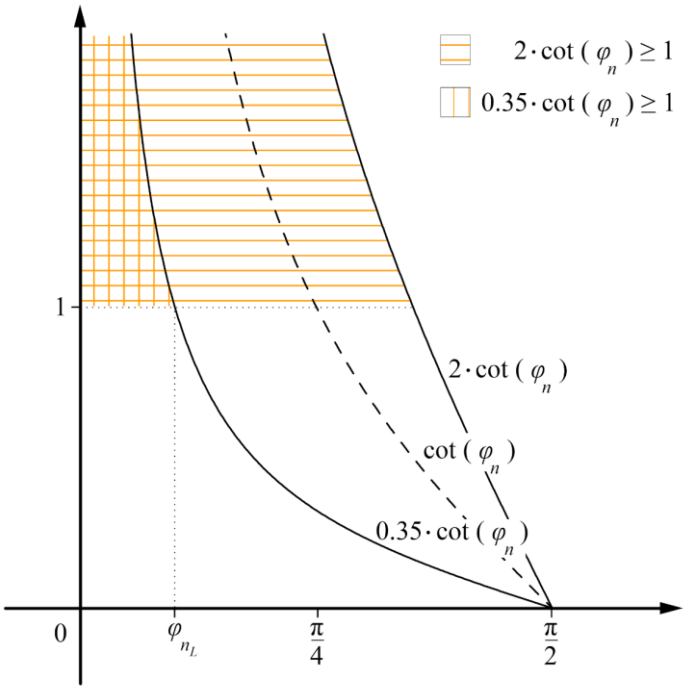

Figure 5.2.3 Representation of condition (7) and the equilibrium limit angle determined by (6) (μ = 0.35 and Ratio $\mathrm{B/H}$ = 2).

Relations (5), (6) and (7) do not consider the presence of any binder, and they describe the situations where the joint are dry-joints, furthermore with approximation, they can depict those situations in which hydraulic binders are used [141]. To represent structures built using fast-setting binders, such as gypsum, (5) (6) and (7) should alter take into account the cohesive mortar ability, the relations above must be reformulated concerning the type of binder used. An approximation could be obtained incrementing the stabilising factor relative to $w^{\perp}$ to represent the cohesive phenomenon. For this particular situation, due to the scale analysed: only a few bricks are considered thus it is possible to estimate the tensile strength which is reasonable in the same order as the tensile strength of mortar.

5.2.2 Global equilibrium step

The **Global equilibrium step**, as mentioned in chapter 5.2, aims to evaluate the stability of the entire built structure. Thus, referring to figure 5.2.4 a), at the n^{th} construction stage, the equilibrium is determined by considering the elements that constitute all i built courses, i.e. all courses comprised between i = 0 up to i = n. The **G.E.S.** must be repeated for all the different construction stages, only if for each stage a balanced state is determined, then, during construction, no failures occur. Due to the scale of the analysis, the **G.E.S.** can be performed using traditional methods such as statics graphic statics, but for each given construction stage, to perform **G.E.S.** the forces defined in **L.E.S.** must be compatible and considered.

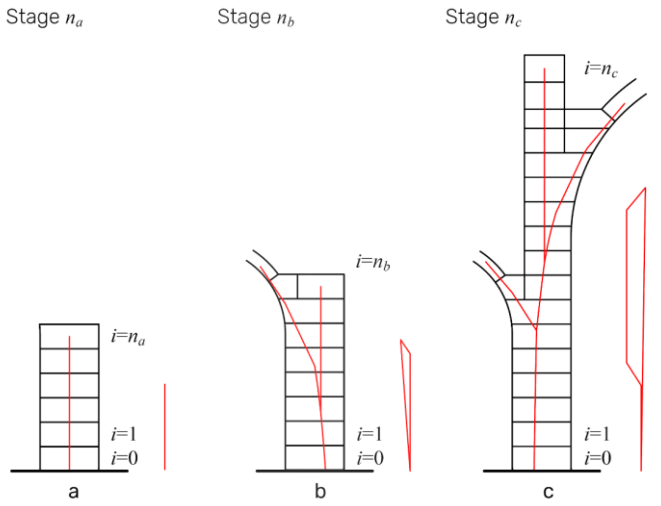

Figure 5.2.4 a), b) and c) **G. E. S.** for three different construction stages n_a, n_b, n_c The geometry of the structure changes during construction, the number i of course increases. For each stage considered a balanced state is found.

6. Two-stepped approach: the cross-herringbone spiralling technology

The two-stepped approach, introduced in chapter 5.2, shows the logic for assessing the balance of masonry structures during construction. It does not provide the tools suitable for performing analyses, but it describes the steps (**L.E.S.** and **G.E.S.**) necessary for the evaluation of the behaviour of the structures in the building phase.

In chapter 6.3, according to the two-stepped approach, a formulation is presented for the determination of the self-balanced state of domes built through the cross-herringbone spiralling technique. Consistently with the factors determined in chapter 5.1, the developed formulation is an example of how the two-stepped approach can be considered the effects of specific building technology for the evaluation of balance state.

The existence of resistant sub-structures, such as arches and plate-bandes, is also proven by the numerical model illustrated in chapter 6.4. Numerical simulations developed with D.E.M. are intended to describe the behaviour of dome during construction, especially in terms of displacements, bricks configuration but above all to verify the existence of these sub-structures.

The models on which the analyses, simulations and the formulation were carried out, derived from the study of the two domes Santa Maria in Ciel d'Oro and Simon Mago are extensively discussed in chapter 4.2. The digital models respect the main geometric characteristics described in that chapter as the ratios of bricks dimensions, the orientation of bricks and the position of nodes.

6.1 Geometry of dome

The formulation developed in the following chapters has been applied to an octagonal dome, whose geometry consisting of eight identical sails, and has been elaborated from the considerations discussed in chapters 4.2.2, 4.2.3 and 4.2.4. on the dome of Santa Maria in Ciel d'Oro. However, under some conditions illustrated in chapter 6.3.2, different dome shapes can be evaluated using the same approach, for example, cases presented in Appendix B reports the analyses performed on the hemispherical dome. As shown in figure 4.2.2 and 6.1.1 the herringbone bricks are laid in regular intervals and placed at the same plane to the horizontal bricks, they are arranged in a radial manner. This geometric property is key to understanding the structural behaviour of the dome under construction. From now on the last complete brick course (thus a closed course) is highlighted in light grey, while the one under construction is dark grey.

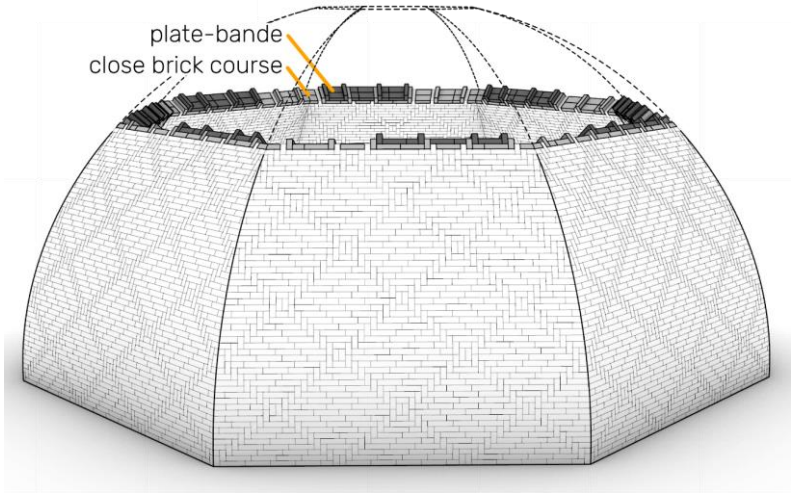

Figure 6.1.1 Octagonal dome during the n^{th} construction stage. The geometry of each block modelled are constituted by the mortar thickness and the brick geometry. The last complete brick course laid $(i = n\text{-}1)$ is coloured light grey, while the one under construction, $(i = n)$ is dark grey.

6.2 The self-balance state of cross-herringbone domes

To understand how the cross-herringbone spiralling pattern allows the construction of a self-balancing octagonal dome, we need to analyse the different construction stages verifying the equilibrium of the dome. To achieve this objective, the resistance structure (global 1) and sub-structures (local 1 and 2) need to be assessed. The first sub-mechanism (local 1) manifests itself when the brick course is completed, and the mason begins to lay a new course. The second sub-mechanism (local 2), the plate-bande, occurs when the bricks are laid in a course which is not yet closed. Both systems are illustrated in figure 6.1.1. In this study, both brick laying phases have been modelled at different heights corresponding to distinct construction stages. Meanwhile, the overall stability of the dome has also been performed; thus, it is possible ensuring a full evaluation of the local and global equilibrium states.

When under construction, the local equilibrium state of a self-balancing cross-herringbone spiralling dome is characterized by two resistance structures: the closed course structure (local 1) and the plate-bande structure (local 2). As described in chapter 2.4.2, it is assumed that the octagonal dome is built through complete courses, only when the previous course is completed, the mason begins to lay a new course of bricks. Thus, any meridian section of the dome, evaluated during the construction stage, can be represented by an incomplete voussoir arch shape. Referring to figure 6.2.1, it is assumed that the voussoir bricks are rigid bodies with a mass. We further assume that they experience friction along with their interfaces and that they can slip as a rigid body on an inclined plane leading to the overturning of the incomplete voussoir arch. Two equilibrium equations are distinguished, both relate to the local equilibrium (local 1 and 2). Using Coulomb's law of friction, the equilibrium can be expressed as:

$$\mu \cdot w_n^{\perp} \geq w_n^{\parallel}$$

$$\frac{\mathrm{B}}{\mathrm{H}} \cdot w_n^{\perp} \geq w_n^{\parallel}$$

where w is the weight of the bricks, μ the mortar friction coefficient, while φ angle represents the inclination of the laying plane with respect to the horizontal plane and the n subscript denotes the last course, i.e. n^{th} identifies the construction stage. As shown in figure 6.2.1, the i index corresponds to the course label. Hence the first course built is denoted with i=0 index and the second i=1, thus each course is uniquely defined by i and n defines the constructive stage.

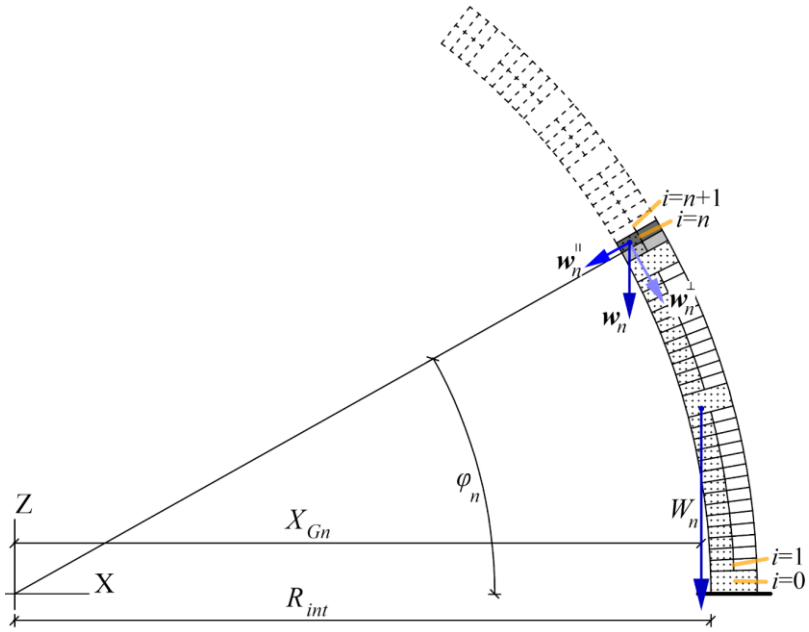

Figure 6.2.1 Meridian section of a dome: the incomplete arch and rigid bodies (n^{th} construction stage).

These inequalities correspond to the number (1) and (2) illustrated in chapter 5.2.1, hence the balance condition is provided by (7). The second equation of equilibrium, which relates to the overturning

moment of the incomplete voussoir arch about its springing, is formulated as:

$$X_{Gn} \geq R_{int} \tag{8}$$

where X_{Gn} is the distance from the origin, defined by the X, Z coordinates system, to the centroid of incomplete voussoir arch, and R_{int} is the distance from the origin to the center of rotation of the voussoir arch (or springing). Only if both inequalities, expressed in equation (7) (local 1 and 2) and (8) (Global 1) are verified, the system of rigid bodies (being the individual bricks and the constructed portion of the sail) is self-equilibrated. This can be expressed by situation 1 (S1):

$$\frac{\mathrm{B}}{\mathrm{H}} \cdot \cot\left(\varphi_n\right) \geq 1 \quad \wedge \quad \mu \cdot \cot\left(\varphi_n\right) \geq 1 \quad \wedge \quad X_{Gn} \geq R_{int} \; ; \quad 0 < \varphi_n \leq \frac{\pi}{2} \tag{S1}$$

Otherwise, if at least one of the two inequalities, (7) and/or (8), is not satisfied, the system of rigid bodies is not able to guarantee a self-balanced state. This can be expressed in situation 2 (S2):

$$\frac{\mathrm{B}}{\mathrm{H}} \cdot \cot\left(\varphi_n\right) < 1 \quad \vee \quad \mu \cdot \cot\left(\varphi_n\right) < 1 \quad \vee \quad X_{Gn} < R_{int} \; ; \quad 0 < \varphi_n \leq \frac{\pi}{2} \tag{S2}$$

In the situation (S2) to achieve a balanced state, a system of auxiliary forces must be considered. The role of the cross-herringbone spiralling pattern is to provide this auxiliary force system through plate-bande action (local 2) to achieve the self-equilibrated state. During all construction stages, sliding and overturning of the bricks are avoided through, the construction of complete courses on one hand and the plate-bandes on the other. The role of the cross-herringbone pattern can also be derived by observing the physical behaviour of brick courses in the different construction stages.

Referring to figure 5.2.3 and recalling the relationship between the dimensions of the bricks $1\text{-}\alpha\cdot 1\text{-}2\cdot\alpha$ ($\alpha>1$), it is possible to understand that the sliding is the first collapse phenomenon that could occur in such type of domes. Therefore, the equilibrium limit angle is defined from (4).

We define the limit course ($i=L$) as the first brick course in which the angle is greater than the equilibrium limit angle, thus the friction forces between the bricks are not sufficient to avoid slippage, the angle (S2). At the limit course ($i=L$) the bricks slide towards the centroid of the dome. However, the presence of the herringbone bricks in the spiralling pattern prevents them from slipping inwards. When the bricks of the limit course try to slip, they collide against the herringbone bricks, which are already laid in a radial manner and fixed into the lower course ($i=L\text{-}1$). This lower brick course is closed and the herringbone bricks at the course ($i=L$) are encastered into that lower brick course so that no sliding of the herringbone bricks can occur.

Further, even if the bricks of the lower course ($i=L\text{-}1$) try to slide, the same mechanism will take place in the previous course ($i=L\text{-}2$). Within the courses, plate-bande systems may be identified. Each of these plate-bande systems is bound by two herringbone bricks fixed into the lower course. The plate-bande systems act to prevent the failures by exerting a thrust against the herringbone bricks which transmit that thrust to the lower completed brick courses. Therefore, even in the case (S2) where the rigid bodies themselves are not sufficient to ensure a state of stable equilibrium, the cross-herringbone spiralling pattern provides internal support so that the dome can be in equilibrium (local 2). These conclusions are further supported by the interpretation of the results of the D.E.M analysis reported in chapter 6.4. Thus, even during the construction, the equilibrium of the masonry dome can be achieved through different systems: in the initial stages of construction, the equilibrium is provided by the system of friction

forces (S1). In the later stages, when these are not sufficient (S2), the cross-herringbone spiralling pattern starts to operate, the structures of the closed brick courses (local 1) and the plate-bandes (local 2) provide the auxiliary forces required to maintain the static equilibrium of the dome under construction.

6.3 Limit analysis for the building phase

Two methods are adopted to analyse the equilibrium states of the spiralling cross-herringbone dome. Both are based on the limit analysis: the thrust line method (T.L.M.) and the modified thrust line method (M.T.L.M.) [89] [142]. The three Heyman hypotheses exposed in chapter 3.2 are made: **I.** sliding of the bricks cannot occur, **II.** the masonry has no tensile strength, and **III.** the masonry has infinite compressive strength [2]. Generally speaking, completed masonry domes experience meridian compressive stresses of one order of magnitude lower than the masonry's crushing strength. The hoop forces experienced in a completed self-balanced dome, are generally low. However, it will be shown in Appendix B, that during construction their value might be larger than the ones experienced in the completed dome, but the stresses are always lower than the masonry's crushing strength. Consequently, for this study, the assumption of infinite compressive strength (**III.**) is valid as the internal compressive stresses are very low. Under construction, when the bricks are being laid, sliding may occur. But even if it occurs, after few settlements, the motion stops and the structure under construction is stable. Therefore, even if the first hypothesis (**I.**) has been removed from our analyses, the limit state analysis can be applied as no significative motion manifests. Even if it is considered finite values of friction angle, as proven by D'Ayala and Casapulla [106], a unique solution exists. According to the Safe Theorem [2], the equilibrium of the dome is guaranteed if a thrust line exists which lies entirely within the cross-section of the dome. Therefore, we adopted a two-stepped approach consisting of **L.E.S.** and **G.E.S.** We perform the T.L.M. to verify the equilibrium state of the completed courses (local 1) and of the brick courses as they are being laid (local 2), that is **L.E.S.**, while we verify the overall equilibrium of the dome under construction using the M.T.L.M. (global 1) which corresponds with **G.E.S.**. The M.T.L.M. combines

Heyman's theory and membrane theory [143]. To perform the analyses with this method some assumptions are required. These assumptions are: the load is uniform and axisymmetric, the hoop forces decrease from the crown to the base of the dome, unlike to meridional forces, which increase from crown to the base. Both the methods T.L.M. (local 1 and 2) and M.T.L.M. (global 1) have been implemented for this study into the graphical editor algorithm Grasshopper for Rhinoceros software.

The analyses have been performed for different construction stages and structures namely for the plate-bande system, for the closed brick course, and for the dome in different construction stages.

6.3.1 L.E.S. and G.E.S. for cross-herringbone dome

As introduced inchapter 5.2, to uniquely identify the brick courses the subscript i has been assumed, but within each course, several plate-bande structures exist. Therefore, as shown in figure 6.3.1, to identify every plate-bande structure, the j subscript has been adopted. Considering one of any courses and referring to figure 6.3.1, j is equal to zero at the south edge of the east sail of the dome, j increases in a right-handed manner. The two-stepped approach, which has been developed to perform the equilibrium state analysis of the dome (both local and global) under all construction stages, is summarized in the flowchart in figure 6.3.2. First of all, for each n^{th} constructive stage it is verified whether the bricks are self-balanced (S1) then analyses are performed to assess the state of each sub-structure namely the plate-bande, the closed brick courses (**L.E.S.**), and subsequently constructed portion of the dome is evaluated (**G.E.S.**). Thereafter all j plate-bandes at the laying course are evaluated. Once the thrust of all plate-bandes in that laying course is computed, the stability of the compressive rings of the underlying closed brick course is verified and finally the overall equilibrium of the dome is verified using M.T.L.M. This

approach, illustrated in figure 6.3.2, is repeated for all construction stages until the last course is laid.

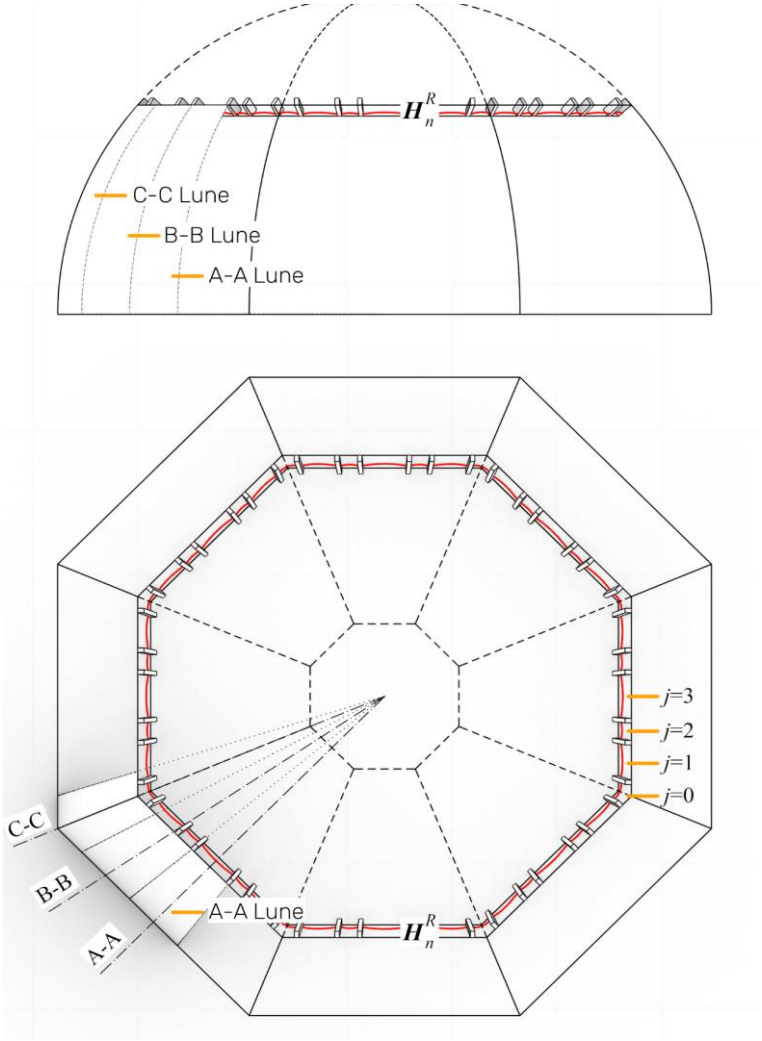

Figure 6.3.1 Elevation (top) plan view (bottom) of octagonal dome under construction. In the plan view: enumeration of plate-bandes within a course, and closed brick course resulting in the n^{th} compression ring (highlighted red). Lunes: A-A, B-B, C-C (plan view and elevation) and their middle section (plan view).

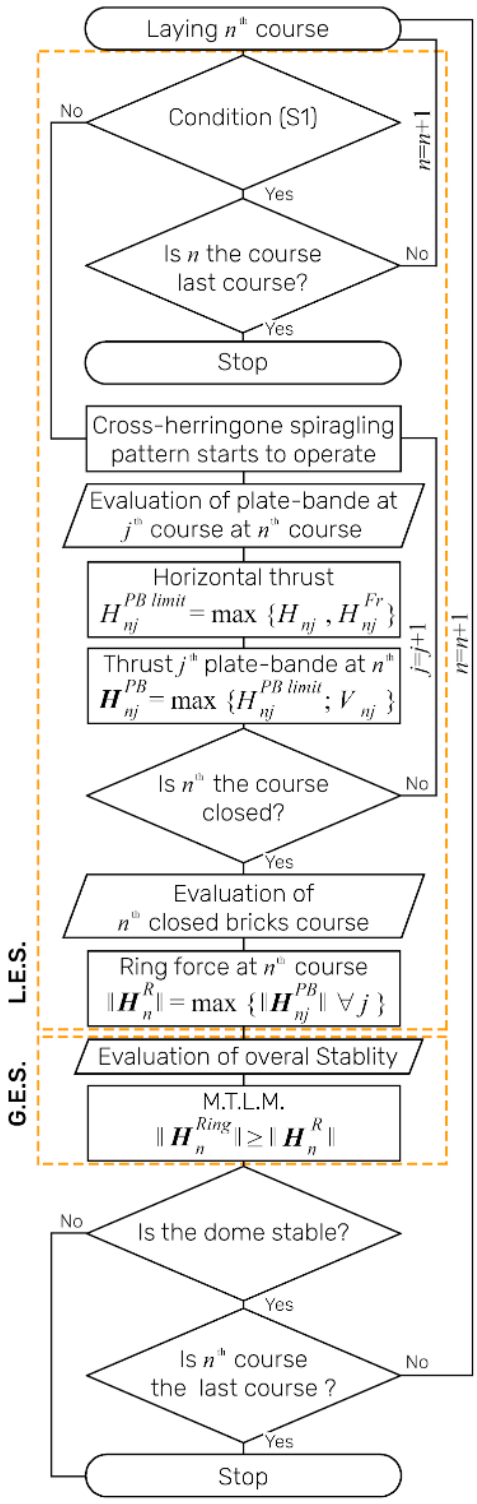

Figure 6.3.2 Flow chart of two-stepped approach for cross-herringbone spiralling technology applied to a dome.

6.3.2 Plate-bande (L.E.S.)

The plate-bande is a straight arch and, because of its geometry, it is impossible to find a collapse mechanism, hence, the maximum thrust of the plate-bande structure is related to the crushing strength of the bricks. The thrust of plate-bande can be defined through considerations of equilibrium. We have adopted two formulations: both do not consider friction on the laying plane (i.e. the bricks are laid onto a smooth surface). This is a conservative assumption and in reality, the bricks would be posed onto a mortar bed which provides frictional resistance. The first formulation respects all Heyman's assumptions, (**I.**), (**II.**) and (**III.**) discussed in chapter 3.2. The limit thrust is related to the loads applied, the length, and thickness of the plate-bande [144]. The length of plate-bande is a function of its location in the dome (i.e. the higher up in the dome, the smaller its length) and it also depends on its position within the course. We define the brick dimensions as multiple of b: b the height (1), 2b the width(α·1) and 4b the length (2·α) (in the model b=6 cm) and the ρ density of bricks. The H horizontal thrust and V the vertical thrust are evaluated through the equilibrium equations (9) and (10) and considering only the parallel component of the self-weight to the φ (the laying plane).

$$w_{nj}^{\parallel} = 2 \cdot \left(l_{nj1} + l_{nj2} \right) \cdot b^2 \cdot \rho \cdot sin\left(\varphi_n \right)$$

$$H_{nj} = \frac{w_{nj}^{\parallel} \cdot l_{nj1}}{32 \cdot b}$$

$$H_{nj} = \frac{\left(l_{nj1} + l_{nj2} \right) \cdot l_{nj1} \cdot b \cdot \rho \cdot sin\left(\varphi_n \right)}{16} \tag{9}$$

$$V_{nj} = \left(l_{nj1} + l_{nj2} \right) \cdot b^2 \cdot \rho \cdot sin\left(\varphi_n \right) \tag{10}$$

Referring to n time of posing, the loads carried by the plate-bande are derived from the component of self-weight parallel to the laying plane as illustrated in figure 6.3.3.

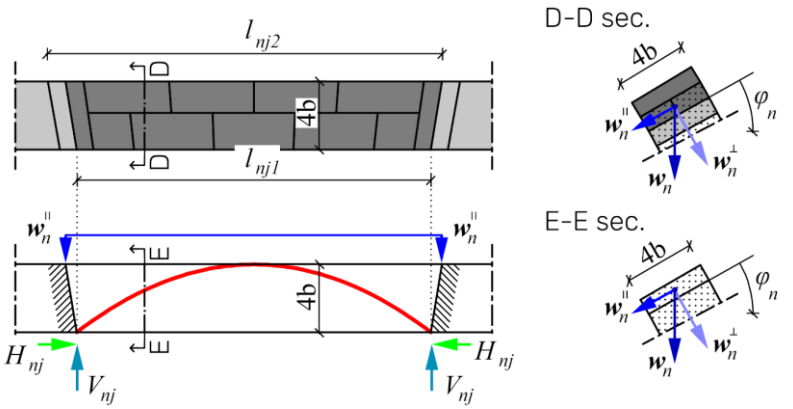

Figure 6.3.3 Plate-bande at the n^{th} course. Plan view (left) and section (right), the graphical representation (top) and free body diagram (bottom).

The other approach is obtained by assuming a finite friction angle and no sliding. Using equation (13), it is possible to evaluate the H^{Fr} horizontal thrust. To differentiate it with respect to the horizontal thrust calculated by equation (9) which relies on the Heyman's assumption of infinite friction, the Fr in the superscript in equation (13), denotes the horizontal thrust defined by taking into account the friction between the faces of herringbone bricks.

As shown in figure 6.3.3, the herringbone bricks have a radial arrangement, with their long side not running parallel to the normal of the imaginary surface of a cylindrical sail. Hence, referring to figure 6.3.4, β angles are defined. These angles are bound by the normal of the imaginary surface of the cylindrical sail and the long side of herringbone bricks, Φ is the friction angle and the γ angle which describes the inclination of the thrust with respect to the intrados of the sail (11). To avoid sliding of the bricks, the γ angle must be defined as described in (12).

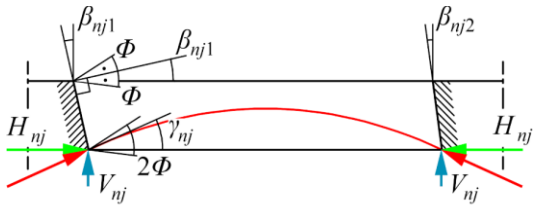

Figure 6.3.4 Plate-bande. Angles: β ,γ and Φ and a thrust line.

$$tan(\gamma_{nj}) = \frac{V_{nj}}{H_{nj}^{Fr}} \tag{11}$$

The limits horizontal thrust which prevents slipping can be determined considering by equations (13).

$$\beta_{njk} - \phi \le \gamma_{njk} \le \beta_{njk} + \phi \qquad k = (0, 1) \tag{12}$$

$$H_{njk}^{Fr} = \frac{(l_{nj1} + l_{nj2}) \cdot b^2 \cdot \rho \cdot sin(\varphi_n)}{tan(\beta_{njk} \pm \phi)} \qquad k = (0, 1) \tag{13}$$

Equation (13) provides an estimate of the minimum horizontal thrust and the maximum horizontal thrust, but in the present formulation, the maximum horizontal thrust is neglected. Even if assuming a low angle of friction (e.g. Φ=20°) the octagonal geometry of the dome allow to do not consider the maximum horizontal thrust defined by (13), indeed the values of the β decrease from base to top dome and in correspondence of the limit course (i=L), defined in chapter 6.2, even assuming γ = 0° the condition (12) is verified. Hence the (13) assumed is:

$$H_{njk}^{Fr} = \frac{(l_{nj1} + l_{nj2}) \cdot b^2 \cdot \rho \cdot sin(\varphi_n)}{tan(\beta_{njk} + \phi)} \qquad k = (0, 1)$$

The limit horizontal thrust in the plate-bande at the time of laying the bricks can be defined as the maximum horizontal thrust (14) required by the two approaches expressed in equations (9) and (13), thus:

$$H_{nj}^{PB\ limit} = max\{H_{nj}\ ,\ H_{njk}^{Fr}\ \ \forall\ k\} \tag{14}$$

At the sail edges, where the two laying planes intersect each other and result in a geometric discontinuity (or fold line), a component of the thrust of the plate-bande pushes the dome outwards. However, due to the symmetry of the dome about that fold line, the reinforcements in the angles and due to the loads, which are of a modest order of magnitude, the outward thrust does not expel the bricks on the fold line, thus it does not lead to failure of the dome. The $\boldsymbol{H}^{PB}$ thrust which acts on herringbone bricks laying on the previous layer is defined as:

$$\boldsymbol{H}_{nj}^{PB} = \left(H_{nj}^{PB\ Limit}\ ; V_{nj} \right) \tag{15}$$

The formulation presented (10) (13) (14) (15) is also validated for hemispherical domes. Indeed figure 6.3.5 shows the possibility to trace a straight line which lies entirely in the thickness of the dome which is bounded by two consecutive herringbone bricks. This geometrical peculiarity indicates that, although the geometry of the dome is hemispherical, the sub-structures can be described by plate-bande. This statement is also complying from (13), i.e. considering a finite friction value (Φ=20°), even in the case of a modest dome, the (12) is verified. Indeed, denoting with S^{Fr} the limit span which allows describing the structural behaviour of arches as plate-bande. For hemispherical dome with inner radius 3.5 meters, the S^{Fr} corresponds of a value greater than 2 meters, but from chapter 4.2.2, the maximum distance between two consecutive loxodromes is lesser than 2 meters, thus a plate-bande behaviour is acceptable. Figure 4.3.6 shows the limit condition to define the

S^{Fr}, when $\beta = \Phi$ if $\beta > \Phi$ the maximum horizontal thrust must be considered.

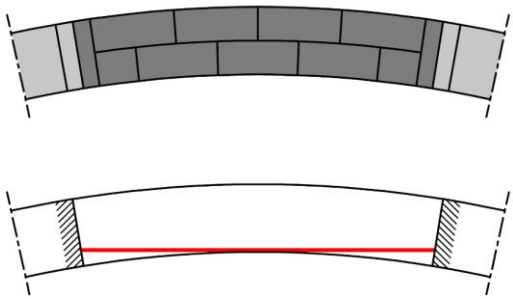

Figure 6.3.5 Portion of a hemispherical dome (radius 3.5 m), the straight line (highlighted red) of thrust lies entirely in the geometry, thus no cinematic mechanism can be individuated.

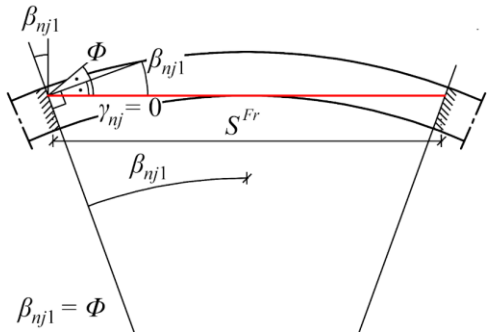

Figure 6.3.6 Plate-bande mechanism and a portion of a hemispherical dome (radius 3.5 meters, γ=0° and $\beta_{nj1} = \beta_{nj2} = \Phi$ = 20°). If S the span of arch, defined by two herringbone bricks, is greater than S^{Fr}, the limit span, than the maximum horizontal thrust is derived by condition (13).

6.3.3 Closed brick course (L.E.S.)

At the n^{th} construction stage, once the entire n^{th} bricks course is completed, a spatial compression ring is formed as shown in figure

6.3.1 (highlighted red). The magnitude of the ring force is estimated as the maximum thrust present in all the plate-bande structures at the n^{th} course or:

$$\| \boldsymbol{H}_n^R \| = max\{ \| \boldsymbol{H}_{nj}^{PB} \| , \forall j \} \quad (16)$$

When the next course is positioned (n+1), the value of compression force in the n^{th} completed ring and in the underlying completed rings changes. To determine the ring compression forces, other approaches could be assumed. For example, the contribution of the normal component of the self-weight of the bricks can be considered, in such manner the friction forces increase and the compression forces required to prevent sliding. Or one could also evaluate the variation of the plate-bande horizontal thrust caused by the slight incline of the herringbone bricks during the laying of bricks, and its effect on the underlying closed brick courses. However, due to hyperstatic nature of the closed brick courses, all approaches proposed under the assumed hypotheses, do not allow for the quantitative definition of the equilibrium state of the rings, but only give a qualitative definition. Equation (16) does allow us to compute the compression force value in the ring at the nth course at the nth constructive stage.

6.3.4 Overall stability (G.E.S.)

The compressive forces in the closed bricks courses act as hoop forces in domes of revolution, thus to evaluate the overall stability of the dome it is possible to assume the existence of a membrane behaviour and to determine a balanced surface [137]. Such surface depends on the compressive forces of the closed brick courses and on the brick's self-weight.

To estimate the balance surface, we adopt M.T.L.M. As shown in figure 6.3.1 (lunes representative A-A, B-B, C-C,) the octagonal dome is sliced by meridian planes into 32 lunes, in a manner so that for example the A-A section of A-A lune lies in the plane of

symmetry of the sail. The balance surface is identified through the thrust traced in all different sections (e.g. sections A-A, B-B, C-C in figure 6.3.1) one for each different lune, thus the thrust in all different sections needs to be assessed.

As denoted in chapter 6.3.3, the compression ring force of each closed brick course is constant, exactly as the hoop forces in domes of revolution. Therefore to trace the thrusts, one for each section, the same distribution of compressive ring forces must be considered. In domes of revolution under axisymmetric loads, the geometry of the hoop forces are described by circles, thus the hoop force can be described through their Δh^{xHoop} x-component and the ϑ angle (17), which is the half angle defining a lune measured on a horizontal plane as shown in figure 6.3.7.

$$\| \boldsymbol{H}_i^{Hoop} \| = \frac{\Delta h_i^{x\,Hoop}}{2 \cdot sin(\vartheta)} \tag{17}$$

However, in the octagonal dome under study, the actual geometry of rings compressive forces is not known they are affected by dome's geometry and by bricks pattern. Even from observing the spans of plate-bande structures, whose lengths vary from course to course it is clear that the shape of ring forces is affected by their shape. Thus, we make the assumption in our analysis that the ring forces H^{Ring} act normal to the lunes side faces, namely, the x component of ring forces can be described by the relation (18).

$$\Delta h_i^{x\,Ring} = 2 \cdot \| \boldsymbol{H}_i^{Ring} \| \cdot sin(\vartheta) \tag{18}$$

This adopted relation does not rely on the description of the actual geometry of ring forces, but it is based on the principle of equilibrium. According to the Safe Theorem [2], the real shape of the compressive rings is not significant, as long as the thrust line of the ring lies entirely within the thickness of the brick courses.

To prove the stability of the dome under construction, we compute the thrust at different construction stages. For each construction stage, the thrust line has been evaluated, at first the section A-A, shown in figure 6.3.7, subsequently, for sections B-B and C-C at the same construction stage (sections A-A, B-B, C-C are referred to figure 6.3.1). To calculate the thrust for sections B-B and C-C, the same distribution of ring forces found in section A-A is assumed. At the n^{th} constructive stage, to guarantee that the ring forces are sufficient to provide the forces required to achieve a stable equilibrium state of the n^{th} closed bricks course, the inequality (19) must be satisfied:

$$\| \boldsymbol{H}_n^{Ring} \| \geq \| \boldsymbol{H}_n^{R} \| \tag{19}$$

Therefore, if all thrusts are compatible with the prescriptions of the Safe Theorem and inequation (19) is verified, it is proven that the dome is in a state of stable static equilibrium.

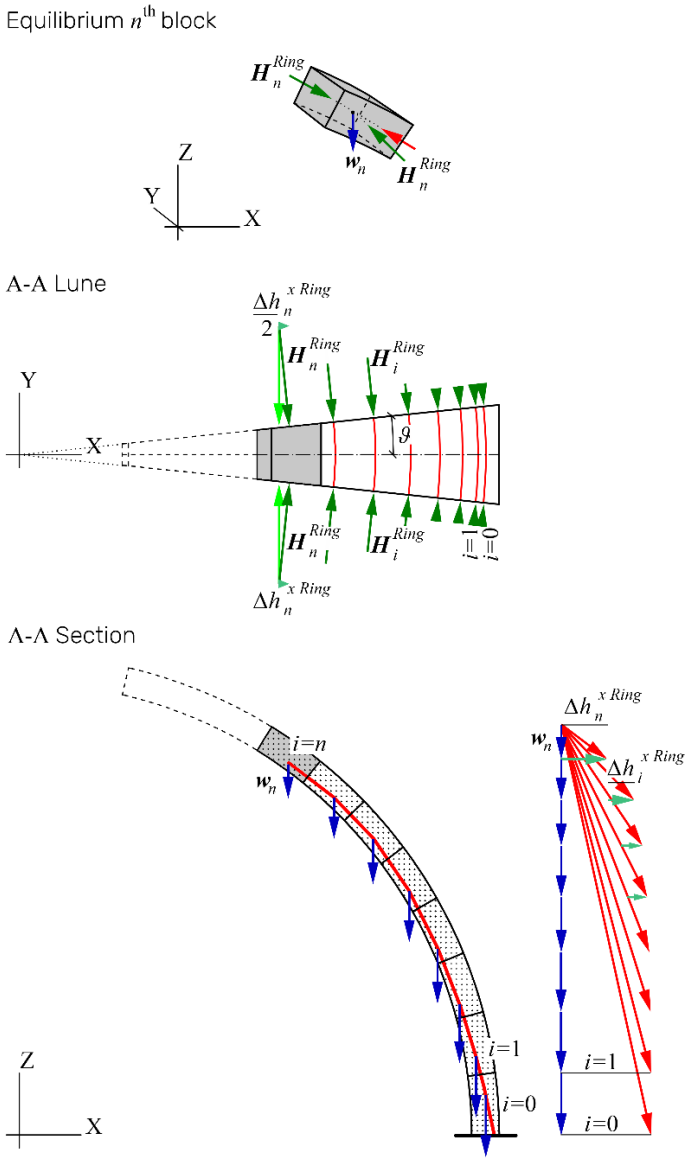

Figure 6.3.7 M.T.L.M for A-A lune at the n^{th} stage: equilibrium of the n^{th} wedge-shaped element (top), plane view of A-A lune and ring forces (center), A-A section and thrust line (bottom).

6.4 The numerical model

The equilibrium states of the dome under construction has also been verified through D.E.M. numerical analysis. The dome analysed has been modelled in the commercially available software 3.D.E.C. (Itasca, Minneapolis, MN, U.S.A.) based on a Discrete Element Modelling (D.E.M.) approach [101].

As introduced in chapter 3.3, discrete element methods can represent the behaviour of discontinuities and that of solid material; consequently, they can model the masonry in each of its parts: the bricks and the joints. In the numerical analyses the structure has been modelled as a system of discrete rigid bodies (the blocks), and their interfaces (the joints). Adopting a central finite-difference procedure, the behaviour of the system of rigid bodies is calculated by the explicit integration of the motion laws (20) (21), where (20) equation describes the translational motion law, while (21) equation corresponds to the rotational motion law, and k subscript denotes the k^{th} centroid of rigid body of the system modelled. D.E.M. can describe the failures of masonry through the contact detection and the evaluation of forces acting on the interfaces.

$$\ddot{x}_k + \alpha \dot{x}_k = \frac{F_k}{m} + g_k \tag{20}$$

$$\dot{\omega}_k + \alpha \omega_k = \frac{M_k}{I} \tag{21}$$

Each rigid body is constituted by the composition of real brick, see chapter 4.2.3, and a portion of mortar that surrounds the brick itself; thus, as mentioned, the joints represented by the interfaces between the blocks should describe all deformations of mortar and bricks and failures which could occur in the real structure.

A Mohr-Coulomb constitutive model has been implemented to represent the mechanical behaviour of the joints, with no cohesive

strength, finite compressive strength and no tensile strength. In the joint tangential direction, the stiffness is ruled by elastoplastic stress-displacement law, while the Coulomb friction coefficient defines the shear strength. Thus the three penalty coefficients govern the behaviour of the interfaces they are jKn the joint normal stiffness, jKs the joint shear stiffness and the Coulomb friction coefficient [111]. The jKn coefficient describes the difficulty of pressing blocks against each other: it rules the intensity of the distributed compression force occurring at a unit depth of the penetration between the two elements [113]. The jKs rules the shear stiffness of the contact, ensures that when a slight relative displacement increment occurs in the tangential direction between two blocks, a tangential force, equal to the displacement increment times the tangential stiffness, arises in the opposite direction, and prevents the contact from unrestricted sliding [113]. The last parameter is Φ, the angle for calculated the friction Coulomb coefficient.

All simulations performed have the purpose of evaluating the equilibrate state of structures. Following the two-stepped approach, the first simulation performed is related to the stability of the plate-bande, whose results are reported in chapter 6.4.1. The second step illustrated in chapter 6.4.2 and in Appendix C is relative to the simulations conducted on dome under construction.

6.4.1 Plate-bande numerical analyses

The numerical tests conducted for the plate-bandes (P.B. test) (L.E.S.) have the purpose of verifying the balanced state of the plate-bande themselves during the construction, thus to simulate different construction stages various inclinations of φ (the inclination of the laying plane) have been taken into consideration, at the top of figure 6.4.1 are reported the course analysed.

The volumic mass assumed in all analyses performed is equal to 2000 kg/m^3 and the gravitational acceleration g=9.81 m/sec^2. Due to

the specific goal of the analyses performed: during the construction, except for the self-weight no other loads have been considered. The values of the penalty coefficients jKn and jKs are not uniquely defined, in the last decades several theories concerning have been developed [110] [145]. To be rigorous and for respecting the composite characteristics of the rigid bodies modelled, they should be defined through a weighted average of mechanical and geometrical properties of joint mortar and bricks. Nevertheless this, to the aim of the P.B. tests (verify the stability of plate bande structure) and due to their low influence in the stability respect the Coulomb coefficient, it has been satisfactory to assume values obtained from literature belonging to similar problems [110] [113] [146]. The implemented values are: E=36 GPa and G =21 GPa [x], thus the values of penalty coefficients adopted are jKn=135 GPa/m, jKs=11 GPa/m.

The influence of Φ (the friction angle) has been detected evaluating a variety of values: 0°, 10°, 15°, 20°, 40°, 60°, 80°, 90° for each laying plane; the results of the P.B. tests shows that the stability of plate-bandes is related to the Φ and to the angle of inclination of laying plane. In particular, as reported in figure 6.4.1 (bottom), if the Φ is equal or larger than 10°, the plate-bande structures are stable. The results also show that for low angles of φ (the inclination of the laying plane) which correspond until the course i=33, the equilibrium of plate-bandes structures is not related to the Φ, and the results are presented in Table 01.

The main outputs recorded through the numerical simulations are these three: the displacement, the z component of velocity (z-velocity) and the unbalanced force. The first two elements are directly related to the motion of the discrete system, they provide information about the motion of specific points of the structure observed.

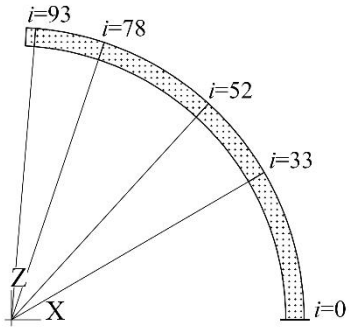

Courses analysed.

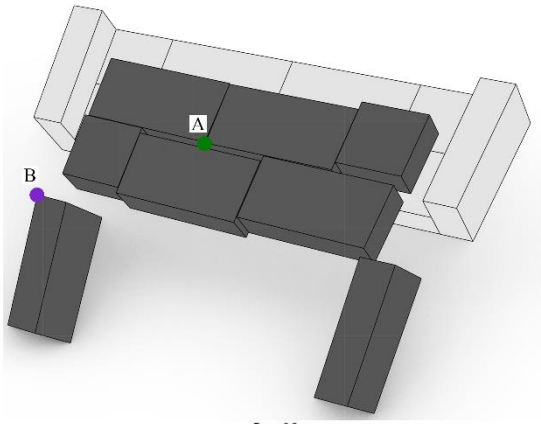

$\Phi = 0°$

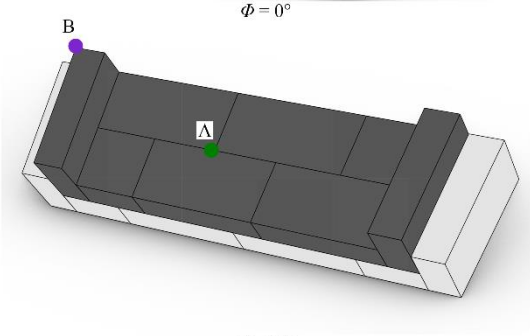

$\Phi = 10°$

Figure 6.4.1 From top to bottom: courses analysed for P.B. tests; plate-bande during collapses (i=52, φ=47°, Φ=0°); plate-bande equilibrates (i=52, φ=47°, Φ=10°).

		Φ	
	φ	0°	⩾10°
i= 33	30°	stable	stable
i= 52	47°	unstable	stable
i= 78	71°	unstable	stable
i= 93	86°	unstable	stable

Table 02 Stability of plate bande.

Referring to figure 6.4.1 for each simulation, displacement and z-velocity are registered for two points (A and B), (B) the first is adopted to illustrate the motion of herringbone bricks and the other (A) for recording the behaviour of the horizontal bricks.

The unbalanced force represents the summation of all nodal forces for each time-step of simulations, for static analyses, the Unbalanced force furnishes global information regarding the state of the system: theoretically, when the equilibrium state is reached the net nodal force vector at the centroid of all rigid bodies is zero, thus the unbalanced force is zero. Nevertheless, for numerical analyses, such quantity tends to zero, but practically this will never reach zero. The discrete system of rigid bodies can be assumed to be at equilibrium when the magnitude of the maximum unbalanced force is small compared to the representative forces of the previous problem [101].

Figure 6.4.2 reports the variation of three quantities (unbalanced force, displacement and z-velocity) calculated for the plate-bande illustrated in figure 6.4.1, during the simulations. For all graphs the

x-axis reports the time-step of analyses, a parameter which describes the progression of the simulation, instead the y-axis illustrates the quantity recorded.

The first graph reports the evolution of the unbalanced force, the red line describes the behaviour of plate-bande analysed with Φ that is $10°$, in this case after few time-steps a peak occurs then the unbalanced forces is almost zero. Consequently, the structure is balanced, after an adjustment phase, where the rigid bodies act one against another. This behaviour is also shown by the z-velocity graph where in correspondence to the unbalanced force peak, the z-velocity is not zero, but after that, this quantity becomes zero and no motion occurs, while the displacement graph is practically zero all through the simulation. In the simulation conducted with $\Phi=0°$, the unbalanced force never attains the zero and z-velocities of the A and B points change variously during the time. At the beginning of the numerical analysis, the two z-velocities have opposite signs, then the sign of B point z-velocity changes and both quantities are negative. This indicates that the vertical blocks, which represents the herringbone bricks, pushes the horizontal elements towards the external of plate-bande, while they slide on the inclined plane in the opposite direction, after a few steps even the horizontal blocks slide down. The displacement graph is coherent to the behaviour described, on the graph three different phases are readable: the first in which A and B displacements increase, a second one correspondents to the inversion of motion and the last one where the A displacement decreases because the horizontal blocks slide on the laying plane. Due to the small number of rigid bodies modelled in the P.B. Test, all of which are involved in an eventual collapse, it can be assumed that the system is balanced when the z-velocity of even just one point is zero and constant for a finite time interval.

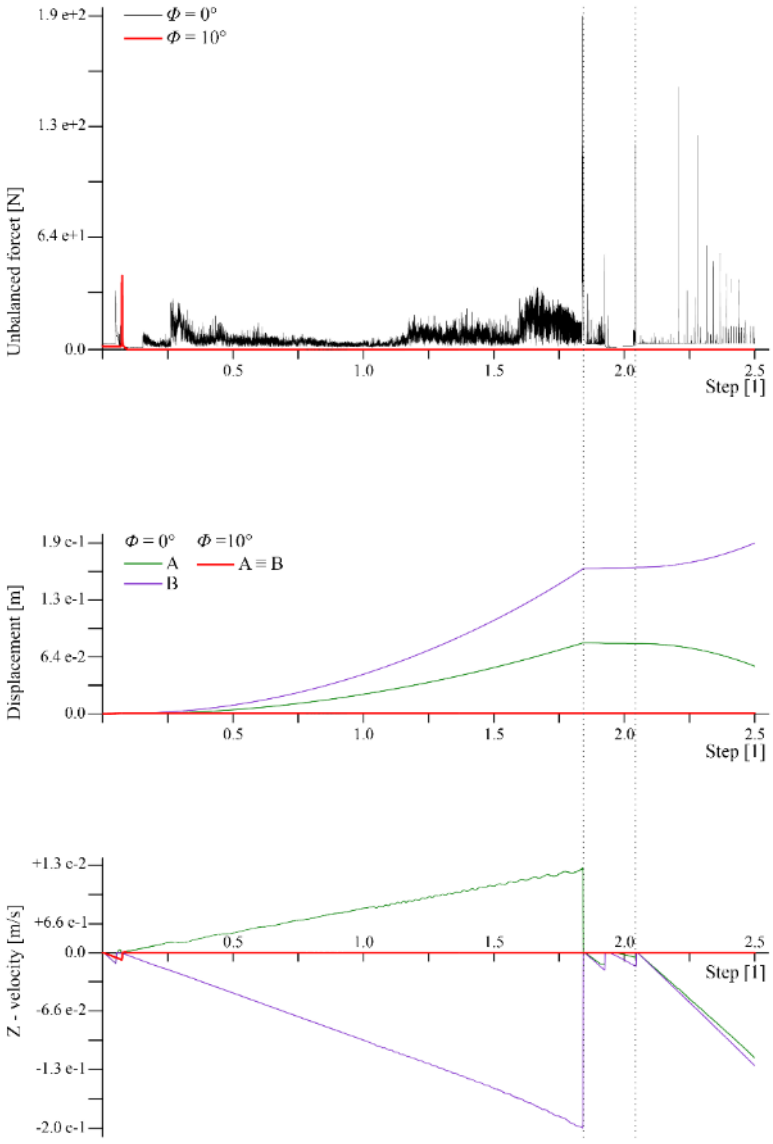

Figure 6.4.2 Graphs for evaluating the state of a plate-bande represented in figure 6.4.1. From top to bottom: unbalanced force, displacement and z-velocity.

6.4.2 Numerical analysis of dome under construction

Following the two-stepped approach presented in chapter 5.2, once verified the stability of plate-bande through the P.B. Tests, two other structures are evaluated for different construction stages (n): the closed bricks course (C.B.C. Test) (L.E.S.) and the dome under construction (D.U.C. Test) (G.E.S).

Two geometrical models have been evaluated: an octagonal dome as Santa Maria in Ciel d'Oro dome, and a hemispherical dome similar to Simon Mago. Both systems of rigid bodies are constituted by blocks which dimensions correspond to the brick dimensions, as described in chapter 6.4.1. The masonry pattern adopted coincide to the pattern formed by cross-herringbone spiralling technique.

Both types of numerical analyses (C.B.C Test and D.U.C. Test) have been assessed simulating the constructive process, i.e. adding one course upon another. Once the equilibrium state has been reached for a given completed course, the next one is added and the overall analysis is performed again to assess the stability of the new overall structure built, in such manner the stability relative of the new construction stage is evaluated. The graph of unbalanced force related to these analyses records numerous peaks at least one for each brick course added, the first graph shown in figure 6.4.3 illustrates the evolution of this quantity recorded for the octagonal dome analysed, while the other two graphs represent the unbalanced force record under different condition. The central graph refers to a complete dome analysed applying g=9.81 m^2/s, while the graph at the bottom describes the same structure but, in this case the gravity value is applied in different time intervals, i.e. first g=0.981 m^2/s, then g=1.96 m^2/s up to g=9.81 m^2/s. This method should reflect the formwork removal operations. The temporal evolution of the unbalanced force in the three graphs reflects the nature of simulations, the alternation of peaks and flat sections readable in the first diagram correctly describes the evolution of the

state of equilibrium during the construction stage of a dome built without the formworks aid.

As shown in Appendix B, the balanced state varies depending on the construction stage: the hoop forces and the meridian forces change during the construction. This variation is intuitable even by the distribution of the unbalanced force, which for each brick course added a peak occurs, and after that, a flat section could manifest, to testify the new state of equilibrium. Figures 6.4.4 and 6.4.5 highlight this concept, where a portion of the dome is displayed e analysed. More precisely, the graphs of figure 6.4.5 are referred to the dome portion modelled in figure 6.4.4. The evaluation of the balance of the courses included between the 28^{th} and 33^{rd} (i=28-33) of an octagonal dome is the subject of the analyses performed. The simulation has been carried out assuming jKn=100 GPa/m, jKs=10 GPa/m and Φ=89° [113], and adding the courses one at a time (as described above), with the exception of the 33^{rd} brick course, where, as shown in figure 6.4.4 (in the centre and bottom), it has been added in two different time intervals: first only three plate-bandes (j=1, 2, 3; i=33), and then the remaining part of the course. As affirmed this process is clearly readable in the graph of the unbalanced forces where seven peaks are recorded, one for each brick course plus another, of lower intensity, for the addition of the three plate-bandes. Figure 6.4.5 each peak is located in a specific and distinct time interval, therefore pursuing the illustrated logic it is possible to determine a correspondence of the different construction stages and the time-steps of analysis.

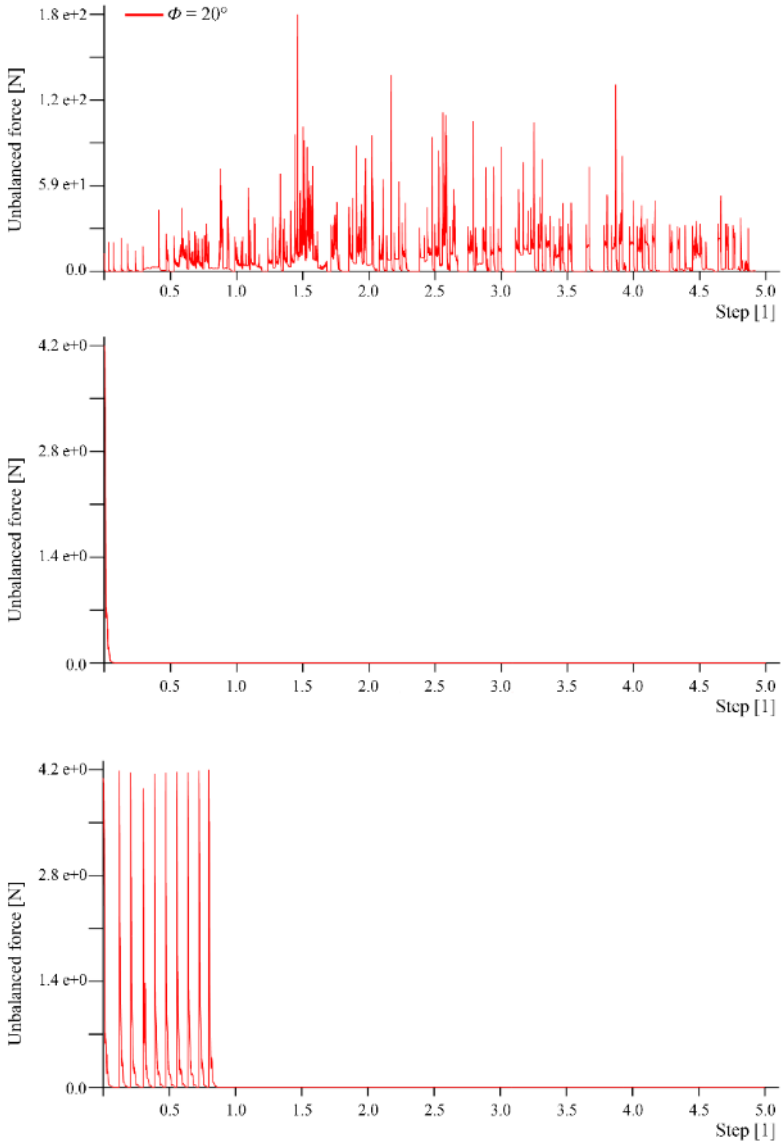

Figure 6.4.3 Unbalanced force graphs. From top to bottom: dome under construction, complete dome (g=9.81 m^2/s), complete dome considering the formwork removal operations (g=9.81, 1.962, ..., 9.81 m^2/s).

The other two graphs of figure 6.4.5 show the evolution of displacement and z-velocity relating to point A and B belonging to 28^{th} bricks of course (see figure 6.4.4), on these graphs no variation is recorded relative to the addition of blocks of plate bande (j=1, 2, 3; i=33). Such behaviour indicates that the perturbation of the balanced state due to the three plate-bandes it is just local confirming the hypotheses proposed in chapter 5.2.

Respect to the displacement graph reported in figure 6.4.2 the same quantity illustrated in figure 6.4.5 highlights the existence of movements due to the adjustment of brick courses laid when a new brick course is added.

To demonstrate the stability of the complete courses, a series of C.B.C Test is performed, precisely at n=28, 52, 65, 78 construction stages for the octagonal dome, while n=27, 43, 66, 70 for hemispherical one. For each stage the same physical properties as for the P.B Test have been observed. The C.B.C Test consists of evaluating the displacement, z-velocity and unbalanced force relative of the last bricks course laid (i=n) at the n^{th} constructive stage. For example, to prove the stability of the 28^{th} complete course, 28 complete courses have been modelled, and the maximum displacement and velocity of the bricks in the 28^{th} course have been recorded. The structural behaviour of the whole domes under construction is assessed (D.U.C. Test), in these numerical analyses the displacement and z-velocity have been recorded at several courses unlike the closed brick course tests, the displacements and velocities. For all numerical analyses (C.B.C Test and D.U.C. Test) only the first laying plane has been constrained and none of the other bricks. The joint penalty coefficients assumed are jKn=100 GPa/m, jKs=10 GPa/m, while a variety of friction angle is investigated.

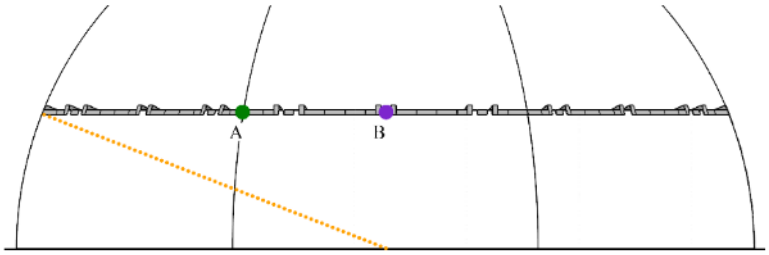

Course analysed: $i = 28$
Construction stage: $n = 28$

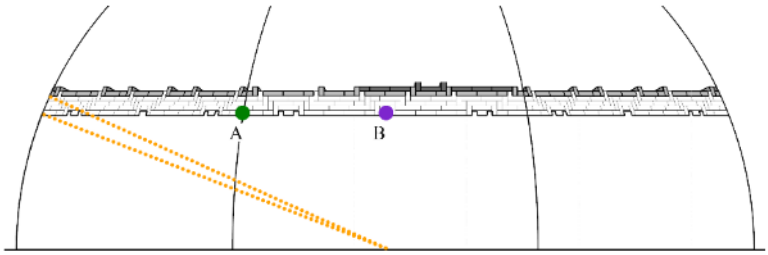

Course analysed: $i = 28$
Construction stage: $n = 33 \quad j = 1, 2, 3.$

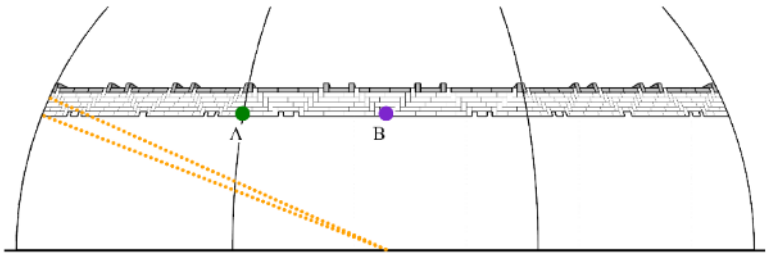

Course analysed: $i = 28$
Construction stage: $n = 33$

Figure 6.4.4 Dome under construction. From top to bottom brick course i= 28, brick courses from i= 28 to i=32 and plate bande j= 1, 2, 3, brick courses from i= 28 to i=32.

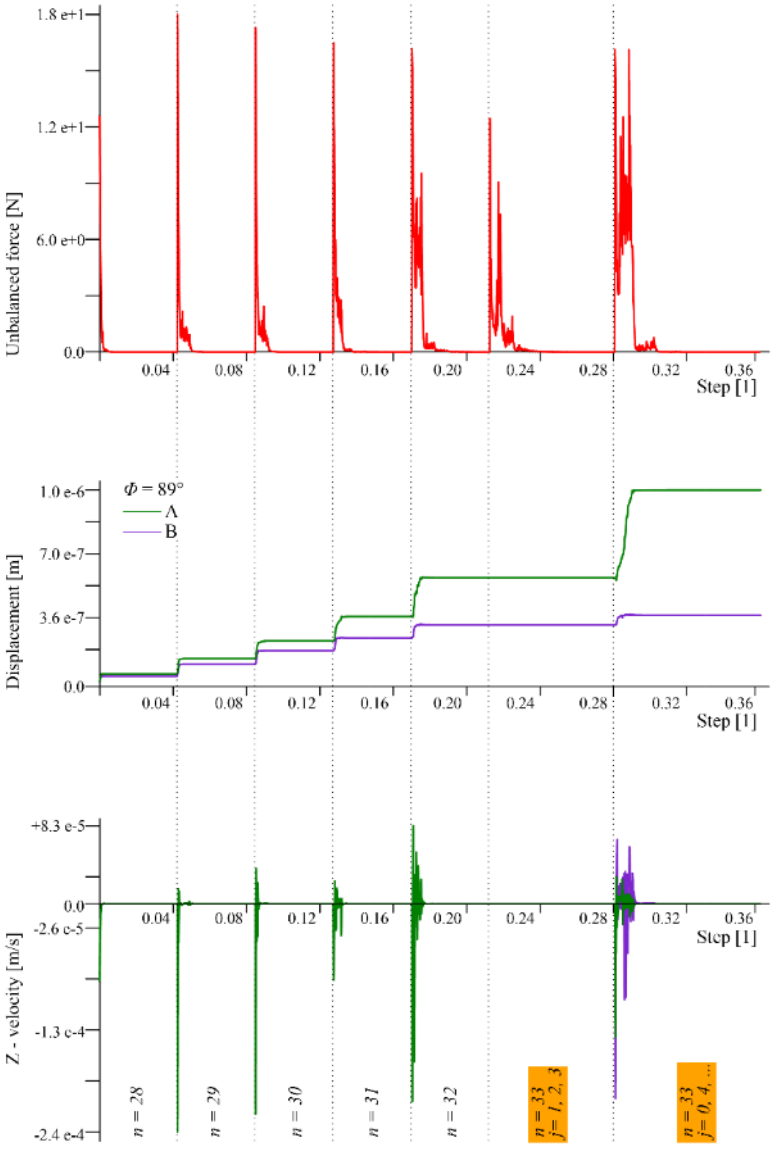

Figure 6.4.5 Graphs of dome under construction shown in figure 6.4.4. From top to bottom: unbalanced force, displacement and z-velocity.

results of C.B.C and D.U.C. Tests show that the maximum z-velocity to which the blocks are subjected coincides with that of the construction stage in which they are laid. Rare high magnitude z-velocities occur randomly, especially in the hemispherical model where the blocks are modelled with some geometrical imperfections, thus these randomly z-velocity could be associated with the presence of imperfections. A resume of the z-velocity graph is reported in Appendix C, where the evolution of z-velocities relative to different points of octagonal and hemispherical domes are graphed.

Table 03 summarizes results of D.U.C. Tests that were executed on octagonal dome modelled considering the interval of brick courses between i=28 up to i=93. The same variety of friction values of P.B. Tests has been. As Appendix C shows, the results in term of stability are coherent with table 03 even for the hemispherical structure analysed.

		Φ	
	φ	0°	⩾10°
i= 28	26°	unstable	stable
i= 52	47°	unstable	stable
i= 65	59°	unstable	stable
i= 78	71°	unstable	stable
i= 93	86°	unstable	stable

Table 03 stability of D.U.C. tests.

Based on the results of the analysis for a wide range of friction angles and construction stages, displacement surfaces relative to

a specific point of the dome under construction can be shaped. Figure 6.4.6 shows the displacements surface recorded for a point in the middle of the sail at the 52nd course of the octagonal dome. Thus, the surface is related to the constructive stages range n=52-93 and to the friction angles between Φ=10° and 89°. Friction angles less than 10° have not been considered because even the plate-bandes structures are not stable at such low friction angles.

Referring to figure 6.4.6 the maximum dome displacement recorded is less than 2 mm, a value really low even for structures built using formworks aid, nevertheless this inaccuracy, the displacement surface provides valuable information relative to the dependence of displacement, friction and construction stages.

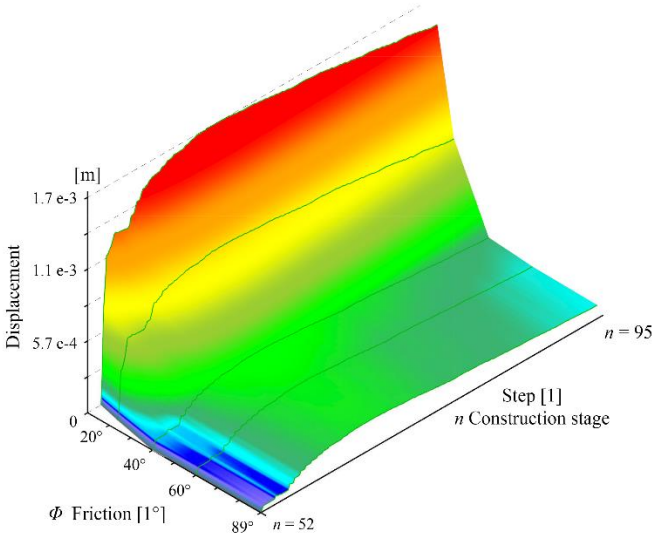

Figure 6.4.6 Graphs of displacement surface relative to A point of an octagonal dome placed in the middle of sail at 52nd brick course.

is to ascribe to values assumed by jKn, jKs and mostly to the Mohr-Coulomb joint constitutive model implemented, more accurate analyses could be conducted changing the constitutive model, but for the purpose of the analyses -testify the existence of plate bande structure in the dome under construction- this inaccuracy does not affect. Even larger displacements can occur when the bricks were laid, but in actual domes during the laying, the cohesion property of mortar is enough to prevent slide for a short time interval, just until the plate bande is formed.

Figure 6.4.6 shows a low correlation between the friction angles and displacement, at least for friction angle values lager of $30°$. This independence is also verified in the other graphs of the same quantity relative to the octagonal model shown in Appendix C. As illustrated in figure 6.4.5 the displacement curves are described by stepped curves, but as figure 6.4.6 displays (e.g. Φ=89°), they present a maximum. The resultant displacement surfaces display a bump region located in the central part of the surface, which reflects the maximum displacement reach for the different friction angles. After that, regardless of friction, the displacements decrease. Therefore the displacement surfaces record the “breath” of the dome under construction [147] which characterised the domes built without any support, starting from these surfaces is possible tracing the movements of the dome during its building. The “breath” phenomenon could be explained by observing the variation of vertical thrust under construction (see Appendix B): once a brick course has been laid, very small settlements toward the centre of the dome occur at this course, but after an initial period the thrust which acts in meridian direction increases and pushes outward the bricks and thus they tend to return to the initial configuration.

Part III

7. Conclusion

The research presented in this dissertation cannot be considered complete and more aspects could be investigated further in this field. However, that, various considerations in the report could be traced. Through the study of historical technologies, the past application of a self-supporting technology has been testified through a case of the cross-herringbone spiralling technique. An approach to evaluate masonry shells during their construction has also been defined: the two-stepped approach.

7.1 The cross-herringbone technology a self-balanced technology

The Brunelleschi herringbone technique was certainly known by the Sangallo architects in the 16th century, who developed the cross-herringbone spiralling technology, a self-supporting construction method for building masonry domes and vaults based on his technique (chapter 4.1).

The herringbone and cross-herringbone were applied for over a century in the central region of Italy. The reason for their limited temporary use and restricted spread have not been investigated, but some assumptions can be derived based on the historical-cultural context they are located within. These two techniques require considerable skills, only a trained master mason could correctly execute, and over this the secret nature of the knowledge of the system, justifies the defined geographical area.

The disappearance of the Sangallo school of architects, the reduced need to build domes in a fast manner, and different political context may have caused the loss of the theoretical and technical knowledge of these vaulting systems.

Nowadays several domes present the herringbone pattern are rediscovered, and a list of them is reported in Appendix A. Among them, due to peculiar characteristics two structures has been studied. They are Santa Maria in Ciel d'Oro and Simon Mago (chapter 4.2.2): both designed by Antonio da Sangallo the Younger, and both with a cross herringbone. These structures are not plastered and are perfectly conserved, providing valuable and relevant information on the peculiarity of the cross-herringbone techniques.

Even in the historical document conserved in the Uffizi museum there are evidence of the existence of cross-herringbone spiralling technology (figure 4.1.2, drawing 1330 (n. 594469) GDSU). This technology is different from the herringbone technology and requires a detailed executive scheme and a precise tracing system as the preliminary operations, without which a self-supporting system cannot be implemented.

7.2 Considerations concerning: the two-stepped approach

From the observation of self-supporting technologies, take into account Heyman's theory and the behaviour of single bricks during their laying, a frame approach needed to assess the state of masonry structure during their construction is proposed. This approach called two-stepped approach (chapter 5.2) is based on the **Local Equilibrium Step** and the **Global Equilibrium Step**.

The two-stepped approach is formulated to verify the state of shells under construction, but it could even provide a process to evaluate the stability of other masonry structures such as arches or walls.

Through the implementation of the two-stepped approach, productivity, and the economic issues can be related to the stability problem and analysed, i.e. to reduce the costs and increase the productivity for building masonry shells it is possible to evaluate the state of the structure under construction and eliminate the unnecessary expenses.

Further, referring to the n^{th} construction stage of a masonry shell, different considerations are proposed:

- 1st independence property: the equilibrium at $i=n^{th}$ brick course, i.e. at the local scale, is related to the building technology adopted, while the overall equilibrium, i.e. referring to the whole structure already built, is ruled by geometry.
- 2nd independence property: the methods to assess the local equilibrium and the overall state can be not related, in particular for evaluating the stability of the nth brick course, the nature of the primary factor (chapter 5.1) must be taken into account.

- 1st dependency property: to achieve a balanced state during the construction, the overall state of shells must satisfy the conditions required at the local scale of structures analysed.
- 2nd dependency property: Even during the construction stage, the Heyman's hypotheses are not violated, thus the overall equilibrium of masonry shells, built using self-supporting technologies, is governed by their geometry.

The two-stepped approach provides a process for evaluating the state of masonry structures during the construction, its implementation must take into account the technology used to build the structure considered.

Within this research it has been developed considering the cross-herringbone spiralling technology. The two-stepped approach has been implemented following the limit analysis, as well as adopting static graphic tools (see chapters 6.3.2, 6.3.3 and 6.3.4). Even the numerical simulations have been performed following the logic of two-stepped approach (D.E.M. simulations, chapters 6.4.1 and 6.4.2).

7.3 Dome behaviour during construction - Case study: the cross-herringbone spiralling technology

During the construction of masonry domes built without shoring or formwork, the overturning of a partially constructed sail and/or the sliding of local bricks or brick courses can lead to an unstable equilibrium state of the dome and ultimately structural failure. Traditional masonry construction technologies do not intentionally address such construction failure mode and resort to costly auxiliary support systems.

The case studies of an octagonal and a hemispherical dome patterned with a spiralling cross-herringbone layout, proves that this brick layout enables self-balancing domes during all phases of construction without formwork or shoring. Through the plate-bande structures found in the incomplete brick course, a resistance mechanism is discovered that enables a self-balanced state by mobilising the underlying completed brick courses through the bonding with the herringbone bricks, linking new incomplete courses to the already completed underlying ones. Once the brick course is closed, the plate-bandes structures are no longer necessary to sustain dome's stability, but instead they start to offer support to fix the herringbone bricks in the next course.

The existence of the plate-bande structures, the closed bricks courses and the stability of the dome under construction is demonstrated through the D.E.M. analysis performed. As highlighted in chapters 6.4.1 and 6.4.2, even for low values of friction between the brick surfaces, the dome finds a balanced equilibrium state.

For real friction angle values, D.E.M. analysis shows maximum displacements of only 1.8 centimetres (hemispherical dome displacement recorded at i=64 brick course and n=73 construction stage, Appendix C). However, what is more relevance is the

evolution of the motion of the bricks once the plate-bande and the closed brick course actions are mobilised. After that initial motion of the bricks, no further motion occurs. Therefore the **I.** Heyman's hypothesis (see chapter 3.2) is not violated even under construction and even the **II.** and **III.** hypotheses are verified (2nd dependency property).

The limit analyses performed during the construction of the two case studies (see Appendix B) highlights the variation of the force required to reach the self-balanced state concerning the building stage analysed. This is independent of the i brick course observed and the maximum compressive ring forces required to achieve the self-stability is recorded in correspondence to the $i = n^{th}$ construction stage. In other words, the most critical construction stage is precisely when the bricks of i course are being laid.

7.4 Future vision

Although the equations of equilibrium defined in chapter 6.3.2, 6.3.3 and 6.3.4 are used to verify the equilibrium state of the dome, they can be easily adapted to design other self-balanced domes. Currently, three-dimensional rigid structural surfaces (such as shells and domes) need formwork and shoring material during construction, which goes to waste once the structure is completed, adding to the economic and environmental cost of the project. In this document, a historic masonry dome construction technique, based on the spiralling cross-herringbone pattern, has been shown to enable statically stable geometries throughout the construction process without the need for any external support system. These self-balancing structures have no theoretical limit to their size. The disruptive potential of this historic masonry pattern comes to the fore for today's construction industry when this technology is viewed in the context of other emerging innovations such as novel structural form-finding approaches and robotic construction technologies [148] [149] [150]. For example, it is envisaged that masonry rigid surfaces could be tailored in their shape through form-finding approaches [19] [151] [152] and patterned with the herringbone pattern to be effectively produced using robots without any falsework and yet be stable during all stages of construction and their service life.

Appendices

Appendix A

List of possible sites

The following list provides an overview of buildings designed by Sangallo architects, especially by Antonio the Younger, in which the herringbone or cross-herringbone spiralling technology was probably applied. These buildings have been chosen because the presence of domes is testified and for other similar structure the herringbone or cross-herringbone technique was applied.

The list was written by consulting various sources but cannot be considered complete. The purpose of this document is to prove that the use of the herringbone technique and or cross-herringbone is not sporadic but rather systematic. The date reported denotes the beginning years of the structure considered. The ** mark labels the structure where the presence of the herringbone or cross-herringbone spiral technique is testified.

List of sites:

Basilica of Santa Casa**
Place: Loreto (Ancona).
Date: 1468.
Architect: Giuliano Sangallo.
Source: [125].

Porta Nova
Place: Colle di Val d'Elsa (Siena).
Date: 1479.
Architect: Giuliano Sangallo.
Source: [125].

Medici Villa
Place:Poggio a Caiano (Prato).
Date: 1480.
Architect: Giuliano Sangallo.
Source: [125].

Santa Maria delle Carceri
Place: Prato.
Date: 1484.
Architect: Giuliano Sangallo.
Source: [125].

Poggio Imperiale**
Place: Poggibonsi (Siena).
Date: 1488.
Architect: Giuliano Sangallo, Antonio Sangallo the Elder.
Source: [62] [125].

Palazzo Della Rovere
Place: Savona.
Date: 1489.
Architect: Giuliano Sangallo.
Source: [58] [123].

Fort Sangallo
Place: Civita Castellana (Viterbo).
Date: 1495.
Architect: Antonio Sangallo the Younger, Antonio Sangallo the Elder.
Source: [58] [123].

Medici Fortress di Sansepolcro**
Place: Sansepolcro, (Arezzo).
Date: 1500.
Architect: Giuliano Sangallo.

Source: [124] [125].

Medici Fortress**
Place: Arezzo.
Date: 1502.
Architect: Giuliano Sangallo, Antonio the Younger and Antonio Sangallo the Elder.
Source: [62] [124].

Church of Santissima Annunziata
Place: Arezzo.
Date: 1503.
Architect: Antonio Sangallo the Elder.
Source: [124]. [153].

Fortress of Nettuno
Place: Nettuno (Rome).
Date: 1503.
Architect: Giuliano Sangallo Antonio Sangallo the Elder.
Source: [124].

Fortress of Castrocaro**
Place: Castrocaro Terme and Terre del Sole (Forlì).
Date: 1504.
Architect: Antonio Sangallo the Younger, Antonio Sangallo the Elder.
Source: [62] [124].

Temple of San Giovanni in Oleo
Place: Rome.
Date: 1509.
Architect: Antonio Sangallo the Younger.
Source: [123].

Church of Sant'Egidio

Place: Cellere (Viterbo).
Date: 1513.
Architect: Antonio Sangallo the Younger,
Source: [123] [124].

Rocca Farnese
Place: Capodimonte (Viterbo).
Date: 1513.
Architect: Antonio Sangallo the Younger,
Source: [123] [124].

Oratorio di Santa Caterina
Place: Bisentina di Capodimonte island, Bolsena lake, (Viterbo)
Date: 1516.
Architect: Antonio Sangallo the Younger.
Source: [124].

Church of San Biagio
Place: Montepulciano (Siena).
Date: 1518.
Architect: Antonio Sangallo the Elder.
Source: [154].

Fortress Vecchia**
Place: Livorno.
Date: 1519.
Architect: Antonio Sangallo the Elder.
Source: [62] [125].

Church of Santa Maria in Ciel d'Oro**
Place: Montefiascone (Viterbo).
Date: 1523.
Architect: Antonio Sangallo the Younger.
Source: [71] [127].

Cappella Cesi in Santa Maria della Pace**
Place: Rome.
Date: 1530.
Architect: Antonio Sangallo the Younger.
Source: [124] [155].

Palazzo Farnese
Place: Caprarola (Viterbo).
Date: 1530.
Source: [123].

Fortezza da Basso**
Place: Florence.
Date: 1534.
Architect: Antonio Sangallo the Younger.
Source: [123]. [124].

Bastion Sangallo
Place: Rome.
Date: 1537.
Architect: Antonio Sangallo the Younger.
Source: [125].

Rocca di Nepi
Place: Nepi (Viterbo).
Date: 1537
Architect: Antonio Sangallo the Younger, Antonio Sangallo the Elder.
Source: [123] [155].

Rocca Paolina
Place: Perugia.
Date: 1540.
Architect: Antonio Sangallo the Younger.
Source: [58] [123].

Simon Mago dome and domes of Octagons in San Pietro**
Place: Roma.
Date: 15--.
Architect: Antonio Sangallo the Younger.
Source: [59] [127].

Appendix B

Limit analysis

The limit analysis has been performed for two different domes, one octagonal and the other hemispherical, the two structures have dimensions comparable to the Santa Maria in Ciel d'Oro dome. The internal diameter of the octagonal dome is 9.4 m and the thickness is 0.24 m, while the hemispherical one has radius 4.0 m and thickness 0.24 m. The two structures present the cross-herringbone pattern, the maximum distance between two loxodromes is 1.4 m measured at the base of hemispherical one. The analyses have been conducted for different construction stages, following the formulation introduced in chapter 6.3 and considering ρ=20 kN/m^3 and Φ=20°. The results are summarised in table 04 and 05 and in following technical sheets. The hemispherical dome has been divided by an angle of ϑ =11.25°, while the three lunes exposed in chapter 6.3.4 has been studied. According to the literature [92] [156] the octagonal dome is not stable, the thrust at the complete dome of C-C section does not lie entirely in the section of the dome, hence fill or abutment should be considered. Nevertheless, the purpose of the analyses is to highlight the variation of the hoop forces during the construction. As expected, the thrust or ring forces, listed in table 04 and 05, change as a function of the construction stage. For all construction stages the ring forces are larger near the last course laid than those located at the first level laid. From these tables it can be seen that the magnitude of ring forces required to achieve stability decreases drastically during construction. At the early construction stages, the magnitude of the ring forces is comparable to the thrust forces required to balance the plate-bandes (octagonal dome) or arches (hemispherical dome), but near the crown, their magnitude increases independently of the plate-bandes thrusts. This observed difference is due to the geometry and dimension of the

plate-bande structure and of the entire dome. The spans of plate-bandes decrease from the base to the dome's crown around 70-80%, unlike the ring forces required to achieve a balanced state of the whole dome, which, at complete construction, increase from the base of the dome to the crown much more than 100%.

Plate-bande			
	Stage $n = i$		
	33	52	93
j	1	3	1
$\|\|H_{nj}^{PB}\|\|$ [N]	104.4	243.6	113.5
Closed brick course			
	Stage n		
	33	52	93
$\|\|H_{n}^{R}\|\|$ [N]	104.4	243.6	113.5
Dome under construction			
	Stage n		
	33	52	93
$\Delta h_{33}^{x\ Ring}$ [N]	210.0	35.6	3.0
$\Delta h_{52}^{x\ Ring}$ [N]		276.0	3.5
$\Delta h_{93}^{x\ Ring}$ [N]			794.0
$\|\|H_{n}^{Ring}\|\|$ [N]	538.2	707.4	2034.9

Table 04 Results of limit state analysis for the octagonal dome analysed.

Arch				
	Stage $n = i$			
	27	59	68	77
$\|\|H_{nj}^{PB}\|\|$ [N]	117.6	152.3	68.0	56.2
Closed brick course				
	Stage n			
	27	59	68	77
$\|\|H_{n}^{R}\|\|$ [N]	104.4	243.6	113.5	
Dome under construction				
	Stage n			
	27	59	68	77
$\Delta h_{27}^{x\ Ring}$ [N]	386.0	15.4	1.9	1
$\Delta h_{59}^{x\ Ring}$ [N]		640.0	34.0	24.0
$\Delta h_{68}^{x\ Ring}$ [N]			720.0	35.4
$\Delta h_{77}^{x\ Ring}$ [N]				918.0
$\|\|H_{n}^{Ring}\|\|$ [N]	989.3	1640.3	1845.3	2352.8

Table 05 Results of limit state analysis for the hemispherical dome analysed.

Octagonal dome

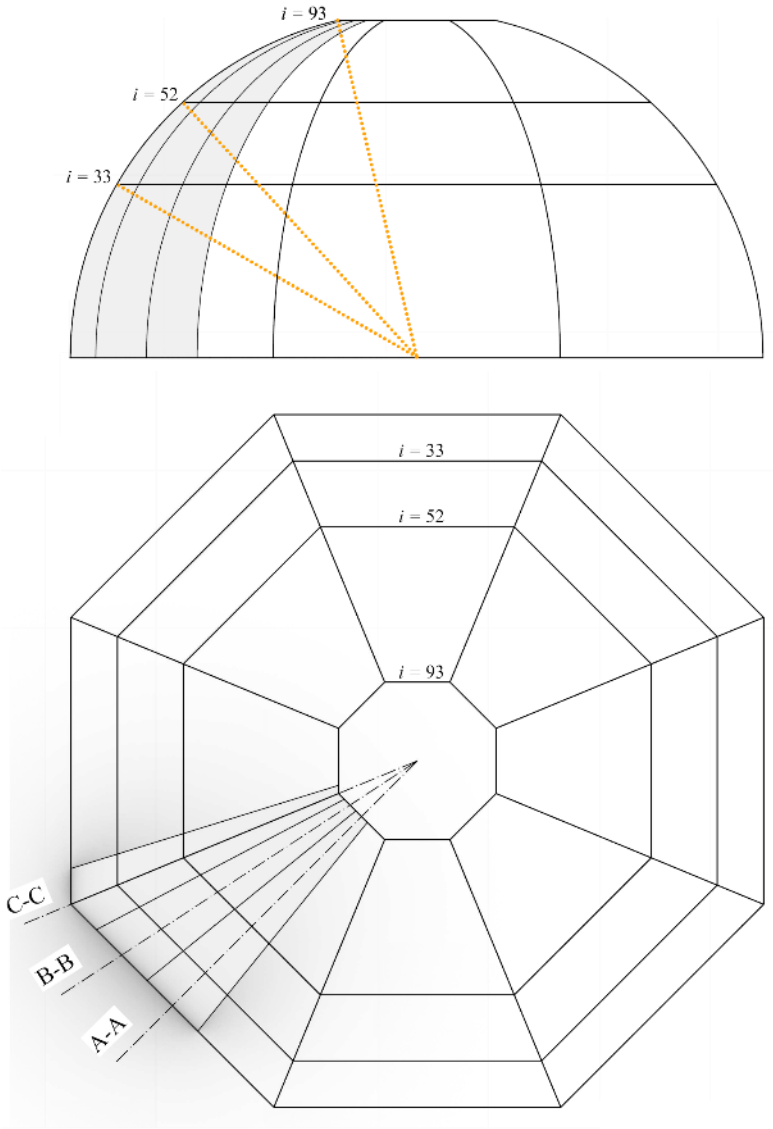

Key-section for analyses:
Constrcution stage analysed: i =33, 52, 93

Construction stage n=33

A-A section

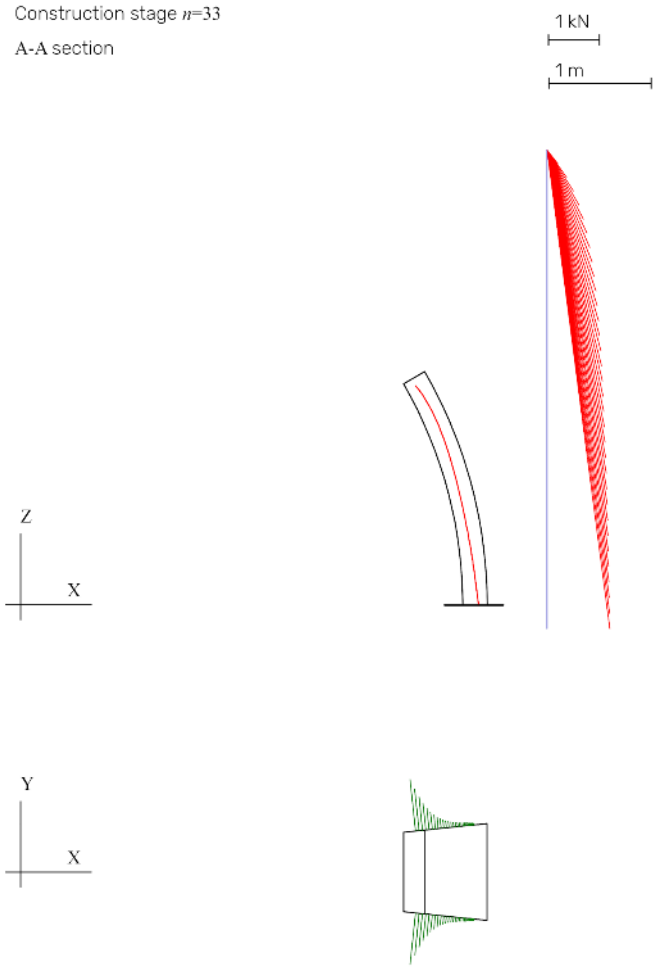

Construction stage n=33

B-B section

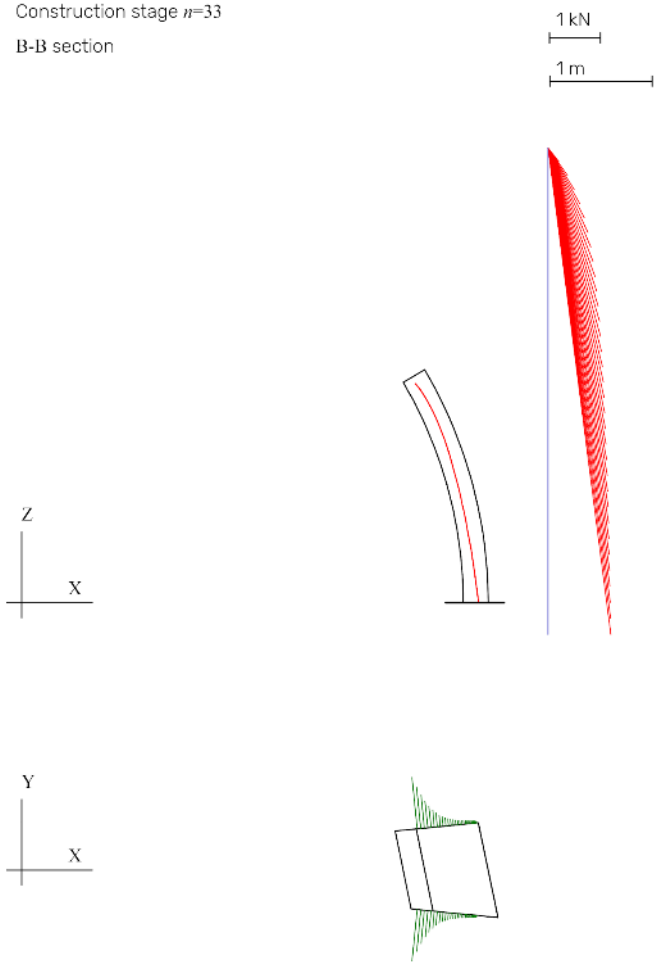

Construction stage n=33

C-C section

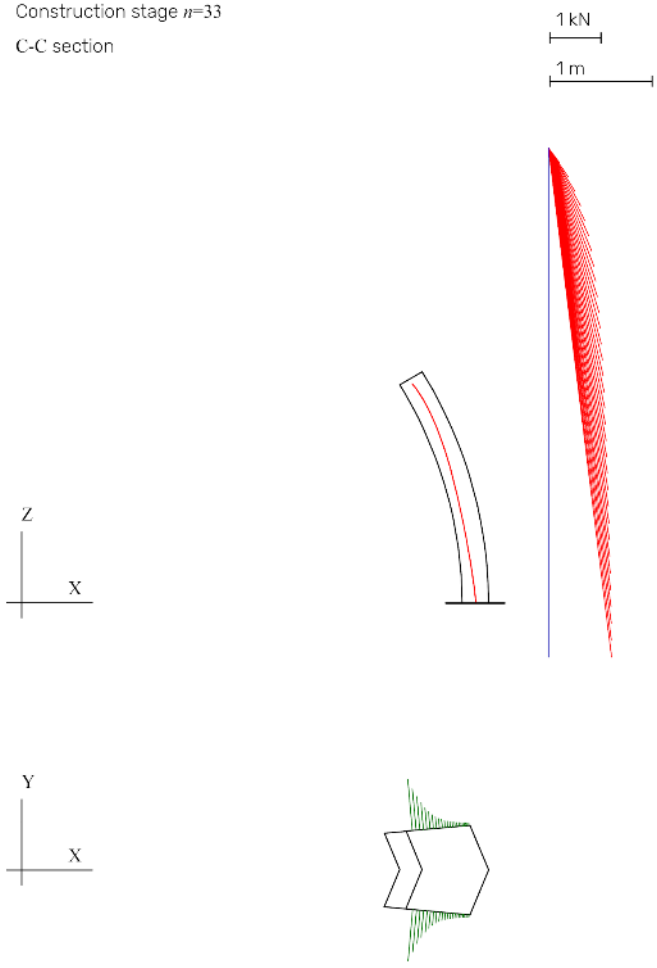

Construction stage n=52

A-A section

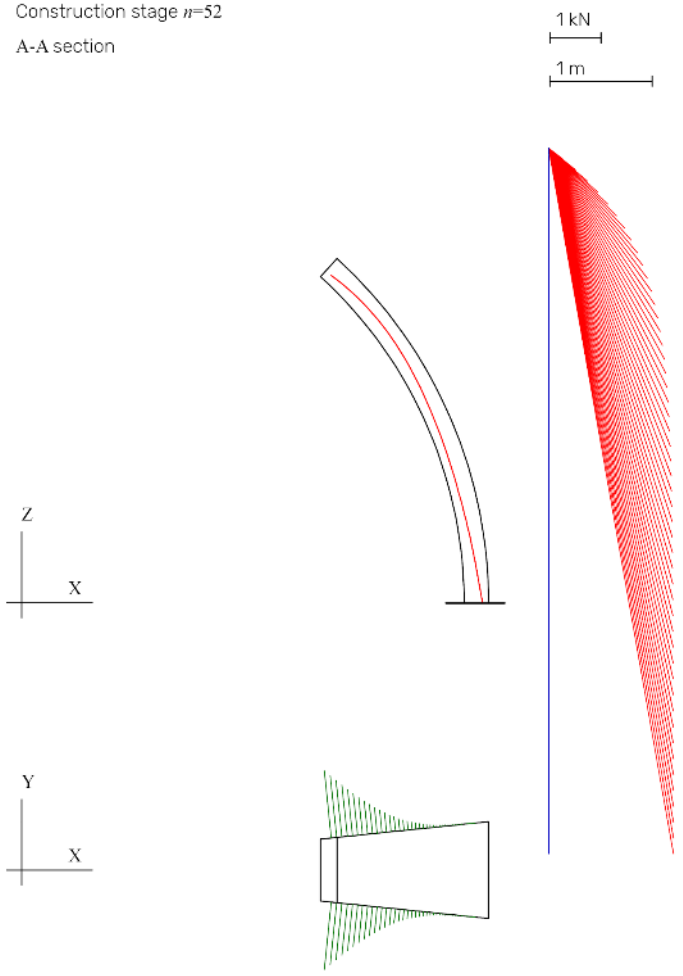

Construction stage n=52

B-B section

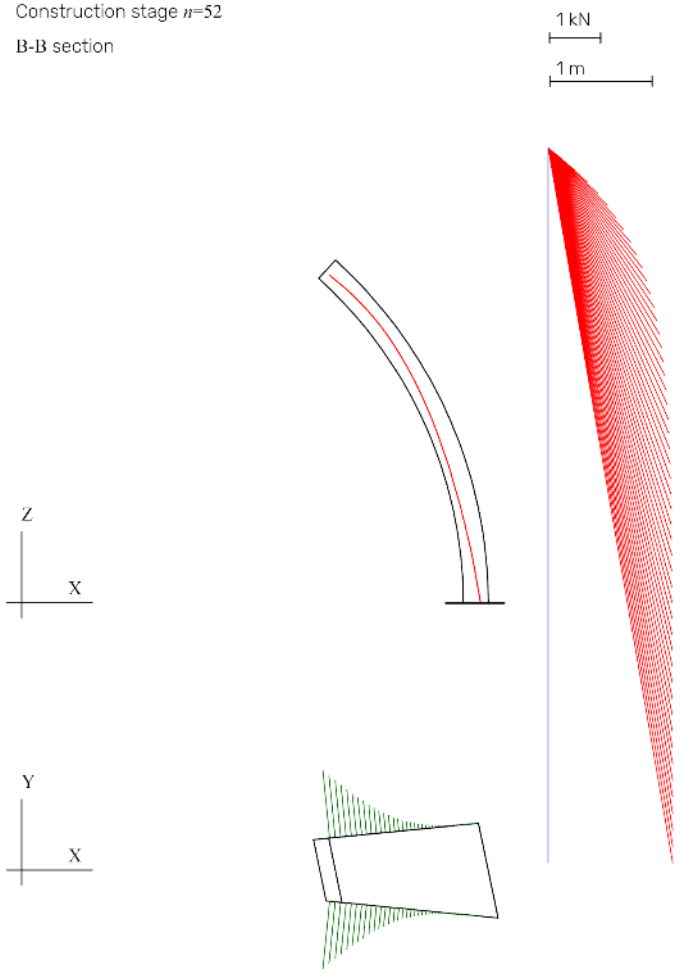

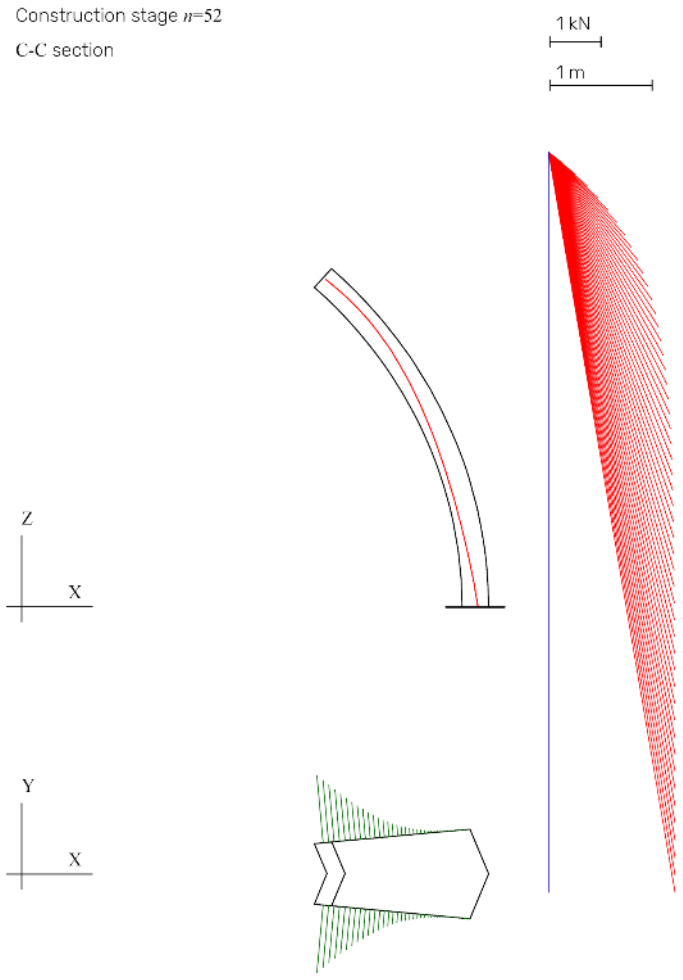
Construction stage n=52
C-C section
1 kN
1 m
Z
X
Y
X

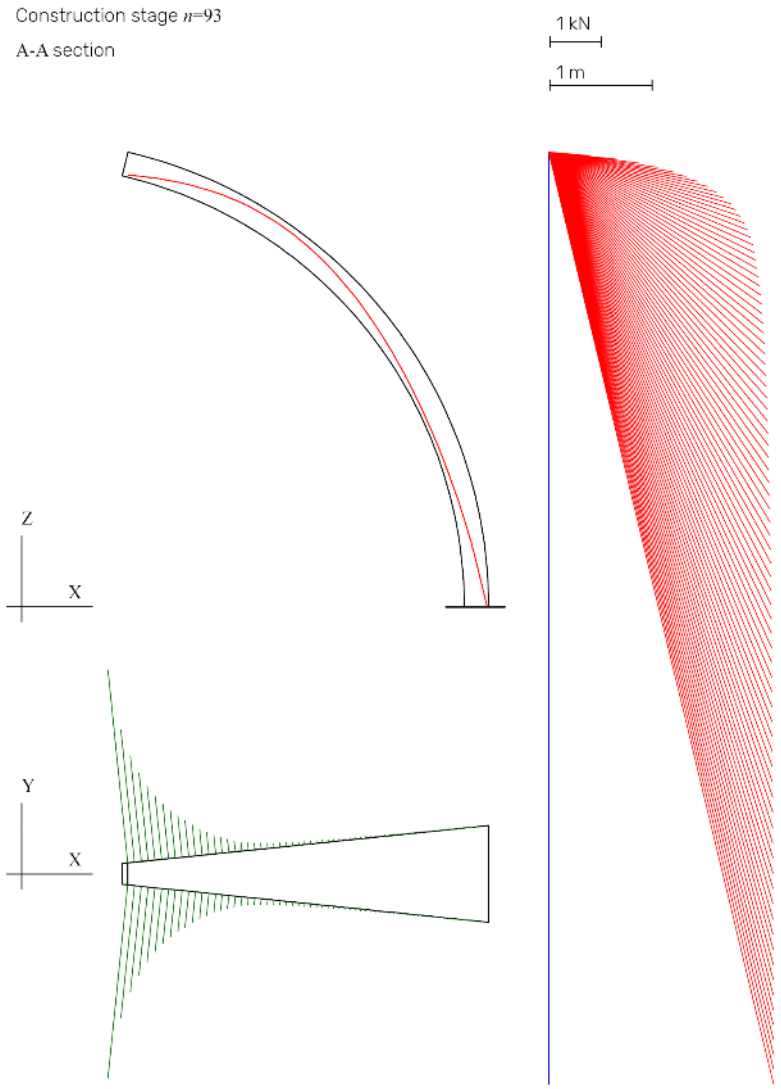
Construction stage n=93
A-A section
1 kN
1 m
Z
X
Y
X

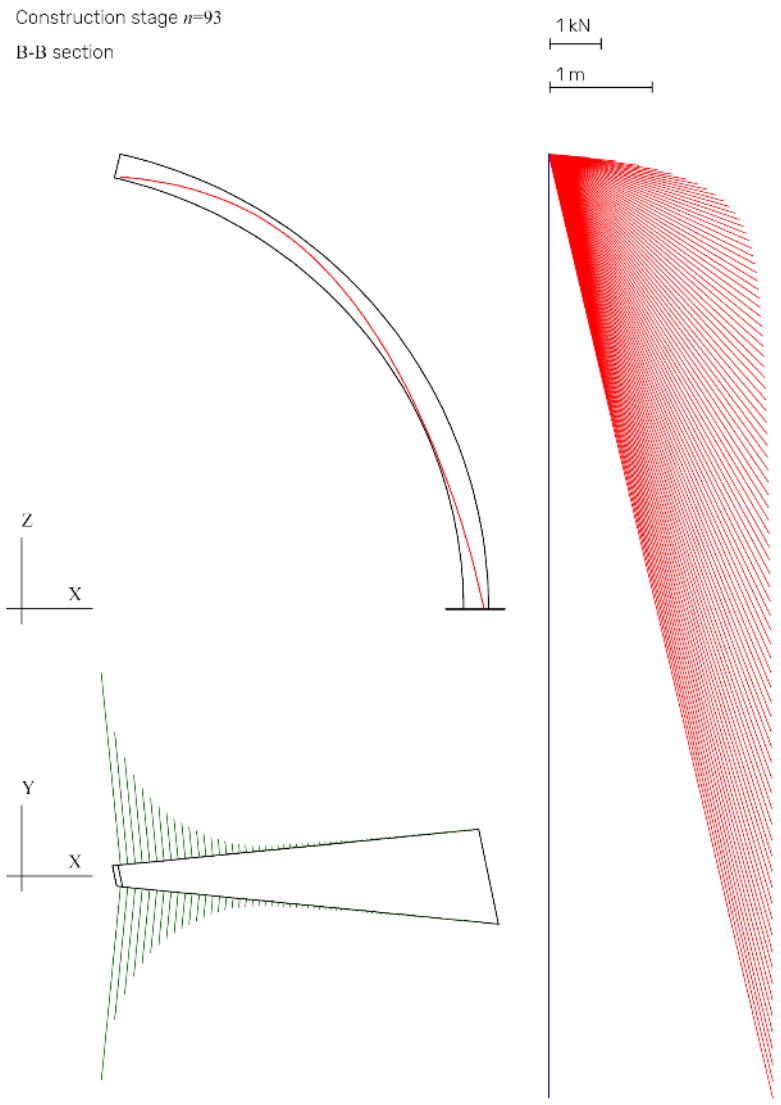
Construction stage n=93
B-B section
1 kN
1 m
Z
X
Y
X

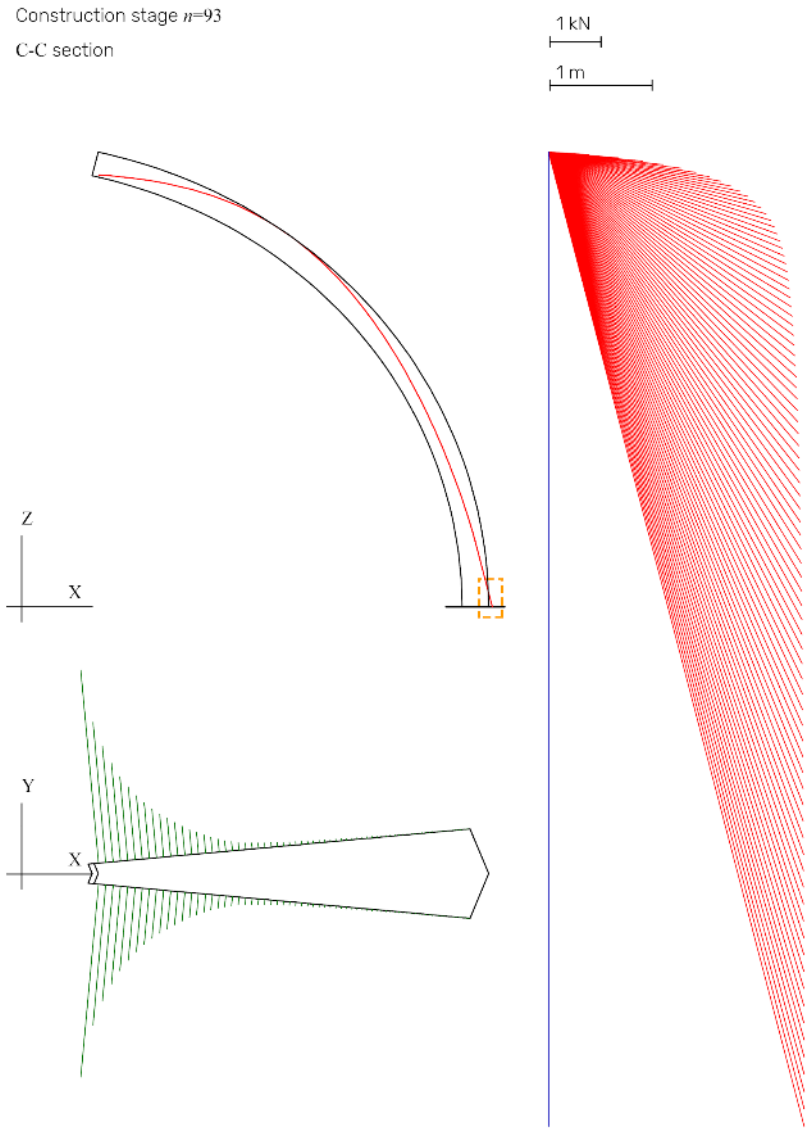
Construction stage n=93
C-C section
1 kN
1 m
Z
X
Y
X

Hemispherical dome

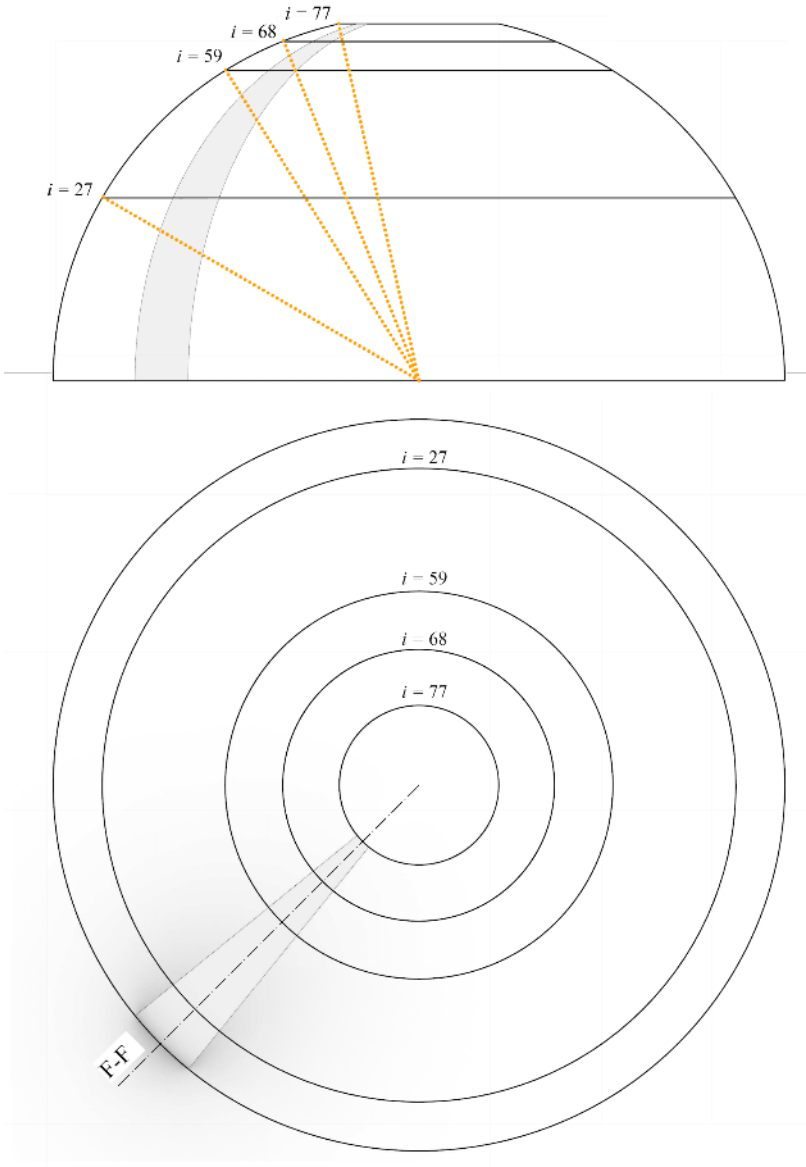

Key-section for analyses:
Construction stage analysed: i =27, 59, 68, 77

Construction stage n=27

F-F section

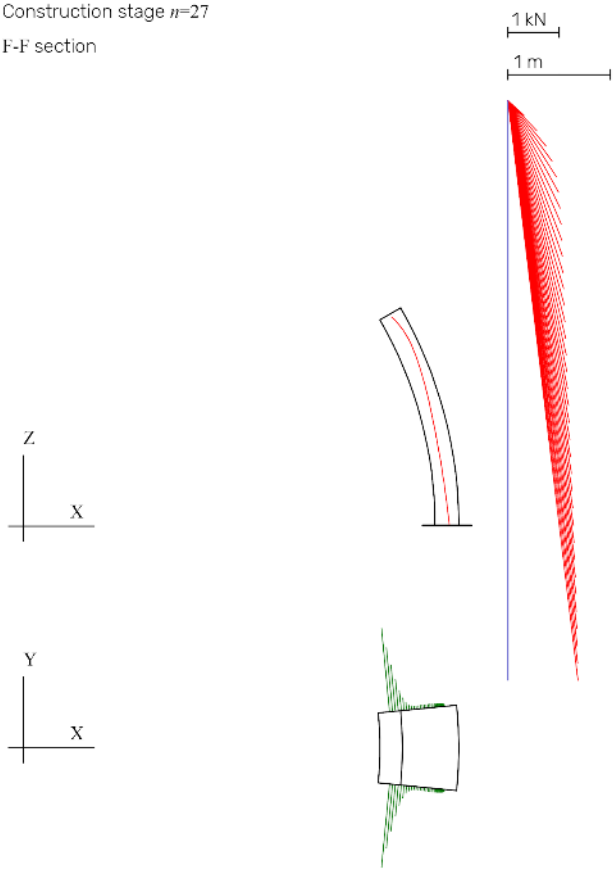

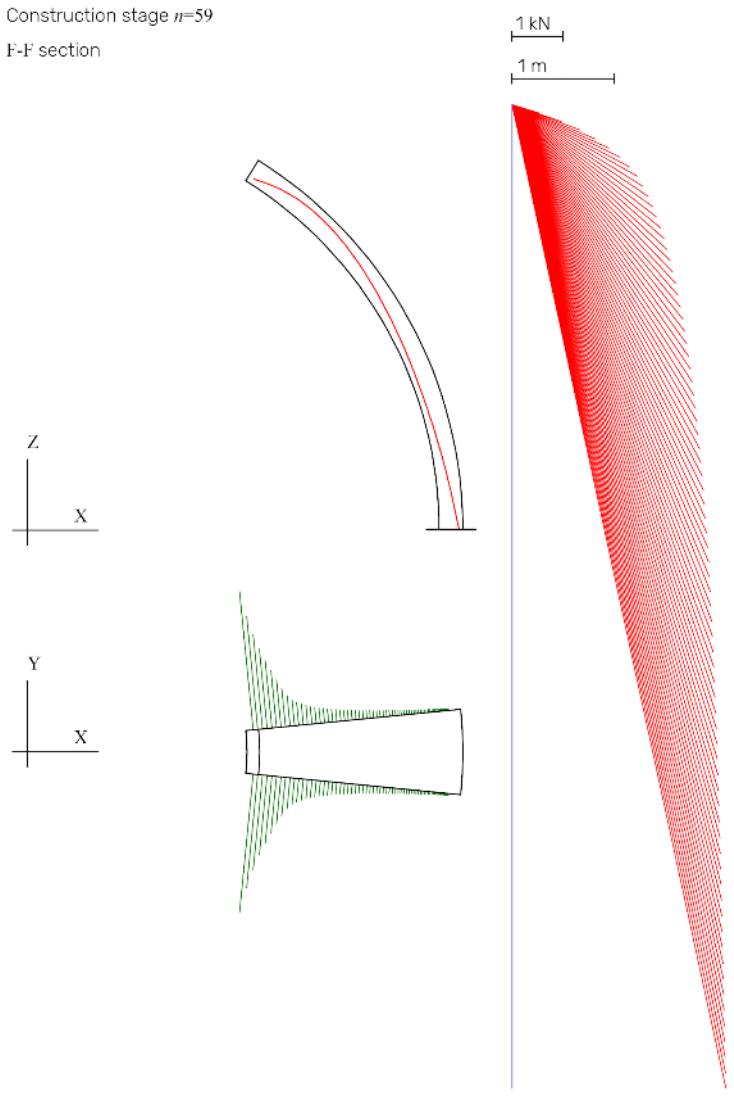
Construction stage n=59
F-F section
1 kN
1 m
Z
X
Y
X

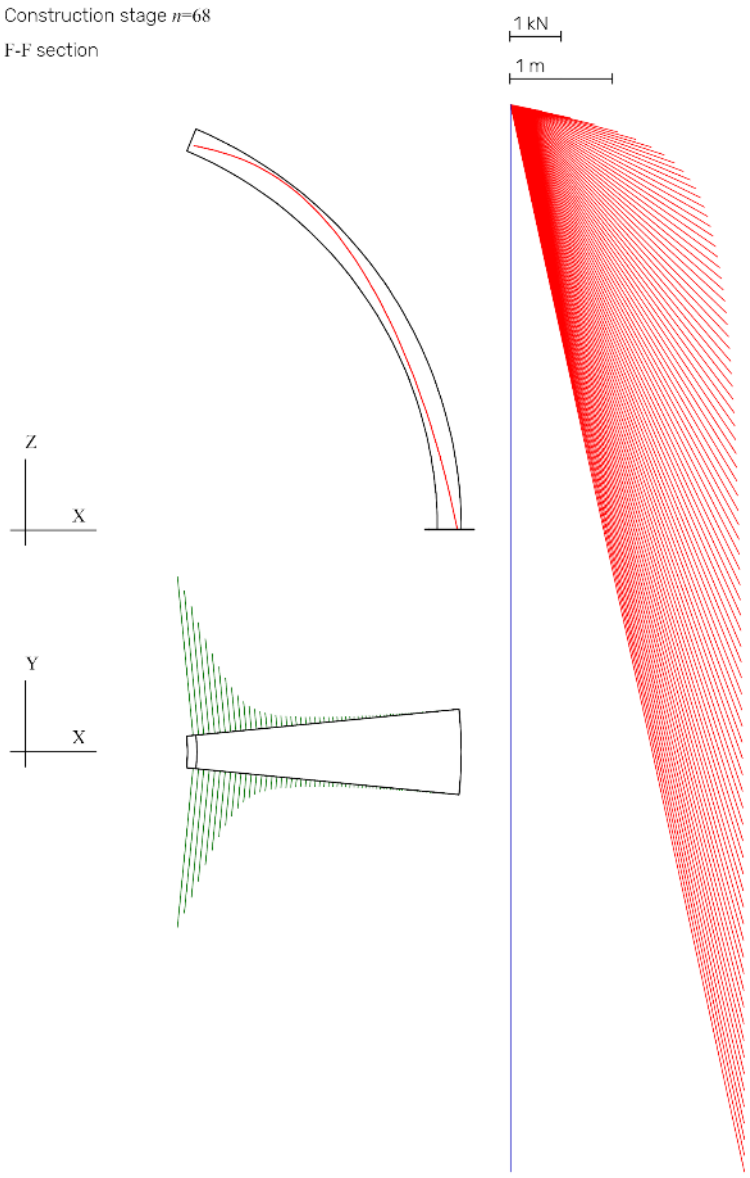
Construction stage n=68
F-F section
1 kN
1 m
Z
X
Y
X

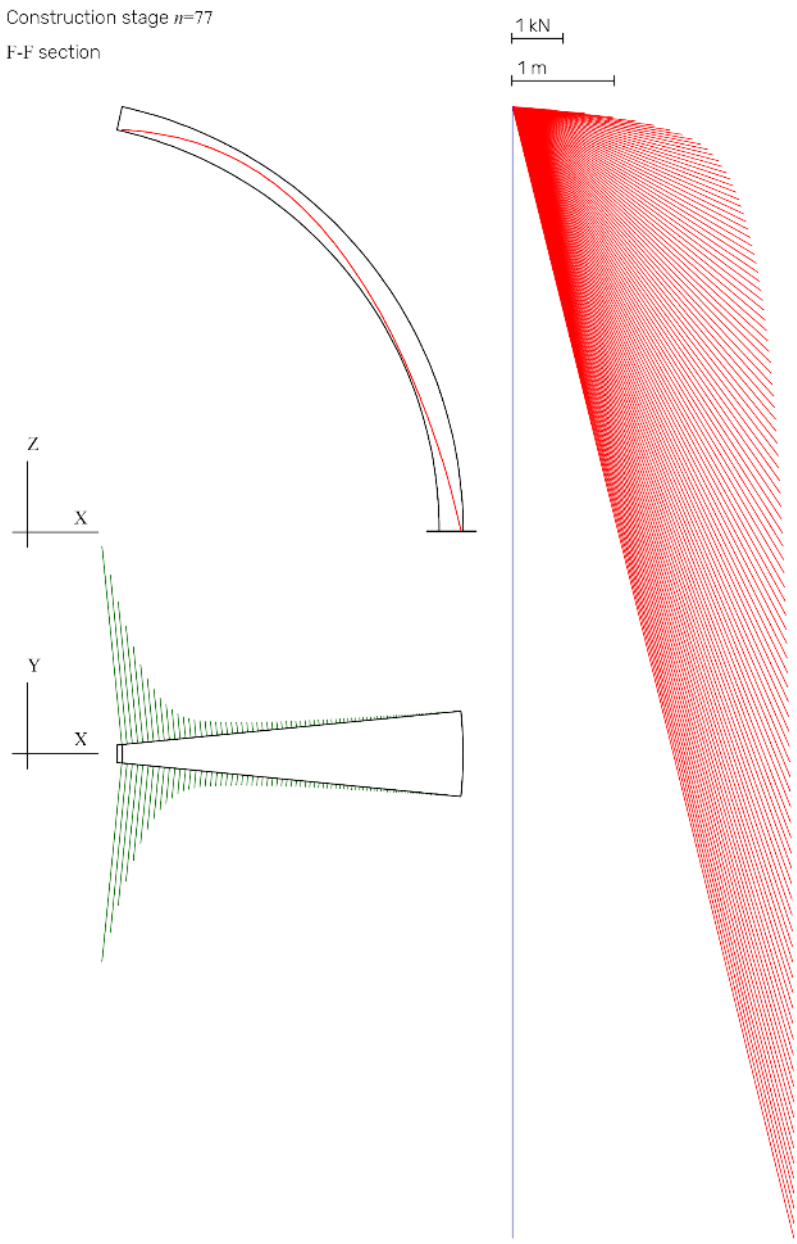
Construction stage n=77
F-F section
1 kN
1 m
Z
X
Y
X

Appendix C

D.E.M. analysis

The structures investigated are the same two domes analysed in Appendix B, an octagonal and a hemispherical structure, but in the D.E.M. analyses the domes are modelled starting from 28^{th} brick course (i=28), the polygonal one, and 27^{th} brick course (i=27) for the hemispherical one. The dimensions of rigid bodies assumed to perform the analyses correspond to the sizes of brick and a portion of mortar which surrounds the brick itself, exactly as described in chapter 6.4. The results reported show the time evolution of the unbalanced force calculated for a friction angle range from Φ=0° up to Φ=89° and z-velocity from Φ=10° up to Φ=89°. As well as the displacement surfaces, the z-velocity graphs have been traced. The graphs illustrate the results obtained relative to the bricks course: i=28, 52, 65, 78 for the octagonal model and i=27, 43, 66, 70 hemispherical structure. All analyses are performed with values of jKn=100 GPa/m, jKs=10 GPa/m.

As mentioned in chapter 6.4.2, the author wants to highlight that the order of magnitude of the displacement surfaces should be non-exact, but their geometries provide interesting information on the time evolution of displacements at different courses, different construction stages and friction values. The bump region of displacement surfaces highlights the settlements occurred during the construction. These movements have really low magnitude, even regarding the order of maximum displacement recorded, they are at least two orders smaller than maximum displacement. Referring to the octagonal dome the "breath" phenomenon is more evident in the courses included in i=28-75 and in the middle of the sails of octagonal dome, this is due to the inclination of the laying plane, as well as this phenomenon is practically absent in correspondence of B point (near the edges of sails). In general, the

displacement surfaces relative to B points have an order lesser of the A points recorded at the same condition (Φ, n).

The introduction of geometrical errors in blocks of the hemispherical dome does not allow the “breath” phenomenon to occur. The displacement surfaces relative to the upper portion of this structure (i=56-77) show a remarkable vertical section in correspondence of the early construction stages which they are recorded. This denotes that the geometrical errors lead to an increasing the settlements but however not such as to compromise the balanced state of the dome.

Octagonal dome

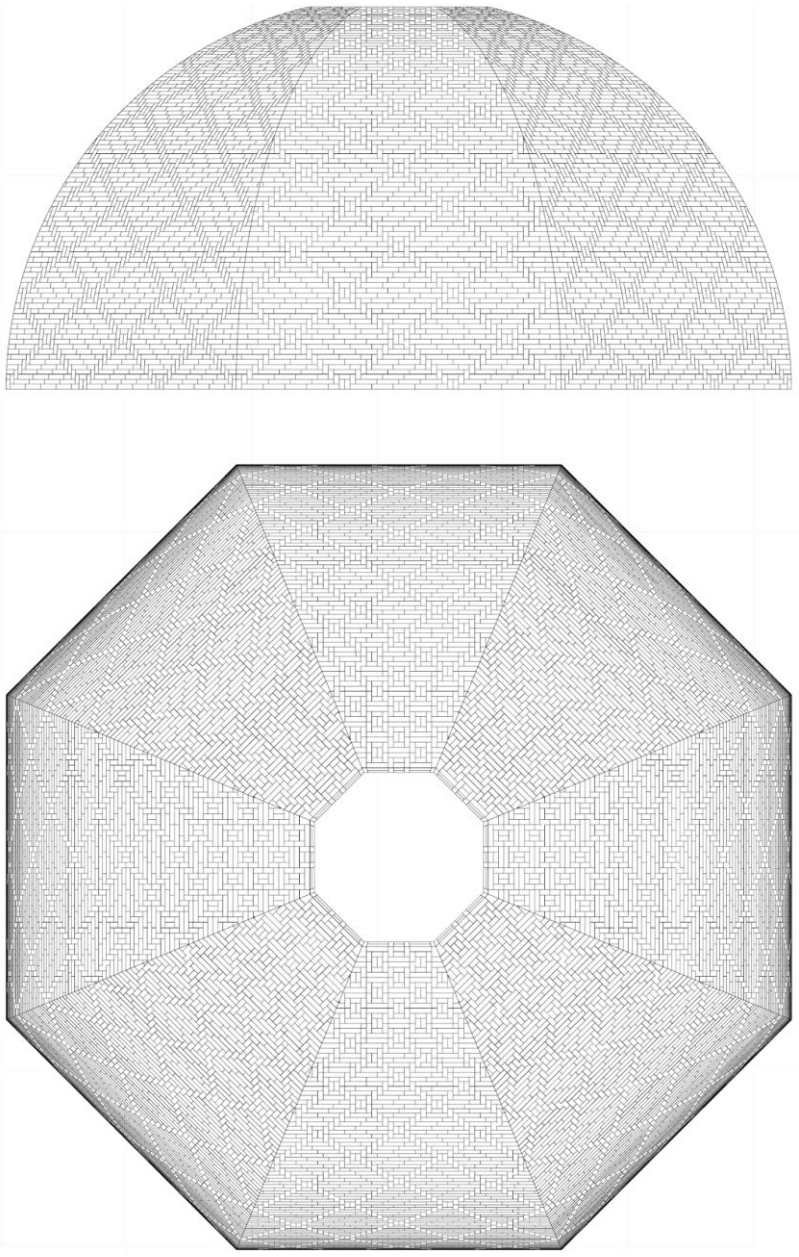

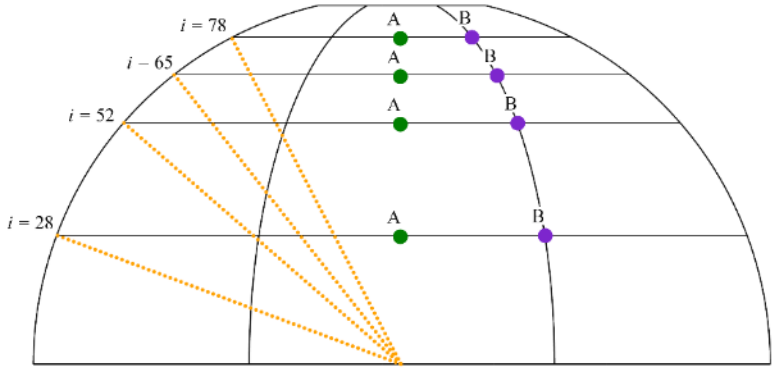

Key-section for analyses:
Courses analysed: i – 28, 52, 65, 78

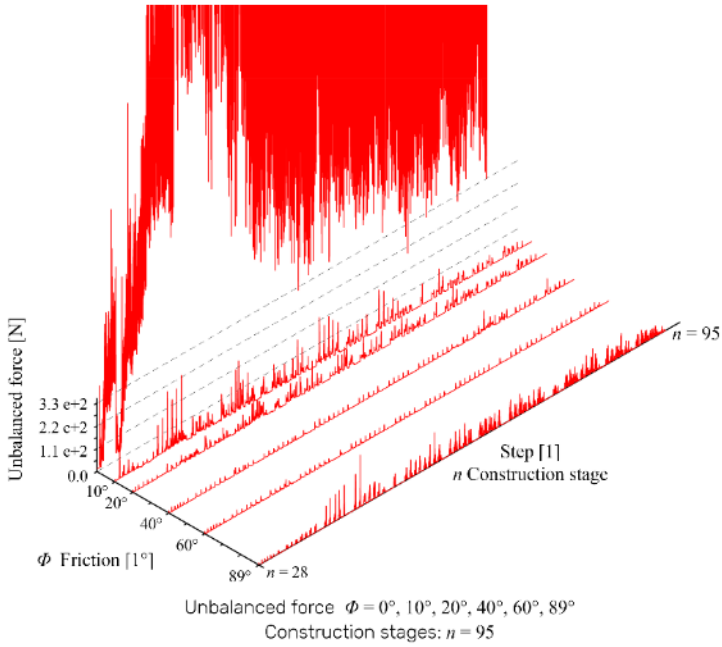

Unbalanced force $\Phi = 0°, 10°, 20°, 40°, 60°, 89°$
Construction stages: $n = 95$

Course $i = 28$, Point A
Construction stages: $n = 95$
$10° < \Phi < 90°$

Z-Velocity

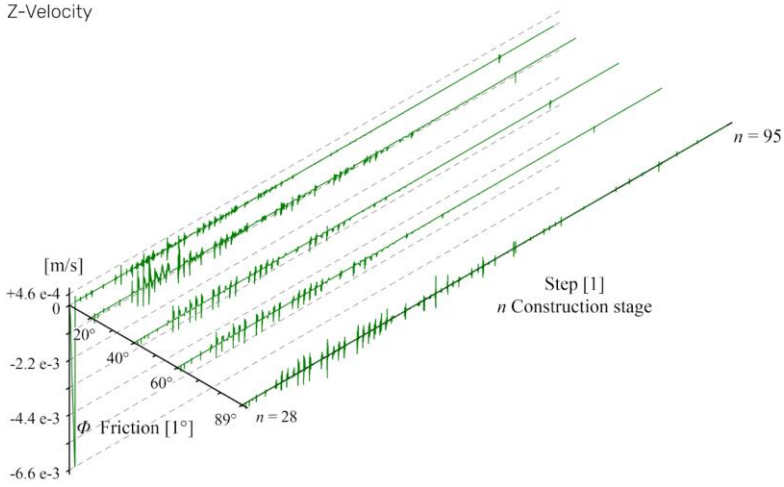

Displacement

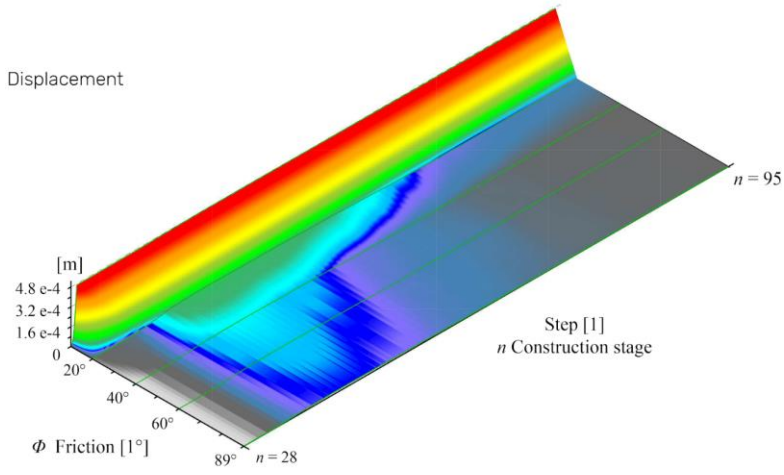

Course $i = 28$, Point B
Construction stages: $n = 95$
$10° < \Phi < 90°$

Z-Velocity

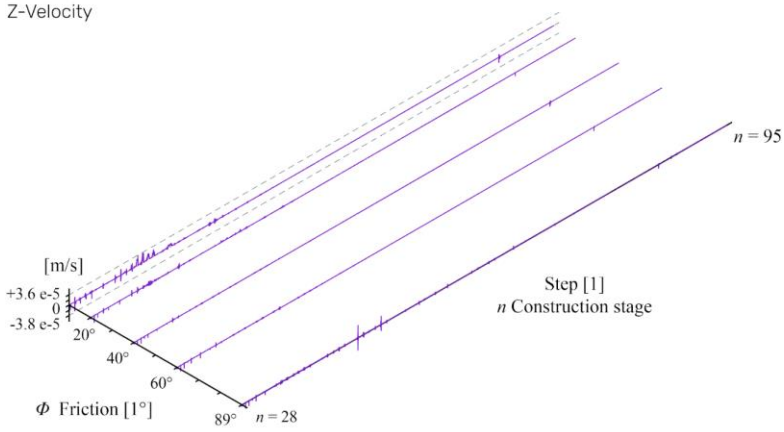

Displacement

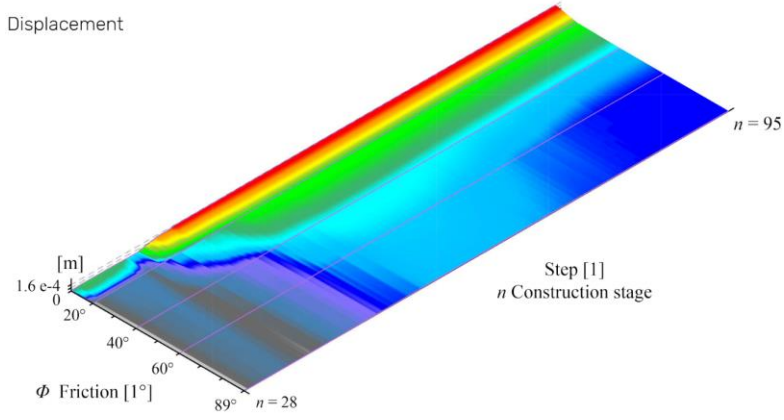

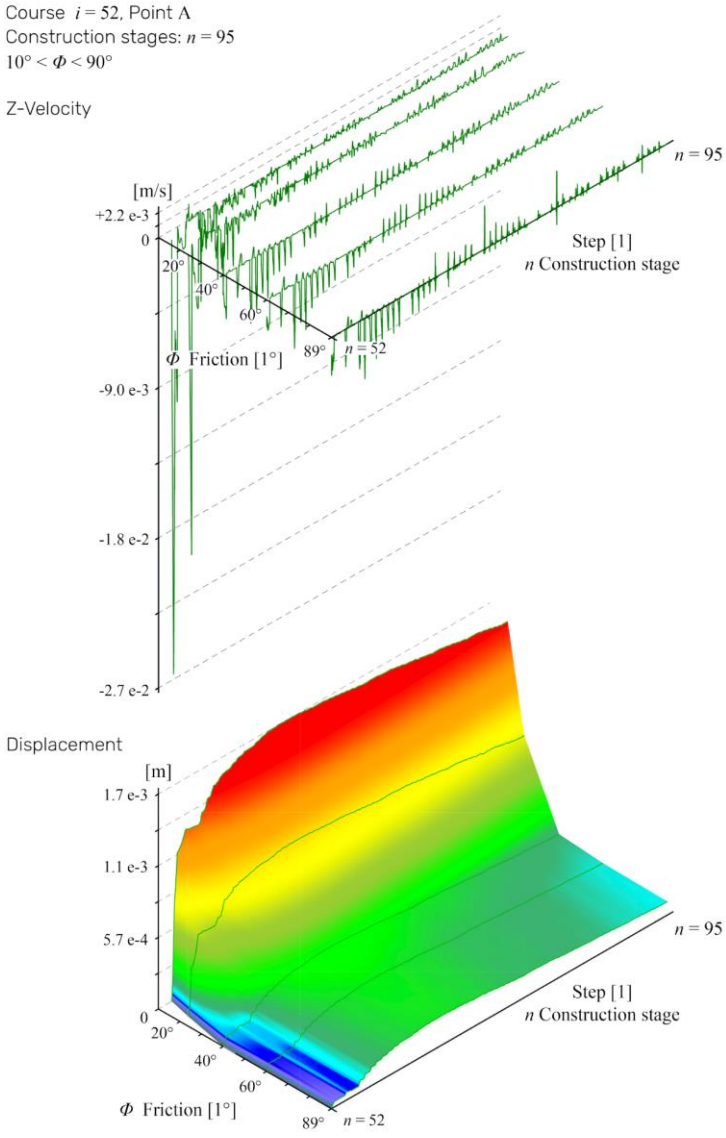
Course $i = 52$, Point A
Construction stages: $n = 95$
$10° < \Phi < 90°$
Z-Velocity
[m/s]
+2.2 e-3
0
-9.0 e-3
-1.8 e-2
-2.7 e-2
20°
40°
60°
89°
Φ Friction [1°]
$n = 52$
$n = 95$
Step [1]
n Construction stage
Displacement
[m]
1.7 e-3
1.1 e-3
5.7 e-4
0
20°
40°
60°
89°
Φ Friction [1°]
$n = 52$
$n = 95$
Step [1]
n Construction stage

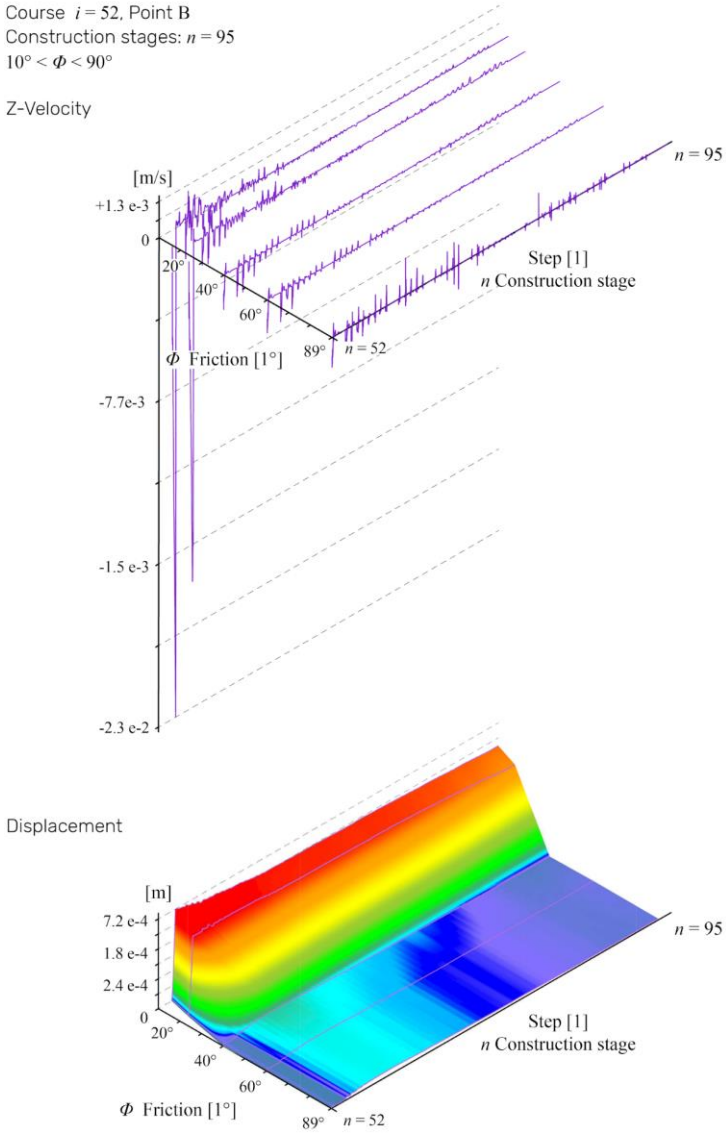
Course $i = 52$, Point B
Construction stages: $n = 95$
$10° < \Phi < 90°$
Z-Velocity
[m/s]
+1.3 e-3
0
-7.7e-3
-1.5 e-3
-2.3 e-2
20°
40°
60°
89°
Φ Friction [1°]
$n = 52$
$n = 95$
Step [1]
n Construction stage
Displacement
[m]
7.2 e-4
1.8 e-4
2.4 e-4
0
20°
40°
60°
89°
Φ Friction [1°]
$n = 52$
$n = 95$
Step [1]
n Construction stage

Course $i = 65$, Point A
Construction stages: $n = 95$
$10° < \Phi < 90°$

Z-Velocity

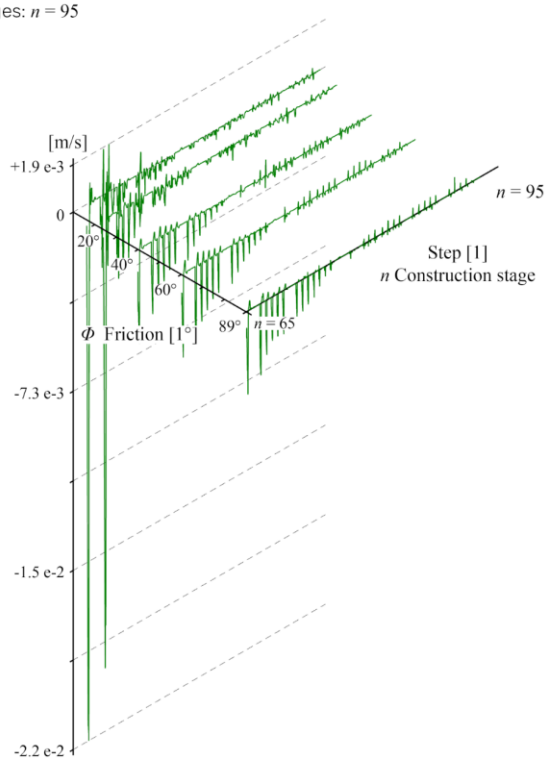

Displacement

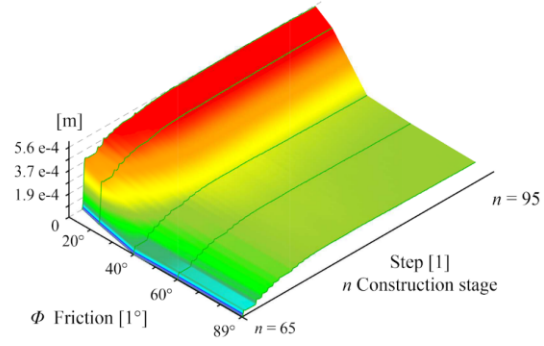

Course $i = 65$, Point B
Construction stages: $n = 95$
$10° < \Phi < 90°$

Z-Velocity

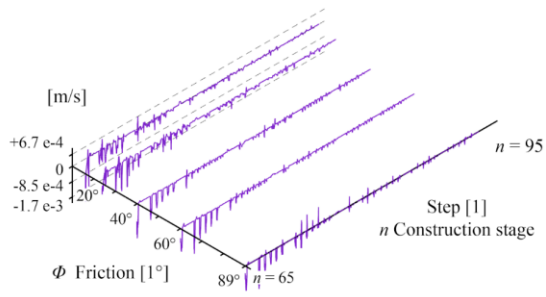

Displacement

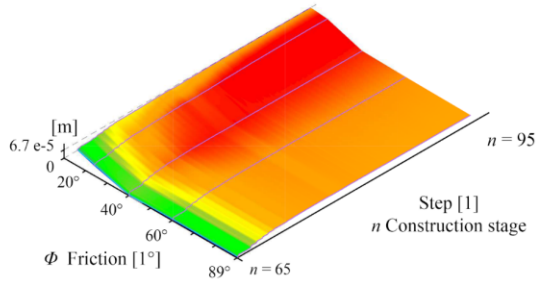

Course $i = 78$, Point A
Construction stages: $n = 95$
$10° < \Phi < 90°$

Z-Velocity

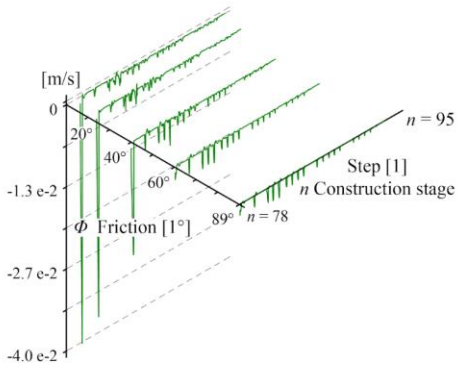

Displacement

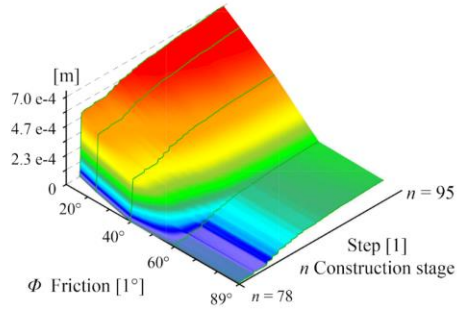

Course $i = 78$, Point B
Construction stages: $n = 95$
$10° < \Phi < 90°$

Z-Velocity

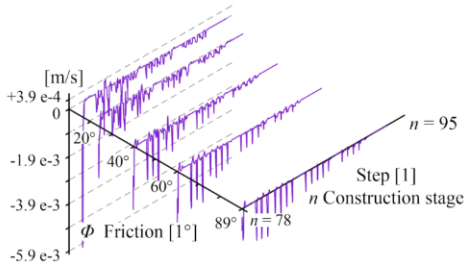

Displacement

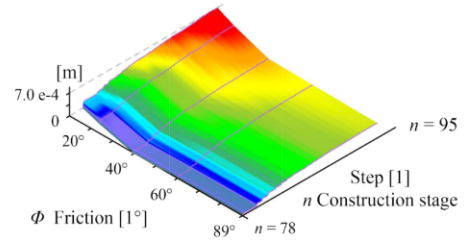

Hemispherical dome

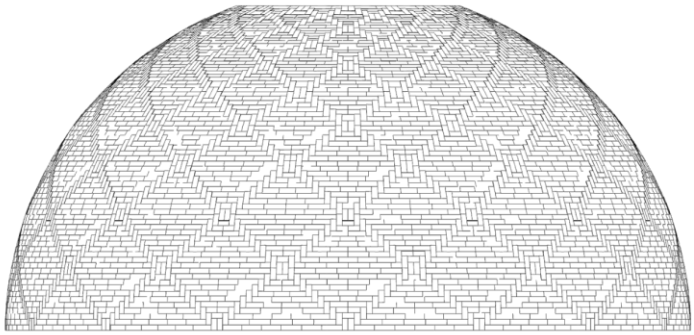

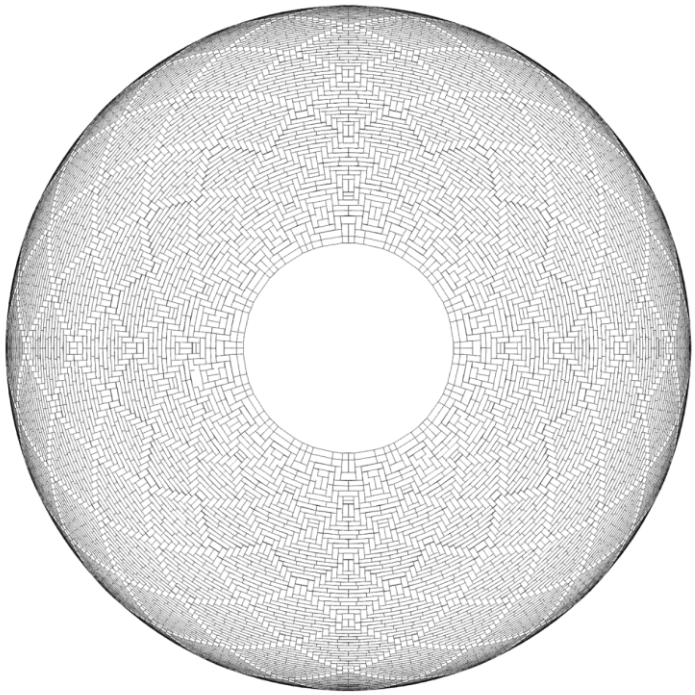

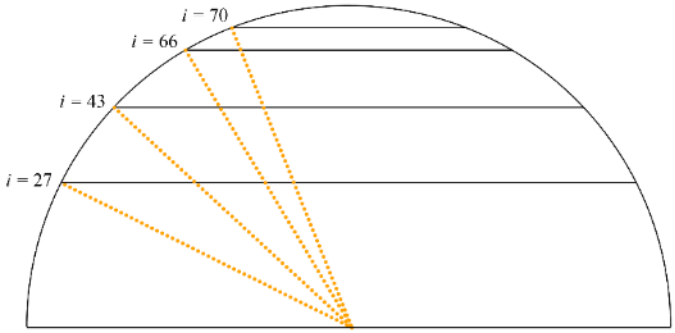

Key-section for analyses:
Courses analysed: i =27, 43, 66, 70

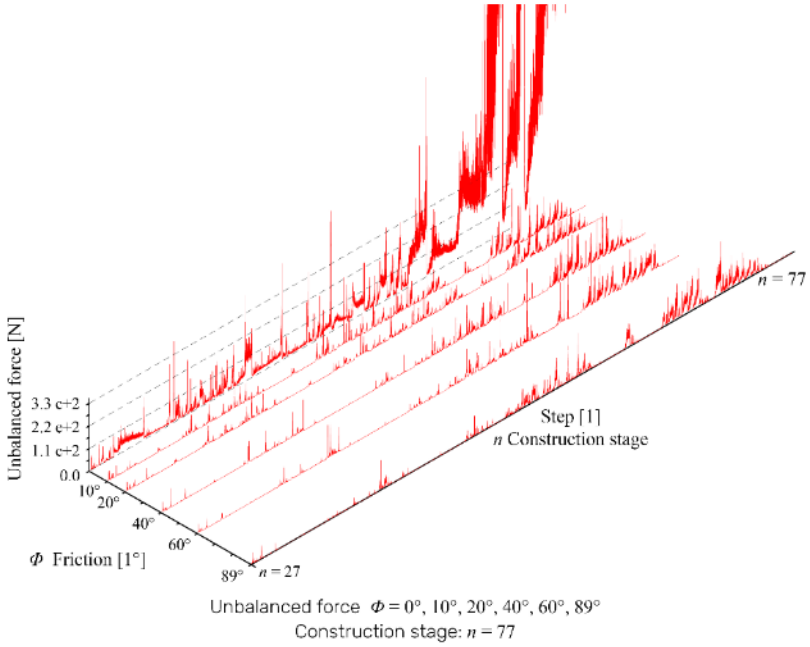

Unbalanced force $\Phi = 0°, 10°, 20°, 40°, 60°, 89°$
Construction stage: $n = 77$

Course $i = 27$
Construction stages: $n = 77$
$10° < \Phi < 90°$

Z-Velocity

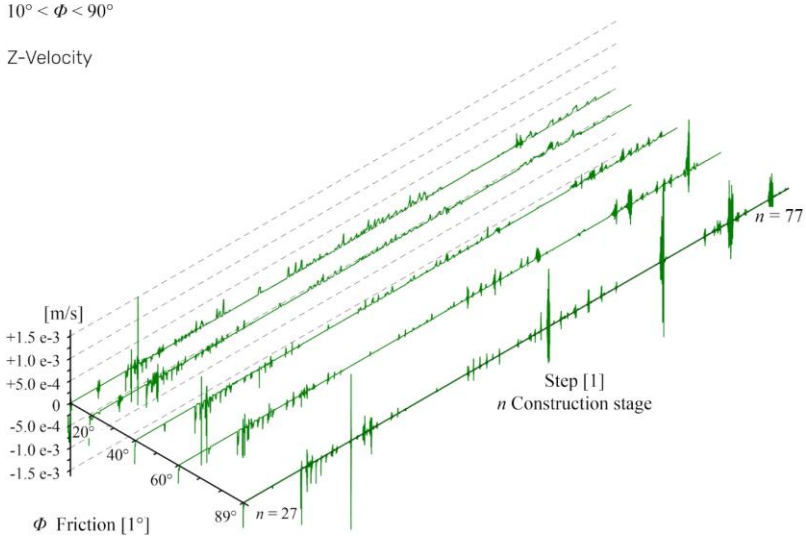

Displacement

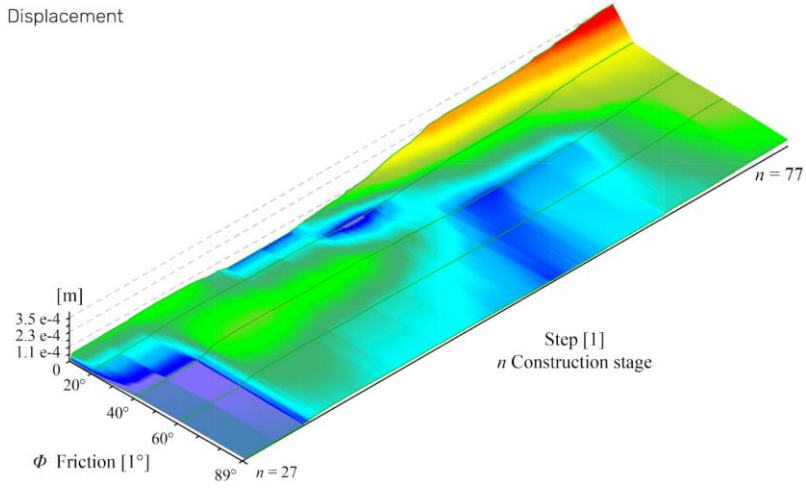

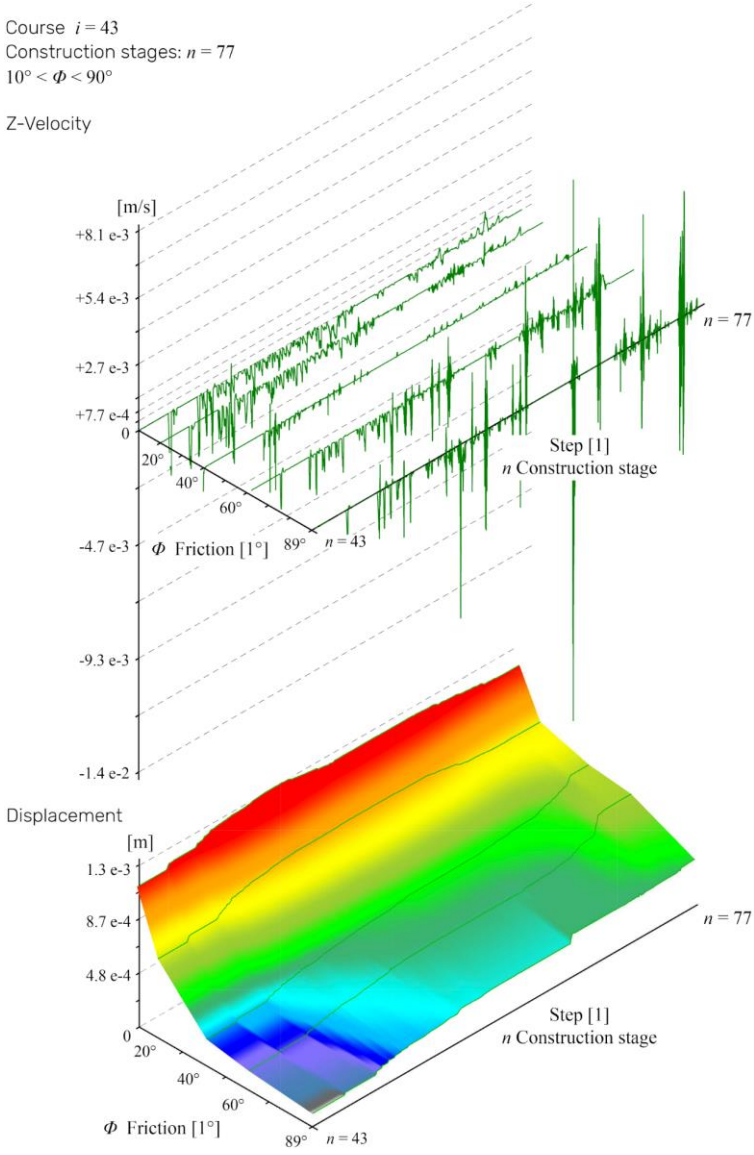
Course $i = 43$
Construction stages: $n = 77$
$10° < \Phi < 90°$
Z-Velocity
[m/s]
+8.1 e-3
+5.4 e-3
+2.7 e-3
+7.7 e-4
0
-4.7 e-3
-9.3 e-3
-1.4 e-2
20°
40°
60°
89°
Φ Friction [1°]
$n = 43$
$n = 77$
Step [1]
n Construction stage
Displacement
[m]
1.3 e-3
8.7 e-4
4.8 e-4
0
20°
40°
60°
89°
Φ Friction [1°]
$n = 43$
$n = 77$
Step [1]
n Construction stage

Course $i = 64$
Construction stages: $n = 77$
$10° < \Phi < 90°$

Z-Velocity

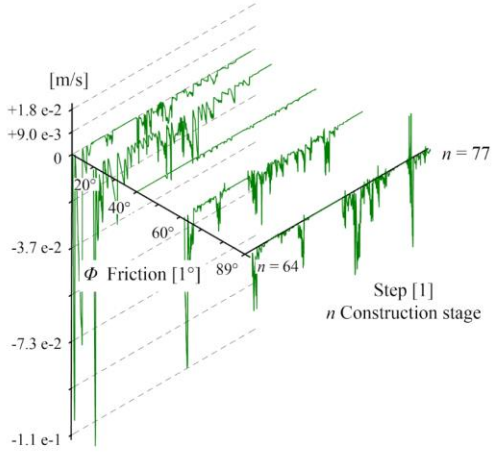

Displacement

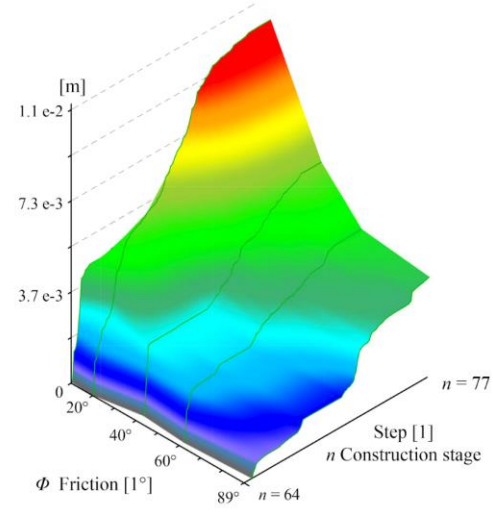

Course $i = 70$
Construction stages: $n = 77$
$10° < \Phi < 90°$

Z-Velocity

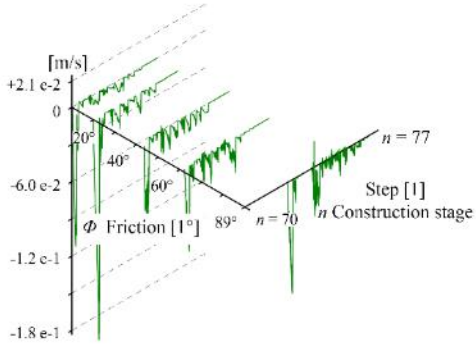

Displacement

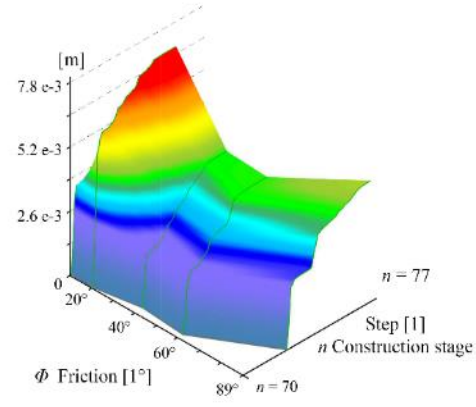

References

[1] P. Block, M. Rippmann, T. Van Mele, and D. Escobedo, "The Armadillo vault balancing computation and tradition craft," in *Fabricate 2017*, JSTOR, Ed. 2017, pp. 286–293.

[2] J. Heyman, "The stone skeleton," *Int. J. Solids Struct.*, vol. 2, pp. 249–279, 1966.

[3] M. Angelillo, L. Cardamone, and A. Fortunato, "A Numerical model for masonry-like structures," *J. Mech. Mater. Struct.*, vol. 5, no. 4, pp. 583–615, 2010.

[4] A. Iannuzzo, F. De Serio, A. Gesualdo, G. Zuccaro, A. Fortunato, and M. Angelillo, "Crack patterns identification in masonry structures with a C° displacement energy method," *Int. J. Mason. Res. Innov.*, vol. 3, no. 3, pp. 295–323, 2018.

[5] A. Tralli, C. Alessandri, and G. Milani, "Computational Methods for Masonry Vaults: A Review of Recent Results," *Open Civ. Eng. J.*, vol. 8, pp. 272–287, 2014.

[6] A. Choisy, *L'art de bâtir chez les Romains*. Paris Librairie générale de l'architecture et des travaux, 1873.

[7] S. F. Huerta, "The geometry and construction of Byzantine vaults: the fundamental contribution of Auguste Choisy," in *Auguste Choisy (1841-1909): L'architecture et l'art de bâtir*, F. J. Girón Sierra and S. Huerta Fernández, Eds. Madrid, 2009, pp. 289–305.

[8] S. Andreani, A. Jyoti, and M. Bechthold, "Flowing Matter: Robotic Fabrication of Complex Ceramic Systems," *SARC. Proc. Int. Symp. Autom. Robot. Constr.*, vol. 29, 2012.

[9] A. MENGES *et al.*, "ROBOTIC FABRICATION OF STONE ASSEMBLY DETAILS," in *Fabricate 2017*, 2019, pp. 106–113.

[10] S. Goessens, C. Mueller, and P. Latteur, "Feasibility study for drone-based masonry construction of real-scale structures," *Autom. Constr.*, vol. 94, pp. 458–480, 2018.

[11] G. McKinsey, "Reinventing Construction. A Route to Higher Productivity. Viitattu 3.11. 2017," 2017.

[12] N. Lepore, "Le volte in muratura: forma e struttura, equilibrio e analisi limite.," Roma Tre, 2018.

[13] S. H. Awad, *Concrete Formwork Svstems*. 1999.

[14] H. A. Rani, "The Impact of Construction Waste to The Environmental on Project Development in Aceh Road material View project Analytic Network Process Method View project," *nternational J. Manag. Inf. Technol. Eng.*, vol. 5, pp. 1–8, 2017.

[15] S. F. Huerta, "Las bóvedas tabicadas en Alemania: la larga migración de una técnica constructiva," in *Actas del Segundo Congreso Internacional Hispanoamericano, Noveno Nacional, de Historia de la Construcción*, Madrid, 2017, pp. 759–772.

[16] J. F. D. Dahmen and J. A. Ochsendorfs, "Earth masonry structures: Arches, vaults and domes," *Mod. Earth Build. Mater. Eng. Constr. Appl.*, pp. 427–460, 2012.

[17] I. J. Oppenheim, D. J. Gunaratnam, and R. H. Allen, "Limit State Analysis of Masonry Domes," *J. Struct. Eng.*, vol. 115, no. 4, pp. 868–882, Apr. 1989.

[18] M. Como, *Statics of Historic Masonry Constructions*, vol. 1. 2013.

[19] T. Michiels and S. Adriaenssens, "Form-finding algorithm for masonry arches subjected to in-plane earthquake loading," *Comput. Struct.*, vol. 195, pp. 85–98, Jan. 2018.

[20] L. C. Lancaster, *Innovative Vaulting in the Architecture of the Roman Empire: 1st to 4th Centuries CE*. Cambridge University Press, 2015.

[21] G. Mirabella Roberti and O. Spina, "Discrete element analysis on the Sardinian 'Nuaraghe,'" in *Strumas V International Symposium on Computer Methods in Structural Masonry*, 2001.

[22] A. Bouet, *Les matériaux de construction en terre cuite dans les thermes de la Gaule Narbonnaise*. Ausonius Éditions, 2019.

[23] S. El-Naggar, "Les voûtes dans l'architecture de l'Égypte ancienne," 1999.

[24] S. Storz, "Tonröhren im antiken Gewölbebau," in *Mainz: Philippe von Zabern*, 1994.

[25] R. Besenval, *Technologie de la voute dans l'orient ancient*. Paris, 1984.

[26] L. Davis, J. Ochsendorf, P. Block, and M. DeJong, "Tile vaulted systems for low-cost construction in Africa," *ATDF J.*, vol. 7, no. 1/2, pp. 4–13, 2010.

[27] D. Wendland, "Traditional vault construction without formwork: Masonry pattern and vault shape in the historical technical literature and in experimental studies," *Int. J. Archit. Herit.*, vol. 1, no. 4, pp. 311–365, 2007.

[28] B. Ward, Perkins; John, "Notes on the structure and building methods of early Byzantine Architecture," in *The Great Palace of the Byzantine emperors. Second Report.', editado por D.T.Rice. Edimbourgh*, Edinburgh:

Walker Trust. and The University of St. Andrews, Eds. D. Talbot Rice. , 1959, pp. 52–104.

[29] H. Fathy, *Architecture for the poor: an experiment in rural Egypt.* University of Chicago press, 2010.

[30] M. Angelillo, *Mechanics of masonry structures*. London, 2014.

[31] F. Ger y Lo´ bez, *Tratado de construcción civil*. Diputación, 1869.

[32] S. Olivier, A.; Storz, "Analyse et restitution d'un procédé de construction antique: réalisation d'une voûte d'arête sur coffrage perdu en tubes de terre cuite," in *Recherches archéologiques franco-tunisiennes à Bulla Regia* , 1st ed., Beschaouch, A.; Hanoune, R.; Khanoussi, M.; Olivier, A.; Thébert, Y, 1983, pp. 11–127.

[33] R. J. A. Wilson, "Terracotta vaulting tubes (tubi fittili): on their origin and distribution," *J. Rom. Archaeol.*, vol. 5, pp. 97–129, 1992.

[34] S. Storz, "La tecnica edilizia romana e paleocristiana delle volte e cupole a tubi fittili," in *Lo specchio del cielo*, 1997, pp. 23–42.

[35] M. L. Stoppioni, "Con la terra e con il fuoco," *Fornaci romane nel Riminese*, 1993.

[36] G. D'ossat De Angelis, "Nuovi dati sulle volte costruite con vasi fittili," *Palladio*, vol. 5, 1941.

[37] G. Mirabella Roberti, N. Lombardini, and H. Faltehr, "Late Roman domes in clay tubes: historical and numerical study of San Vitale in Ravenna," in *Iass international Symposium*, 1955, vol. 2.

[38] J. Durm, "Die Baukunst der Etrusker," *Die Baukunst der Römer*, vol. 2, 1905.

[39] A. Almagro, "Bóvedas tabicadas en la Cartuja de Granada: el final de un proceso evolutivo," in *Actas del Simposio Internacional sobre Bóvedas Tabicadas*, 2011.

[40] A. Zaragozá. Catalán, "A propósito de las bóvedas de crucería y otras bóvedas medievales," in *Anales de Historia de l'arte*, Pubblicaciones Universidad Complutense de Madrid, Ed. Madrid, 2009, pp. 96–126.

[41] A. Zaragozá. Catalán, "Hacia una Historia de las Bóvedas Tabicadas," in *Construyendo Bóvedas Tabicadas*, 2011.

[42] I. M. Varela,Botella; Bevia, S.; Garcia, "Restauracion Catillo de la Atalya, dos fases," *Praxis Edilizia 10 anos con el Patrimonio Arquitectonico Resturacion*. Valencia, pp. 94–197, 2010.

[43] G. R. Collins, "The Transfer of Thin Masonry Vaulting from Spain to America," vol. 27, no. 3, pp. 176–201, 2018.

[44] J. Ochsendorf, *Guastavino vaulting: the art of structural tile*. Princeton Architectural Press, 201AD.

[45] C. Espie, *Manière de rendre toutes sortes d'édifices incombustibles*. Paris: Duchesne, 1754.

[46] M. H. Ramage, J. Ochsendorf, P. Rich, J. K. Bellamy, and P. Block, "Design and Construction of the Mapungubwe National Park Interpretive Centre , South Africa," pp. 14–23.

[47] Á. Truñó, *Construcción de bóvedas tabicadas.* Reverte, 2004.

[48] L. Moya Blanco, *Bóvedas tabicadas*. 1947.

[49] R. Guastavino, *Essay on the theory and history of cohesive construction applied especially to the timbrel vault*. Ticknor, 1892.

[50] L. Davis, M. Rippmann, T. Pawlofsky, and P. Block, "Innovative funicular tile vaulting: A prototype vault in Switzerland," *Struct. Eng.*, vol. 90, no. 11, pp. 46–56, 2012.

[51] A. Choisy, *Histoire de l'Architecture*. Paris: G. Béranger, 1899.

[52] D. Melonie, Bayl-Smith; Block, Philippe; Pigram, "Pass me the mixing bucket: The Ribbed Catalan studio as a design/research case study," *Brookes eJournal Learn. Teach.* , no. 8.1/2, 2016.

[53] H. Saalman, *Filippo Brunelleschi: The Cupola of Santa Maria del Fiore*. London: Zwemmer, 1980.

[54] S. Di Pasquale, *Brunelleschi: la costruzione della cupola di Santa Maria del Fiore*. 2002.

[55] F. Ottoni, "La lunga vicenda delle fabbriche cupolate. Note storiche sulla stabilità, tra dibattito e sperimentazione.," Università degli Studi di Parma. Dipartimento di Ingegneria Civile ed Architettura, 2009.

[56] A. Pizzigoni, "Brunelleschi.pdf." Zanichelli, p. 192, 1989.

[57] A. Pizzigoni, "Brunelleschi's Bricks," *J. Int. Assoc. Shell Spat. Struct.*, vol. 56, no. 2, pp. 137–156, 2015.

[58] G. Vasari, *Le vite dei più eccellenti pittori, scultori e architetti*, Vol.1. presso l'Ufficio Generale di Commissioni ed Annunzi, 1876.

[59] G. Zander, "Gli ottagoni di San Pietro riconosciute nel disegno Arch.Uff. N.

1330," *Palladio*, vol. 1, pp. 62–82, 1998.

[60] E. Galdieri, "Da Gerusalemme a Dakha: mille anni di cupole islamiche," in *Lo specchio del Cielo*, Caludia Conforti, Ed. MIlano: Electa, 1997, pp. 53–66.

[61] Shukur Askaro, *The Architecture of the Temurids*. Tashkent: San'at, 2009.

[62] S. Conti, Giuseppe; Guidelli, Sandra; Livi, "La spinapesce nel Rinascimento tra Filippo Brunelleschi, i Sangallo e Bernardo Buontale nella Grotta Grande del Giardino di Boboli : alcune considerazioni matematiche," *Bollettino della Società di Studi fiorentini*, Emmebi Edizioni, 2013.

[63] D. De Rosa, "Il pontificato di Vittore III: un riesame critico." Aracne, 2008.

[64] M. S. Elsheikh, "Tracce di presenza arabo-musulmana in Toscana," *Plurilingual e-journal Lit. Relig. Hist. Stud.* , 2016.

[65] C. G. De Montauzan, *Les aqueducs antiques de Lyon: étude comparée d'archéologie romain*. E. Leroux, 1909.

[66] C. Gurrieri, Francesco; Acidini Luchinat, *La cattedrale di Santa Maria del Fiore a Firenze*, Vol. 1. Giunti gruppo editoriale, 1994.

[67] V. Lanza, "La ventilazione naturale dei bādgir nell'architettura contemporanea. Il ruolo della tradizione nel condizionamento ad impatto zero: quattro esempi di ventilazione naturale nei Paesi del Golfo e in Occidente," Università Ca'Foscari Venezia, 2017.

[68] "Ardestan, Zavareh and Abarquh," 2018. .

[69] "Ardesan Friday Mosque," 2013. [Online]. Available: http://www.selcuklumirasi.com/architecture-detail/ardestan-friday-mosque.

[70] "Noan Dishan." [Online]. Available: https://www.noandishaan.com/.

[71] A. Pizzigoni, V. Paris, M. Pasta, M. Morandi, and A. Parsani, "Herringbone naked structure," in *Iass*, 2018.

[72] G. Conti, B. Sedili, and A. Trotta, "Le curve Lossodromiche in Architettura," *Chief Ed.*, vol. 65, no. 2, 2014.

[73] V. Paris and A. Pizzigoni, "La struttura nascosta," *STRUCTURAL*, pp. 1–15, 2016.

[74] A. Pizzigoni, "Herringbone, Gualandrino and Brunelleschi's Bricks," 2014.

[75] S. F. Huerta, "The analysis of masonry architecture: A historical approach: To the memory of professor Henry J. Cowan," *Archit. Sci. Rev.*, vol. 51, no.

4, pp. 297–328, 2008.

[76] K. Karl-Eugen, *The history of the theory of structures*. 2018.

[77] M. Corradi, *Edoardo Benvenuto: l'arte e la scienza del costruire*. Genova: Edizioni di Storia, Scienza e Tecnica &, 2008.

[78] J. Heyman, *Coulomb's memoir on statics: an essay in the history of civil engineering*. Imperial Collage Press, 1972.

[79] P. de La Hire, *Traité de mécanique, où l'on explique tout ce qui est nécessaire dans la pratique des Arts, et les proprietés des corps pesants lesquelles ont eu plus grand*. Paris: Imprimerie Royale, 1695.

[80] P. de La Hire, "Sur la construction des voûtes dans les édifices," 1712.

[81] B. F. de Belidor, *"La" science des ingenieurs dans la conduite des travaux de fortification et d'architecture civile*. Chez Charkes Antoine Jombert, 1739.

[82] P. Roca, M. Cervera, G. Gariup, and L. Pela', *Structural analysis of masonry historical constructions. Classical and advanced approaches*, vol. 17, no. 3. 2010.

[83] P. de T. Couplet, "Seconde partie de l'examen de la poussée des Voûtes," 173AD.

[84] S. F. Huerta, "Thomas Young's theory of the arch: thermal effects," in *Mechanics and architecture between episteme and techne*, 1st ed., A. Sinipoli, Ed. Roma, 2010.

[85] J. Weale, J. Hann, H. Moseley, R. Stevenson, and W. Hosking, *The Theory, practice, and architecture of bridges of stone, iron, timber, and wire: with examples on the principle of suspension*. 1843.

[86] H. Moseley, " L. On a new principle in statics, called the P rinciple of least P ressure ," *London, Edinburgh, Dublin Philos. Mag. J. Sci.*, vol. 3, no. 16, pp. 285–288, Oct. 1833.

[87] E. Méry, "Sur l'équilibre des voûtes en berceau," vol. 19, pp. 50–70, 1840.

[88] S. F. Huerta, "Mechanics of masonry vaults: The equilibrium approach," *3rd Int. Semin. Hist. Constr. Guimarães, Port.*, no. February, pp. 47–70, 2001.

[89] H. T. Eddy, *Researches in graphical statics*. D.Van Nostrand Publisher, 1878.

[90] E. Benvenuto, M. Corradi, A. Becchi, and F. Foce, *La scienza delle costruzioni e il suo sviluppo storico*. Edizioni di storia e letteratura7, 2010.

[91] S. F. Huerta, "The analysis of masonry architecture: A historical approach: To the memory of professor Henry J. Cowan," *Archit. Sci. Rev.*, vol. 51, no. 4, pp. 297–328, 2008.

[92] G. Ungewitter, "Lehrbuch der gotischen Konstruktionen," 1892.

[93] D. C. Drucker, "A more fundamental approach to plastic stress-strain relations," in *1951*.

[94] A. Kooharian, "Limit analysis of voussoir (segmental) and concrete archs," *1952*, vol. 49, no. 12.

[95] W. Prager, "An Introduction to Plasticity. Addison Wessley," 1959.

[96] P. Block, M. Dejong, and J. Ochsendorf, "As hangs the flexible line: Equilibrium of masonry arches," in *Nexus Network Journal*, 2006, vol. 8, no. 2, pp. 13–24.

[97] M. Angelillo, P. B. Lourenço, and G. Milani, "Masonry behaviour and modelling," in *CISM International Centre for Mechanical Sciences, Courses and Lectures*, vol. 551, Springer International Publishing, 2014, pp. 1–26.

[98] R. Hart, P. A. Cundall, and J. Lemos, "Formulation of a three-dimensional distinct element model-Part II. Mechanical calculations for motion and interaction of a system composed of many polyhedral blocks," *Int. J. Rock Mech. Min. Sci.*, vol. 25, no. 3, pp. 117–125, 1988.

[99] Cundall. P. A, "Formulation of a three-dimensional distinct element model—Part I. A scheme to detect and represent contacts in a system composed of many polyhedral blocks," *Int. J. Rock Mech. Min. Sci. Geomech.*, vol. 25, no. 3, pp. 107–116, 1988.

[100] V. Sarhosis, K. Bagi, J. V. Lemos, and G. (College teacher of M. Milani, *Computational modeling of masonry structures using the discrete element method*. .

[101] *Manual, Theory and Background*. Minneapolis, Minnesota, USA: Itasca Consulting Group. iInc.

[102] A. Fraddosio, N. Lepore, and M. D. Piccioni, "Lower Bound Limit Analysis of Masonry Vaults Under General Load Conditions," *RILEM Bookseries*, vol. 18, pp. 1090–1098, 2019.

[103] J. Heyman, *Structural analysis: a historical approach*. Cambridge University Press, 2010.

[104] J. Heyman, "On shell solutions for masonry domes," *Int. J. Solids Struct.*, vol. 3, no. 2, pp. 227–241, 1967.

[105] W. H. Barlow, "On the existence (pratically) of the line of equal horizontal

thrust in arches, and the mode ofdeterminf it by geomerical construction.," *Minutes Proc. Inst. Civ. Eng.*, vol. 5, no. 1846, pp. 162–172, Jan. 1846.

[106] D. D'Ayala and C. Casapulla, "Limit state analysis of hemispherical domes with finite friction," *Hist. Constr. possibilities Numer. Exp. Tech.*, no. 1977, pp. 617–626, 2001.

[107] B. Cipriani and W. Lau, "Construction Techniques in Medieval Cairo: the Domes of Mamluk Mausolea (1250 AD-1517A. D.)," *Second Int. Congr. Constr. Hist.*, pp. 695–716, 2006.

[108] A. Romano and J. A. Ochsendorf, "The mechanics of Gothic masonry arches," *Int. J. Archit. Herit.*, vol. 4, no. 1, pp. 59–82, Jan. 2010.

[109] D. Ferretti and E. Coisson, "A New Numerical Approach to the Structural Analysis of Masonry Vaults Monitoraggio storico View project Analysis of masonry structures by Discrete Element Method (DEM) based on non-smooth dynamic View project," 2017.

[110] J. McInerney and M. J. Dejong, "Discrete Element Modeling of Groin Vault Displacement Capacity," *Int. J. Archit. Herit.*, vol. 9, no. 8, pp. 1037–1049, 2015.

[111] I. N. Psycharis, J. V Lemos, D. Y. Papastamatiou, and C. Zambas, "Numerical study of the seismic behaviour of a part of the Parthenon Pronaos," *Earthq. Eng. Struct. Dyn.*, vol. 32, no. January 2002, pp. 2063–2084, 2003.

[112] Ž. Smoljanović, Hrvoje; Živaljić, Nikolina; Nikolić, "A combined finite-discrete element analysis of dry stone masonry structures," *Eng. Struct. Elsevier*, vol. 52, pp. 89–100, 2013.

[113] J. Simon and K. Bagi, "Discrete element analysis of the minimum thickness of oval masonry domes," *Int. J. Archit. Herit.*, vol. 10, no. 4, pp. 457–475, 2016.

[114] B. S. A. Tatone and G. Grasselli, "A calibration procedure for two-dimensional laboratory-scale hybrid finite-discrete element simulations."

[115] A. Munjiza and K. R. F. Andrews, "Penalty function method for combined finite-discrete element systems comprising large number of separate bodies," *Int. J. Numer. Methods Eng.*, vol. 49, no. 11, pp. 1377–1396, Dec. 2000.

[116] B. Valentina, R. Gianni, and T. Alessandro, "A non-smooth-contact-dynamics analysis of Brunelleschi's cupola: an octagonal vault or a circular dome?," *Mecc. Elsevier*, pp. 1–23, 2019.

[117] I. Caliò, M. Marletta, and B. Pantò, "A new discrete element model for the evaluation of the seismic behaviour of unreinforced masonry buildings," *Eng. Struct. Elsevier*, vol. 40, pp. 327–338, 2012.

[118] L. B. Alberti, *De re aedificatoria*. Florence, 1443.

[119] M. Haines, "Myth and mangement in the construction of brunelleschi's cupola," *I Tatti Stud. Ital. Renaiss.*, vol. 14/15, pp. 47–101, Jan. 2011.

[120] M. Ricci, "L'accusa di Giovanni di Gherardo Gherardi a Filippo Brunelleschi: spiegazione integrale della pergamena, dei disegni e relativi contenuti tecnici," 1987.

[121] M. Haines, "Gli anni della cupola," 2015. [Online]. Available: http://duomo.mpiwg-berlin.mpg.de/.

[122] M. Viganò, "L'architettura militare nell'età di Leonardo.'Guerre milanesi' e diffusione del bastione in Italia e in Europa," in *Atti del Convegno*, 2007.

[123] G. Giovannoni, *Antonio da Sangallo, il Giovane*. Tipografia regionale, 1959.

[124] P. Portoghesi, *Dizionario enciclopedico di architettura e urbanistica*. Roma: Istituto editoriale romano.

[125] G. Da Sangallo and L. Zdekauer, "Il taccuino senese di Giuliano da San Gallo: 49 facsimili di disegni d'architettura, scultura ed arte applicata," 1902.

[126] A. Pizzigoni and V. PAris, "Il dispositivo a spinapesce: attualità e futuro della tecnologia costruttiva brunelleschiana - Laterizio.it," *Speciale "Cupola del Brunelleschi,"* 2019. [Online]. Available: http://www.laterizio.it/cil/storia-e-restauro/482-il-dispositivo-a-spinapesce-attualita-e-futuro-della-tecnologia-costruttiva-brunelleschiana.html. [Accessed: 09-Mar-2020].

[127] R. Docci, Mario; Migliari, "La costruzione della spinapesce nella copertura della sala ottagonale di Simon Mago nella fabbrica di San Pietro," *Palladio*, vol. 3, pp. 61–72, 1989.

[128] P. Sanpaolesi, *Brunelleschi*. Milano: Club del Libro, 1962.

[129] G. Breccola, *La Chiesa di Santa Maria in Montedoro, Montefiascone*. MOntefiascone, 2000.

[130] A. Pizzigoni, V. Paris, and G. Ruscica, "Herringbone technique : truth and history of a cutting-edge technology," *Proc. IASS Annu. Symp.*, 2018.

[131] C. Ragghianti, "Filippo Brunelleschi: un uomo, un universo," 1977.

[132] S. Rebora, "Scoperto il modello della Cupola del Brunelleschi? A Firenze c'è aria di scoop, attorno ai lavori per l'ampliamento del Museo dell'Opera del Duomo | Artribune," *Artribrune*, 2012. [Online]. Available: https://www.artribune.com/tribnews/2012/12/scoperto-il-modello-della-cupola-del-brunelleschi-a-firenze-ce-aria-di-scoop-attorno-ai-lavori-per-lampliamento-del-museo-dellopera-del-duomo/. [Accessed: 19-Oct-2019].

[133] M. Ricci, *Il genio di Filippo Brunelleschi : e la costruzione della Cupola di Santa Maria del Fiore*. Sillabe, 2014.

[134] M. Rippmann, P. B.-P. of the IABSE-IASS, and undefined 2011, "Digital Stereotomy: Voussoir geometry for freeform masonry-like vaults informed by structural and fabrication constraints," *block.arch.ethz.ch*.

[135] P. Block, T. Van Mele, A. Liew, M. DeJong, D. Escobedo, and J. Ochsendorf, "Structural design, fabrication and construction of the Armadillo vault," *Struct. Eng.*, vol. 96, no. 5, pp. 10–20, 2018.

[136] D. V Oliveira, P. B. Lourenço, and C. Lemos, "Geometric issues and ultimate load capacity of masonry arch bridges from the northwest Iberian Peninsula."

[137] M. Angelillo and A. Fortunato, "Equilibrium of Masonry Vaults," 2004, pp. 105–111.

[138] G. Milani and P. B. Lourenço, "3D non-linear behavior of masonry arch bridges," *Comput. Struct.*, vol. 110–111, pp. 133–150, Nov. 2012.

[139] M. Como, "A static analysis of the Brunelleschi's Dome in Florence," in *Symposium of the International Association for Shell and Spatial Structures (50th. 2009. Valencia). Evolution and Trends in Design, Analysis and Construction of Shell and Spatial Structures : Proceedings.*, 2009, pp. 1661–1674.

[140] A. Giuffrè, "Letture sulla meccanica delle murature storiche.," 1991.

[141] L. Coppola, "Concretum," 2007.

[142] W. W. . Lau, "Equilibrium analysis of masonry domes," B.S., Civil Engineering Michigan State University, 2006.

[143] J. Zessin, W. Lau, and J. Ochsendorf, "Equilibrium of cracked masonry domes," *Proc. Inst. Civ. Eng. - Eng. Comput. Mech.*, vol. 163, no. 3, pp. 135–145, 2010.

[144] J. Heyman, "'Gothic' Construction in Ancient Greece," *J. Soc. Archit. Hist.*, vol. 31, no. 1, pp. 3–9, 1972.

[145] E. Çaktı, Ö. Saygılı, J. V. Lemos, and C. S. Oliveira, "Discrete element modeling of a scaled masonry structure and its validation," *Eng. Struct.*, vol. 126, pp. 224–236, 2016.

[146] D. L. Fang, "Assessing the stability of unreinforced masonry arches and vaults: a comparison of analytical and numerical strategies," 2017.

[147] P. Solomita, "Pier Luigi Nervi architetture voltate Verso nuove strutture," Bologna, 2012.

[148] W. David, *Lassaulx und der Gewölbebau mit selbsttragenden Mauerschichten: Neumittelalterliche Architektur um 1825-1848*. Verlag , Micheal Imhof, 2008.

[149] T. Bock, "Concept of building system for robotization," *Int. Symp. Autom. Robot. Constr.*, 1987.

[150] T. Bock and T. Linner, *Robotic Industrialization*. Cambridge University Press, 2015.

[151] J. N. Richardson, S. Adriaenssens, R. Filomeno Coelho, and P. Bouillard, "Coupled form-finding and grid optimization approach for single layer grid shells," *Eng. Struct.*, vol. 52, pp. 230–239, 2013.

[152] S. Adriaenssens, P. Block, D. Veenendaal, and C. Williams, *Shell structures for architecture: form finding and optimization*. 2014.

[153] D. Dragoni, *Antichità e Reiguardevolezza della venerabil compagnia della SS. Annunziata d'Arezzo, e della sua chiesa altrimenti detta dipoi di S. Maria delle Lagrime*. 1759.

[154] A. Schiavo, "Documentazione. La Madonna di San Biagio a Montepulciano (1518-45)," *Boll. del Cent. di Stud. di Stor. dell'Architettura*, vol. vi, pp. 33–50, 1952.

[155] F. Gurrieri and P. Mazzoni, *La Fortezza da Basso: un monumento per la città*. 1990.

[156] J. Heyman, "Hemingbrough spire.," *Struct. repair Maint. Hist. Build. Gen. Stud. Mater. Anal.*, vol. 1, pp. 12–22, 1991.